INVESTIGATION OF CLIMATE CHANGE IMPACT ON HURRICANE WIND AND FRESHWATER FLOOD RISKS USING MACHINE LEARNING TECHNIQUES

BY

CHI-YING LIN

DISSERTATION

Submitted in partial fulfillment of the requirements
for the degree of Doctor of Philosophy in Civil Engineering
with a minor in Statistics
in the Graduate College of the
University of Illinois Urbana-Champaign, 2021

Urbana, Illinois

Doctoral Committee:

Assistant Professor Eun Jeong Cha, Chair
Professor Paolo Gardoni
Professor Zhuo Wang
Assistant Professor Ruoqing Zhu

ABSTRACT

Hurricane causes severe damage along the U.S. coastal states. With the potential increase in hurricane intensity in changing climate conditions, the impacts of hurricanes are expected to be severer. Current hurricane risk management practices are based on the hurricane risk assessment without considering climate impact, which would result in a higher level of risk for the built environment than the intended. For the development of proper hurricane risk management strategies, it is crucial to investigate the climate change impact on the hurricane risk. However, investigation of future hurricane risk can be very time-consuming because of the high resolution of the models for climate-dependent hazard simulation and regional loss assessment. This study aims at investigating the climate change impact on hurricane wind and rain-ingress risk and freshwater flood risk on residential buildings across the southeastern U.S. coastal states. To address the challenge of computational inefficiency, surrogate models are developed using machine learning techniques for evaluating wind and freshwater flood losses of simulated climate-dependent hurricane scenarios. It is found that climate change impact varies by region and has a more significant influence on wind and rain-ingress damage, while both increases in wind and flood risks are not negligible.

ACKNOWLEDGEMENTS

I would like to express my sincere appreciation to my advisor, Dr. Eun Jeong Cha, for her enduring help, guidance, and encouragement in my Ph.D. life. Her high standards in tackling research problems and her optimism while facing difficulties inspire me and shape me to be a competent researcher. I have thoroughly enjoyed working with her and expect to carry on what I have learned and the insights to the next chapter of my life.

I appreciate my dissertation committee members: Dr. Paolo Gardoni, Dr. Zhuo Wang, and Dr. Ruoqing Zhu, who provided me constructive suggestions from various aspects enriching the content of this research.

I gratefully acknowledge the funding support from the Taiwan Ministry of Education-University of Illinois at Urbana Champaign fellowship. The constant support always reminds me how much I want to contribute to society and taxpayers in my hometown.

Thanks also go to my friends and colleagues in this department, especially to Sami Pant, Xian He, Vamshi Krishna Gudipati, and lovely members of the R4 group, who provide me invaluable help and suggestions throughout my Ph.D. study.

Most importantly, I would like to give special thanks to my wife, Ling-Chieh, for being unconditionally supportive throughout these years. The work and this degree are not attainable without your companion. Special thanks also go to my parents, who endow me the chance to write this acknowledgment today and always care about my well-being much more than my achievement.

TABLE OF CONTENTS

LIST OF ABBREVIATIONS

Abbreviation	Explanation
AAG	approach angle
AEP	annual exceedance probability
ANN	artificial neural network
AOGCMs	Atmosphere–Ocean General Circulation Models
AOR	annual occurrence rate
AR	autoregressive
ASCE	American Society of Civil Engineers
BAM	Beta-Advection Model
CBO	U.S. Congressional Budget Office
CMIP5	Coupled Model Intercomparison Project Phase 5
CPD	central pressure difference
CPDHH	central pressure difference of high-intensity hurricanes
CPDLH	central pressure difference of low-intensity hurricanes
CTBT	Cloud-Top Brightness Temperature
DEM	digital elevation model
DHS	U.S. Department of Homeland Security
ECMWF	European Centre for Medium-Range Weather Forecasts
ERSST	Extended Reconstructed Sea Surface Temperature
FEMA	U.S. Federal Emergency Management Agency
FFBP-ANN	Feed-forward back-propagation ANN
FIA	Federal Insurance Administration
FIRM	Flood Insurance Rates Maps
FPHLM	Florida Public Hurricane Loss Model
FRC	filling rate constant
GBM	gradient boosting machine
GFS	Global Forecast System
HMON	Hurricanes in a Multi-scale Ocean-coupled Non-hydrostatic
HURDAT	Hurricane Databases
HWM	high-water mark
HWRF	Hurricane Weather Research and Forecasting
IBTrACS	International Best Track Archive for Climate Stewardship
ICOADS	International Comprehensive Ocean-Atmosphere Data Set
IPCC	Intergovernmental Panel on Climate Change
LGEM	Logistic Growth Equation Model
LHS	Latin hypercube sampling

MCPD	annual mean central pressure difference
MH	major hurricane
MSE	mean square error
NA	non-tropical Atlantic Ocean
NARX	nonlinear autoregressive network with exogenous inputs
NASA	National Aeronautics and Space Administration
NFIP	National Flood Insurance Program
NH	non-major hurricane
NI	non-tropical Indian Ocean
NOAA	National Oceanic and Atmospheric Administration
NP	non-tropical Pacific Ocean
NWS	National Weather Service
PERSIANN	Precipitation Estimation from Remotely Sensed Information using Artificial Neural Networks
R-CLIPER	Rainfall Climatology and Persistence
RCP	relative concentration pathway
RHH	ratio of the number of high-intensity hurricanes to the number of all hurricanes
RMSE	root mean square error
RMW	radius of maximum wind speed
RNN	recurrent neural network
SE	standard error
SHIPS	Statistical Hurricane Intensity Prediction Scheme
SRTM	Shuttle Radar Topography Mission
SST	sea surface temperature
SSTD	sea surface temperature difference
TA	tropical Atlantic Ocean
TC	tropical cyclone
TCGI	Tropical Cyclone Genesis Index
TDL	tap delay line
TI	tropical Indian Ocean
TP	tropical Pacific Ocean
TRMM	Tropical Rain Measurement Mission
TWI	topography wetness index
TWS	translation wind speed
USACE	U.S. Army Corps of Engineers
USGS	United States Geological Survey

CHAPTER 1: INTRODUCTION

1.1 Background and Motivation

Hurricanes, as one of the most devastating natural disasters, have caused record-breaking deconstruction to the U.S. in recent years. The U.S. Congressional Budget Office (CBO) estimates that the expected annual economic loss caused by hurricanes is $54 billion with respect to 2017 values, which accounts for 0.3 percent of the nation's current gross domestic product (CBO, 2019), and $34 billion (63%) is to the residential sector. Among the $34 billion residential sector loss, $14 billion (41%) results from wind damage, and $20 billion (59%) results from flood damage caused by storm surges or freshwater flooding. Martinez (2020) estimated a 38% and 7% chance of annual hurricane losses exceeding U.S. $10 billion and U.S. $100 billion, respectively. A study by Tonn and Czajkowski (2018) showed freshwater flooding accounts for 62% of the number of insurance claims, 51% of the total damage, for 28 U.S. landfalling tropical cyclone-related flood events from 2001 to 2014. Therefore, in terms of expected loss to the residential sector, hurricane wind, storm surge, and freshwater flooding approximately account for 40%, 30%, and 30%, respectively. The significance of hurricane wind loss is manifested by the resulted average loss ratio. In addition, hurricane-induced damages are not limited to the coastal area but potentially occurred also in hundreds of kilometers away from storm center caused by freshwater flooding (Villarini et al., 2011; Atallah et al., 2007).

Worse still, the hurricane risk has been predicted to change by climate change (Hallegatte, 2007; Vecchi et al., 2008; IPCC, 2013; Holland & Bruyère, 2014). A warming trend has been reported by the United Nations Intergovernmental Panel on Climate Change since the 1950s with the increasing greenhouse gas concentration, decreasing amounts of snow and ice, and rising sea level (IPCC, 2013). There are spatial and temporal variations in climate-related observations, and

the natural climate changes periodically and possesses cyclic variability within atmospheric and oceanic systems at the continental or subcontinental level (Olsen, 2015). However, anthropogenic global climate change alters climate patterns that could not be attributed to natural variability (Solomon et al., 2011). The changing temperature pattern, significant warming throughout the 20th century could be recognized with recorded data as a reduction in the occurrence of cold temperatures and an increase in the occurrence of warm temperatures (Alexander et al., 2006). According to the latest report by the United Nations Intergovernmental Panel on Climate Change (IPCC, 2018), if the warming continues at the current rate, the global-mean temperature might reach the crucial threshold, increasing 1.5°C above pre-industrial levels as early as by 2030. Beside the changing temperature pattern, changing meteorological phenomena and increasing number of extreme events have also been observed. The extreme weather event is defined by IPCC (2007) as the weather events being more extreme than its 10th or 90th quantiles of the recorded probability density function. The number of extreme high temperatures, precipitations, snowstorms and category 3 to 5 hurricanes has been observed to be increased significantly in recent decades relative to the average number in time period 1951 to 1980 (Wuebbles et al., 2014).

More extreme climate events have been observed in recent decades and have impacted civil infrastructures, although global warming and its consequences are still highly debated issues (Hein & Jenkins, 2017). The recognition of the impact of seasonal climate on daily weather conditions is essential in civil engineering practice and design. Civil infrastructures are exposed to severer natural hazards caused by climate change, and engineering awareness of the importance of civil infrastructures has risen by repeated and more devastating natural disasters (Stewart and Deng, 2015; Coppola, 2015). Although the essential way to mitigate the negative effect of changing

climate is to reduce the greenhouse gas emission, it is equally important and urgent for civil engineers to evaluate the potential impact as climate change happens.

The hurricane risk has been predicted to be aggravated in changing climate conditions due to increasing hurricane intensity and hurricane-induced precipitation. Since 1980, it has been found that there is an increasing trend in the intensity, duration, and frequency of North Atlantic hurricanes. Furthermore, the frequency of the most destructive hurricanes (Saffir-Simpson categories 4 and 5) has increased as well (Garfin et al., 2014; Olsen, 2015). According to Kossin et al. (2020), the frequency of the major hurricane (Saffir−Simpson categories 3, 4, and 5) in the North Atlantic increases 38% per decade based on homogenized data record for the period 1979 to 2017. The intensity of a hurricane is directly related to the sea surface temperatures (SST) at the storm center (Emanuel, 1991; Shen et al., 2000). The rising temperature induces more water vapor in the atmosphere due to the exuberant evaporation and fuel hurricanes to be more destructive, together with the warmer SST (Bengtsson et al., 2007; Emanuel, 1987; Emanuel, 2005). Several studies (Oouchi et al., 2006; Emanuel, 2008; Knutson et al., 2010) found the maximum hurricane wind speed increases under the IPCC A1B scenario (Nakicenovic et al., 2000). Specifically, Emanuel (1987) suggested that the peak wind speed should increase theoretically by 5% as the tropical ocean temperature increases 1°C, and Elsner et al. (2008) found 1°C increase in SST rises 80^{th} percentile wind speed by 1.9 ± 2.9m/s and 90^{th} percentile wind speed by 6.5 ± 4.2m/s through a quantile regression. IPCC (2018) suggests limiting global warming to 1°C compared to 2°C above pre-industrial levels to reduce the potential impact. The 2°C global warming will likely increase the tropical cyclone intensity by 1 to 10% (Knutson et al., 2019).

In terms of cyclone-induced rainfall in climate change, the warmer air holds more moisture, which induces higher precipitation (IPCC, 2013; Coumou and Rahmstorf, 2012). Seneviratne et

al. (2012) reported that heavy rainfall associated with tropical cyclones is likely to increase under increasing global warming. According to Knutson et al. (2019), for a 2°C global warming scenario, rainfall rates averaged within about 100 km of the storm will likely increase 10 to 15%. The anthropogenic influence on tropical cyclones is found to go beyond the Clausius-Clapeyron relationship, which indicates a 7% saturation specific humidity per 1°C of warming (Patricola and Wehner, 2018; Trenberth et al., 2018). For instance, two studies (Risser & Wehner, 2017; Van Oldenborgh et al., 2017) suggested that the precipitation brought by Hurricane Harvey was increased by 15 to 38% or more due to the current 1°C of global warming relative to the pre-industrial levels. Emanuel (2017) estimated that the 1% annual probability of 500 mm rainfall in the period 1980-2000 will increase to 18% in the late 21st century under the IPCC projected RCP8.5 scenario. Consequently, hurricane-induced flood risk is expected to increase in the changing climate conditions (Anthes et al., 2006; Van Aalst, 2006; Emanuel, 2008; Zahmatkesh et al., 2015; Contento et al., 2019).

Another parameter that measures hurricane hazards is hurricane genesis frequency. It is still debated whether the hurricane frequency will be changed in the future climate. Based on the analysis of the Hurricane Database (HURDAT), several studies (Mann and Emanuel, 2006; Mudd et al., 2013; Liu, 2014) have suggested that the annual frequency of hurricanes is increasing in climate change. Elsner et al. (2008) found the 1 °C increase of sea surface temperature would result in 31% increase in the global frequency of strong cyclones. Emanuel (2013) projected an increase in global mean frequency in the range of 10% to 40% during the first three-quarters of the 21st century. Bhatia et al. (2018) recently projected that the storm frequency has a 9% increase globally and a 23% increase in the Atlantic basin by the end of the 21st century. However, other studies (Vecchi and Knutson, 2008 Knutson et al., 2010; Landsea et al., 2010) suggested the statistical

significance of the increasing trend in hurricane frequency is reduced after considering the number of missing cyclones due to a lower density of cyclone-reporting ships and observational limitations prior to satellite and aircraft reconnaissance era. Despite no consensus on the trend of hurricane frequency in the future climate, many studies agree on an increasing trend in high-intensity storms (IPCC, 2013; Bengtsson et al., 2007; Bender et al., 2010; Knutson et al., 2015; Knutson et al., 2019). Holland and Bruyère (2014) concluded that there has been a substantial regional and global increase in the proportion of category 4 and 5 hurricanes relative to all hurricanes at a rate of 25-30% per 1°C of global warming.

The hurricane translation speed is also a hurricane attribute that could be affected by climate change and has a negative effect on the hurricane risk. Although a slower-moving hurricane might have a lower peak wind speed, the heavy precipitation as a result of a stalling storm can cause greater flood damage. Hurricane Harvey brought an extreme amount of rainfall, pouring more than 40 inches of rain to many areas as the hurricane slowly moved over the State of Texas (Risser & Wehner, 2017; Van Oldenborgh et al., 2017). Kossin (2018) showed a 10% decrease in the global tropical cyclone translation speed over the period 1949-2016. The change in translation wind speed varied by region: 6% and 16% decreases were found in the North Atlantic basin over water and over land, respectively. Lee et al. (2020) found a slightly decreasing trend in the tropical cyclone translation speed globally at a rate of -6×10^{-3} kph/year by conducting a statistical–dynamical downscaling projection. The study also found a 1-2% increment in the probabilities of translation speeds below 15 kph. Zhang et al. (2020) suggested that weather perturbations near 30°N related to the poleward shift of the midlatitude westerlies will be reduced as a result of anthropogenic warming, which might contribute to a slowdown of tropical cyclone motion. However, several studies proposed different findings regarding the change in translation

speed. Lanzante (2019) suggested the observed decreases in tropical cyclone translation speed are likely a result of a combination of natural internal climate variability and abrupt changes in early measurement practices. Chan (2019) made a similar conclusion, suggesting an indetermination of change in tropical cyclone translation speed, and even found a significant global speedup trend over land. Kim et al. (2020) investigated the trend of tropical cyclone translation speed during the post-satellite period (1982–2017) and found global mean tropical cyclone translation speed increased by 0.31 kph per decade over the period.

The increasing trend of global temperature is expected to continue and has a potential effect on hurricane risk. However, existing literatures do not provide a full picture of the future hurricane risk considering climate change, which delays the development of proper risk mitigation strategies. Specifically, existing studies focused mostly on the climate change impact on hurricane hazards but not impacts. Since hurricane loss is a more direct measure of risk, the investigation result of the climate change impact on hurricane losses would provide more useful information for risk management. Also, other than wind and storm surges, there are limited studies on the potential climate change impact on hurricane risk, such as rainfall-induced flooding. Furthermore, existing studies on investigating climate change impact on hurricane risk focus on smaller regions. Without a proper future hurricane risk assessment, built-infrastructure hurricane risk management practices continue based on the risk assessment with stationary hurricane occurrence assumption. The design wind load specified in ASCE 7-16 was derived based on long-term averaged hurricane statistics and did not consider possible future climate conditions. Similarly, the National Flood Insurance Program (NFIP), which accounts for 95% of residential flood insurance (CBO, 2019), assesses flood risk and delineates flood boundaries based on its Flood Insurance Rates Maps (FIRM) without considering the impact of climate change. The NFIP keeps updating map panels based on

the change of flood risk as well as refining the terrain model using remote sensing techniques (Maune, 2016; Carswell, Jr and Lukas, 2018). However, the update of flood maps does not consider the impact of climate change (Lehmann, 2020). Such practice might underestimate the flood risk in the changing climate conditions and put the built environment of the nation at risk. The U.S. Department of Homeland Security (DHS) also points out the need for improving the flood mapping program of the U.S. Federal Emergency Management Agency (FEMA) to provide reliable flood vulnerability measures (DHS, 2017). Therefore, it is imperative to assess the climate change impact on hurricane risk of wind damage and freshwater flooding for adapting design codes and standards.

Thus, the goal of this study is to investigate the climate change impact on hurricane wind and freshwater flood risks across the southeastern U.S. coastal states. To investigate the hurricane risk in changing climate conditions, it is necessary to conduct hurricane simulation using a climate-dependent hurricane model and estimate the consequent losses. One biggest challenge for such investigation is the high computational complexity and high computation time of sophisticated hurricane models and hurricane loss estimation tools. This study tackles the challenge by developing statistical surrogate models. The study will utilize machine learning techniques, especially the artificial neural network (ANN), as surrogate statistical models to establish the relationship between climate variables and hurricane parameters for conducting climate-dependent hurricane simulation. Moreover, ANNs will also be applied to develop surrogate loss estimation models for efficiently assessing regional hurricane wind and freshwater flood losses of simulated hurricane scenarios across the southeastern U.S. coastal states. The change of hurricane wind and freshwater flood losses under the projected climate scenario (IPCC, 2013) will be investigated by using the developed surrogate models. The hurricane wind and freshwater flood risk assessment

can be used by insurance industry as loss analysis tool as well as provide a guidance for amending building design codes and standards to incorporate potential climate change impact to hurricane-prone states. The following sections discuss the objectives and tasks of this study.

1.2 Research Objectives and Tasks

This research aims at investigating the climate change impact on hurricane risks, specifically, the hurricane wind and freshwater flood risks to residential buildings in the southeastern U.S. coastal states. Below are the main research tasks and associated subtasks to accomplish the objective.

(1) Develop a statistical model for predicting nonstationary hurricane parameters under changing climate conditions.

   i. Collect climate variable data including sea surface temperature and relative humidity as predictors and nonstationary hurricane parameters as responses

   ii. Conduct feature selection to identify the driving climate variables

   iii. Develop and validate a time-series regression model for hurricane parameters prediction

   iv. Use the developed model to predict nonstationary hurricane parameters for climate-dependent hurricane scenario simulation

(2) Develop statistical hurricane loss assessment models for residential buildings for wind and freshwater flood losses.

   i. Develop a hurricane wind loss model for residential buildings

   ii. Develop a hurricane flood loss model for residential buildings

(3) Evaluate the hurricane wind and freshwater flood risks across the southeastern U.S. coastal states in climate change scenarios.

i. Obtain the building inventory for study regions

ii. Simulate climate-dependent hurricane scenarios for current climate conditions and the projected climate change across study regions

iii. Evaluate hurricane wind loss for current climate conditions and the projected climate change scenario across study regions

iv. Evaluate hurricane flood loss for current climate conditions and the projected climate change scenario across study regions

v. Compare climate change impact to hurricane wind and flood losses across study regions

1.3 Organization

This dissertation comprises eight sections. Chapter 2 reviews climate-dependent hurricane simulation methods and the existing work on the investigation of climate change impact on hurricane risk. Chapter 3 introduces the basic concepts and model setups of ANNs that are used in this study. Chapter 4 presents the nonstationary hurricane parameter projection and a proposed approach to simulate hurricanes considering nonstationary hurricane parameters. Chapters 5 and 6 introduce the ANN-based hurricane wind loss model and the ANN-based hurricane freshwater flood loss estimation model developed in this study, respectively. Chapter 7 demonstrates the hurricane risk assessment results for hurricane wind and freshwater flood loss separately. Chapter 8 summarizes the investigation results of this study and discusses future works.

CHAPTER 2: EXISTING STUDIES ON CLIMATE-DEPENDENT HURRICANE RISK

2.1 Climate-Dependent Hurricane Simulation Methods

Hurricane simulation models can be categorized into dynamical, statistical, and statistical-dynamical models (National Hurricane Center, 2009). The dynamic model utilizes supercomputers solving the physical equations of motion governing the atmosphere and initial conditions based on available observations from satellites, buoys, and reconnaissance aircraft to forecast hurricane conditions. Two of the most well-known models, U.S. National Weather Service's Global Forecast System (GFS) and the European Centre for Medium-Range Weather Forecasts (ECMWF), are used for track forecasting; on the other hand, Hurricane Weather Research and Forecasting (HWRF) model and Hurricanes in a Multi-scale Ocean-coupled Non-hydrostatic (HMON) model are used for hurricane intensity prediction (Cangialosi, 2018). Dynamic models can forecast or simulate hurricanes that comply with environmental physical relationships, but these sophisticated models are known to be complex and time-consuming. For instance, an end-to-end run of HWRF would take about 4 hours with available resources, including access to 5440 cores with 16 2.6 GHz cores per node (Biswas et al., 2017). Statistical-dynamical models, such as Statistical Hurricane Intensity Prediction Scheme (SHIPS) and Logistic Growth Equation Model (LGEM), utilize a statistical model that predicts storm behavior by using environmental conditions estimated by dynamic models (Demaria & Kaplan, 1994). Lee et al. (2018) developed a statistical-dynamical model comprising a genesis model (Tropical Cyclone Genesis Index, TCGI), a beta-advection track model (Beta-Advection Model, BAM), and an autoregressive (AR) intensity model. The TCGI, developed by Tippett et al. (2011), predicts the expected number of genesis events by climate variables, including absolute vorticity, relative humidity, SST relative to tropical mean SST, and vertical shear between the 850 and 200 hPa levels. The BAM, developed by Marks

(1992) and adopted in Emanuel et al. (2006), combines beta drift and a linear combination of winds of 850 and 250 hPa levels to determine the storm track after genesis. The AR intensity model developed by the same author (C. Y. Lee et al., 2015) is a second-order vector autoregressive linear model with external environmental variables as inputs, including potential intensity, 800 – 200 hPa deep-layer mean vertical wind shear, and 500 – 300 hPa midlevel relative humidity. This model is able to capture the tropical cyclone genesis, track, intensity and landfall statistics. However, similar to dynamic models, the statistical-dynamic models might not be practical for hurricane risk assessment due to the high computation time and computational complexity.

On the other hand, statistical methods are commonly adopted to resample the historical data and create synthetic hurricane scenarios for risk assessment (Nakamura et al., 2015). The realization of synthetic hurricanes based on historical data usually utilizes Monte Carlo simulation or Markovian simulation. Hurricanes can be simulated directly at landfall (Clark, 1986; Chu & Wang, 1998), or from genesis to a complete storm track (Vickery et al., 2000; Emanuel et al., 2006; Hall & Jewson, 2007; Rumpf et al., 2007). Vickery et al. (2000) proposed a regression model to simulate hurricane direction, translation speed, and intensity on a six-hour interval as linear functions of the corresponding values from previous steps and SST. Emanuel et al. (2006) presented two track models. The first model utilized the Markov chain model, whose transition probability depending on position, season, and previous states (heading and translation speed) with statistics fitted to historical observations, and the second model utilized a beta-advection track model. Hall and Jewson (2007) developed a non-parametric model using an out-of-sample jackknife procedure to maximize the likelihood of historical observations to propagate the cyclone at the six-hour interval. Rumpf et al. (2007 and 2009) developed a basin-wide cyclone model using Monte Carlo simulation. The model utilized a local fitting kernel estimator to sample movement,

translation speed, and wind speed. The generated track needs to conform to a predefined historical track cluster that it generated from to be accepted as a valid storm track sample. Considering the possible divergence in simulation by Markovian models, Nakamura et al. (2015) developed a cyclone track simulation model that using a kernel density function to sample from the nonparametric conditional distribution to create a shift to historical hurricane track at each transition location.

Therefore, sophisticated dynamic and statistical-dynamic hurricane models are not suitable for sampling hurricane distribution due to the high computation time and computational complexity, and most statistical hurricane models assume a linear relationship between SST and hurricane wind speed or no relationship between changing climate conditions and hurricane parameters. Therefore, climate-dependent hurricane simulation in hurricane risk assessment can be improved by establishing a statistical model that captures the relationship between hurricane parameters and multiple climate variables.

2.2 Studies on Hurricane Wind and Freshwater Flood Risk Assessment Considering Climate Change

2.2.1 Wind risk assessment

The hurricane intensity is expected to increase due to climate change and would induce severer wind losses. Bjarnadottir et al. (2011) proposed a probabilistic framework to assess hurricane risk considering climate change. They assumed nonstationary wind speed due to climate change for future hurricane intensity to estimate the hurricane risks. Bjarnadottir et al. (2014) further proposed a loss estimation framework considering the damage due to hurricane wind and hurricane-induced surge along with rising sea level and also concluded that climate change would

induce a significant impact on hurricane risk. Mudd et al. (2014a) proposed a framework to investigate the hurricane hazard considering the effect of climate change. This study especially focused on the effect of changes in SST and trends in hurricane genesis frequency and hurricane track. Empirical and event-based hurricane models were built, and considering a climate change scenario (RCP8.5), the wind hazard was investigated. The authors suggested the need for an increase in design wind speed, and the same conclusion is found in their related studies (Mudd et al. 2014b; Rosowsky et al., 2016). Li et al. (2016) evaluated the hurricane damage to Miami-Dade County by considering the nonstationary hurricane intensity due to climate change, and the annual mean hurricane wind speed is assumed as linearly increasing with time. The authors conclude that annual hurricane damage is more sensitive to the change in wind speed comparing to the hurricane occurrence rate. Cui and Caracoglia (2016) thoroughly investigated the structure repair cost accounting for a series of future climate scenarios. A statistical hurricane track model was examined and applied with sea surface temperature data to simulate characteristics of hurricanes in the Atlantic Ocean, and a prototype building was used for evaluating the lifetime costs due to the aggravating hurricane hazard. Both hurricane frequency and intensity increased as a result of the warming climate and induced rising hurricane losses. Wang and Rosowsky (2018) evaluated the hurricane loss in the coastal region of South Carolina, USA, considering the changing SST on the Atlantic basin. Bivariate hazard events of simulated hurricanes were considered in the study, and the associated loss was estimated by using HAZUS-MH. Pant and Cha (2018) investigated hurricane damage for residential buildings considering four representative concentration pathways (RCPs) proposed by the IPCC, and the relationship between the SST and hurricane central pressure difference was established for the hurricane simulation under changing climate conditions.

2.2.2 Freshwater flood risk assessment

Hurricane rainfall-induced freshwater flood risk is expected to increase under climate change due to increasing precipitation resulting from warming temperature. Despite the need to understand changing hurricane freshwater flood risk, there exists no study investigating the impact of climate change on hurricane rainfall-induced freshwater flood risk. The study of climate change impact on hurricane risk has started in recent years, and the studies are mostly focused on winds or storm surge losses only. Li et al. (2012) investigated the correlation between hurricane wind and storm surge and estimated the loss due to the combined effect. The assessment of combined loss showed the overestimation of superposing individual losses. A few studies investigated climate change impact on hurricane-induced freshwater flood risk by focusing on one segment of the whole risk assessment processes, such as climate change impact on rainfall rate or impact of rainfall intensity increase on flood loss. Mudd et al. (2017) developed a probability-based tropical cyclone rainfall model conditioned on maximum surface wind speed and sea surface temperature (SST), which provides flexibility to capture extreme rates of rainfall that the operational R-CLIPER model is not capable of. To investigate the climate change impact, the study simulated tropical cyclones in the current and RCP8.5 scenario considering the change of SST. The projected maximum value of rainfall rate increases over 40% for the 700-year mean return intervals for the northeast U.S. coast comparing to current climate conditions. Emanuel (2017) estimated the annual probability of 500 mm rainfall would increase from 1% in the 2000s to 18% in the 2100s under IPCC representative concentration pathway 8.5 (RCP8.5). Czajkowski et al. (2017) used insurance claim data of 28 historical U.S. landfalling tropical cyclones to establish the statistical relationship between physical hazard and economic impact, and the study suggested a 20% increase in rainfall intensity result in a 17% increase in the number of flood claims.

2.2.3 Limitations of existing studies on future hurricane risk assessment

Literature review on the existing studies on assessing the future hurricane risk in change climate revealed significant gaps in the research. Firstly, compared to the studies on the climate change impact on hurricane hazards (introduced in Section 1), there are limited studies on the climate change impact on hurricane losses. Since hurricane loss is a more direct measure of risk, the investigation of the climate change impact on hurricane losses would provide more useful information for risk management. Secondly, existing studies on the potential climate change impact on hurricane risk are focused on wind and storm surge, and limited studies exist on other hazard types, e.g., rainfall-induced flooding. The hurricane rainfall-induced freshwater flood is one major hazard that caused significant losses historically. Thirdly, existing studies on investigating climate change impact on hurricane wind damage focus only on smaller regions, while a large regional study such as the southeastern U.S. coastal states can provide a more thorough understanding of the difference in regional climate change impact. This is mainly due to the high computational complexity and high computation time of existing hurricane loss estimation tools. For example, regional hurricane loss assessment models such as the Hazus-MH (Vickery et al., 2006) and the Florida Public Hurricane Loss Model (FPHLM) (Pinelli et al., 2008) are used for detailed estimation of hurricane wind damage. Both models conduct detailed load and resistance comparison on structural components to evaluate exterior physical damage and the consequent wind penetration. The process requires iterations to assess the final damage state with balanced structure internal pressure. For flood risk assessment, the National Water Model provides a detailed prediction on stream discharge and stage for water management and flood risk mitigation, and it also can be utilized in flood inundation prediction (Liu et al., 2018 and Shastry et al., 2019). It is a high-resolution model that manages to predict up to 250m gridded water cycle

behavior. The FPHLM is also expected to incorporate freshwater flood loss estimation as one of loss model components. These high-resolution models can be used to predict the consequence of a single event well. However, these models need more strict designation of initial and boundary conditions and more computation time attributed to model complexity, making them unsuitable for assessing hurricane risk that requires a large number of simulations. For the risk assessment, a large number of hurricane simulations are needed to construct a representative probability distribution, especially for investigating the extreme events, and high-resolution models are not feasible due to the high computational complexity and high computation time. Therefore, there is a need for developing a more efficient regional hurricane loss assessment model for a proper investigation of climate change impact on future hurricane risk.

CHAPTER 3: APPLICATION OF ARTIFICIAL NEURAL NETWORKS TO THE INVESTIGATION OF FUTURE HURRICANE RISKS

3.1 Basic Concept and Network Configuration

Several options for surrogate models (e.g., ensemble learning, regularized regression, decision trees, etc.) exist, and their adequacy is known to be problem-dependent (Brodley & Smyth, 1995; Rivas-Perea et al., 2013). Artificial neural networks (ANNs), inspired by human brain functioning, have been used effectively in fields such as regression analysis, classification, data processing, robotics, control, etc. (Geman et al., 1992; Jain et al., 1999; Jang, 1993; Schaal, 1999). This study adopts ANN since ANN models have been adopted to model and solve problems in many studies in civil engineering since the late twentieth century, especially in hydrology-related areas such as modeling of rainfall-runoff, groundwater, forecasting of precipitation, streamflow, water resource management, etc. (Tokar and Johnson, 1999; Cheng et al., 2002; Rogers & Dowla, 1994; Hsu et al., 1997; Poff et al., 1996; Liong et al., 2000; Nayak et al., 2004; Iliadis & Maris, 2007; Baños et al., 2011; Kia et al., 2012; Akbari Asanjan et al., 2018). For instance, Akbari Asanjan et al. (2018) proposed a framework for Short-term precipitation forecasting using an artificial recurrent neural network (RNN). The RNN is adopted to predict the time series of Cloud-Top Brightness Temperature (CTBT) images, and precipitation pattern is projected by using the predicted CTBT images with the Precipitation Estimation from Remotely Sensed Information using Artificial Neural Networks (PERSIANN). The main advantage of ANN is its flexibility in model configuration and the ability to recognize the underlying highly nonlinear pattern in the problem. One drawback of using ANNs is that it is hard to be used for interpretation. In other words, although it can predict the response well, it is not straightforward to know the influence of individual predictors on the response. Since the ANN is used as a prediction tool

rather than for clarifying the relationship between predictors and the response, it is considered to be an appropriate method for this study.

ANN is a mathematical model that can be trained to learn patterns and conduct regression or classification based on what it has learned. Feed-forward back-propagation ANN (FFBP-ANN) is one of the most used network algorithms used as generalized regression tools for modeling causal relations (Geeraerts et al., 2007). FFBP-ANN consists of three parts: an input layer, one or more hidden layers, and an output layer, and Figure 1 shows the schematic diagram of an ANN with n input variables and m output variables. Data used to train the network are fed forward passing nodes and links with network parameters, and the errors, i.e., the difference between target t and prediction $\hat{y}$, calculated at the output layer, are backpropagated to adjust the network parameters to help the network recognize the inherent pattern in the data. The input and target relationship could be expressed in a series formula formed by the weight and bias matrices. A series of inputs form an input vector $\boldsymbol{X} = (x_1, x_2, \dots, x_i, \dots, x_n)$, and a series of weight leading to the node j form a weight vector $\boldsymbol{W}_j = \left(w_{1j}, \dots, w_{ij}, \dots, w_{nj}\right)$, where w_{ij} represents the connection weight from the ith node in the previous layer to node j in the current layer. There is a bias or threshold value b_j associated with each node, and it serves as the threshold of the activation function. In a node, the weight has the effect of changing the slope, and the bias has the effect of shifting the location of the activation function. The activation function decides the output response of a node based on the functional form of the function. The output of node j, expressed as y_j, is obtained by computing the value of an activation function $f(.)$ with respect to the inner product of vector $\boldsymbol{X}$ and $\boldsymbol{W}_j$ minus b_j. This relation could be expressed as follows

$$y_j = f\left(\boldsymbol{X} \cdot \boldsymbol{W}_j - b_j\right), \tag{1}$$

where the activation function or called transfer function $f(.)$ determines the response of a node to the total input. The activation function is monotonically increasing, continuous, and piecewise differentiable; for instance, the sigmoid function is one of the commonly used activation function, given as

$$f(x) = \frac{1}{1 + e^{-x}}. \tag{2}$$

The output of a node in the hidden layer will be the input of the following hidden layers or the output layer.

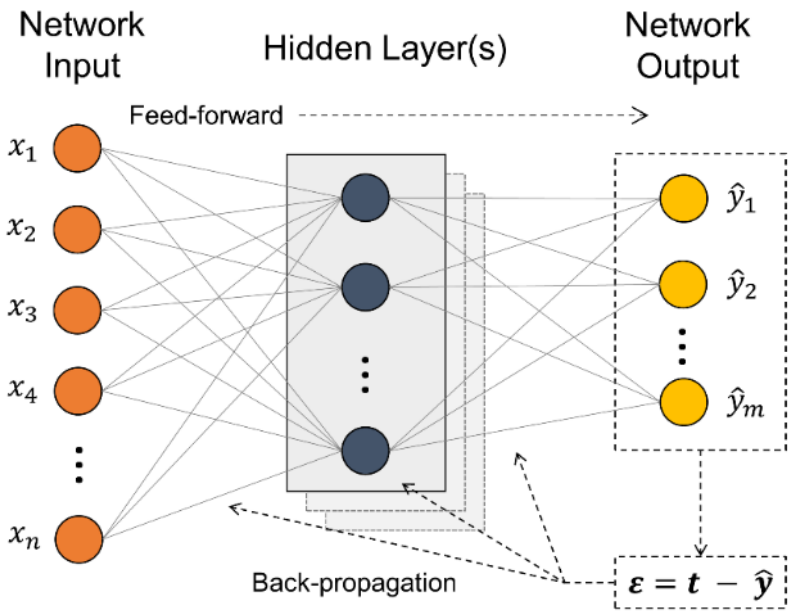

Figure 1. Illustration of a feedforward neural network

3.2 Network Training and Model Tuning

3.2.1 Network training

In supervised learning, a set of input and corresponding target data is provided for the network to learn the inherent pattern. The target values are used to evaluate the network performance based on the network-predicted output. For improving the training efficiency, data are pre-processed before fed into the network. The pre-processed data are multiplied by a pre-assigned weight matrix and added by a bias vector to form net input, which is fed into a node in the next layer with an activation function. The process keeps going until the last layer, the output layer. The processed data produced from the output layer are post-processed to transform the response back to the original form as the prediction result. The prediction error is calculated as the difference between the target values and the network-predicted outputs at the end of each iteration. This error is propagated backward to adjust the weight matrix and the bias vector, and then the updated network is used to generate the output of the next iteration. Generally, the training algorithm decides how the weight and bias are adjusted in this optimization process of minimizing the error from the output layer, and the gradient descent and the chain rule are often employed in the training algorithm. The selection of learning rate determines how much the error is propagated backward to adjust the network. A low learning rate makes the network converge slowly, and if the learning rate is too large, the gradient descent might diverge. Reviews of common network training algorithms can be found in Neelakantan et al. (2002), Ilonen et al. (2003), and Mustafa et al. (2012).

If all available observed data are used to train the network simultaneously, the network may overfit the dataset, which means, besides the underlying pattern of the data, the network also captures the unnecessary noises in the data. To avoid overfitting, the observed data are divided

into training, validation, and testing datasets. During the network training of each dividing, only the training dataset is used to train the network. Meanwhile, the unseen validation dataset is used to check whether the overfitting happens. If the prediction error in training data decreases but increases in the validation data, it means the network starts overfitting. The training should be terminated here, and the network with the current set of weights and biases is ready for the prediction. The unseen test dataset provides an unbiased evaluation of the network performance and is then used for comparison between other networks.

3.2.2 Model tuning and cross-validation

For ANNs, the number of hidden layers, number of hidden nodes, learning rate, etc., are called hyperparameters or tuning parameters for the model, i.e., the parameter of the algorithm. In section 0, the data is divided into training, validation, and testing datasets to train an ANN and avoid overfitting for a set of tuning parameters. The test result of the ANN is used to evaluate the performance of the tuning parameters. To ensure the choice of hyperparameter, cross-validation is usually conducted, and this process is called model tuning. This study incorporates k-fold cross-validation in model development. When there are several models to be selected, a train-test split is implemented, and the model is chosen with the best test performance. However, the train-test split process cannot guarantee the unbiasedness of estimation, i.e., the model might be tested on a certain portion of data that cannot represent the whole observed data distribution. In k-folds cross-validation, the observed data is divided into k folds, and each observation has the chance of being assorted to training and test datasets. In the k^{th} iteration, the k^{th} fold of data is held as the test data, and the remaining k-1 folds of data are used to train the model. Finally, the average of the test error of each holdout test data, i.e., the cross-validation error, is used to unbiasedly evaluate the model performance and for further model selection.

3.3 ANNs for Time-series Prediction

Although ANN can be used as a prediction tool for interpolation purposes, its use for extrapolation has been known to be limited (Lohninger, 1999). Since SST is expected to increase in the future and may produce samples outside the original SST sample space used to train the ANN, the usual FFBP-ANN is inappropriate for the hurricane parameters forecasting purpose. Considering the assumption of nonstationarity and the underlying causal relationship between variables, time series regression can be adopted to handle this problem instead. The ANN can be used to conduct the time series regression as it can model the dynamic relationship between variables. In this study, the time series modeling is achieved by using the nonlinear autoregressive network with exogenous inputs (NARX). The NARX is a recurrent dynamic network because it connects the output to the input layer enclosing the network. The recurrent output is used in the regression as well as the external input to achieve dynamic feedback of the network. Furthermore, one or more tap time delays are applied to the input u as well as the recurrent output y, and this discrete-time nonlinear system can be expressed as

$$y(t) = f\left(y(t-1), y(t-2), \cdots\ y\left(t-n_y\right), u(t), u(t-1), \cdots\ u(t-n_u+1)\right) +\ \varepsilon(t), \quad (3)$$

where y(.) is the output variable and u(.) is the external input variable; $\varepsilon(t)$ is the noise term; n_y and n_u represent the number of past time steps of output and input variables used in the regression, and they are set the same for input and output in this study. Except for using the recurrent output and the tapped time delay input and output variables, the basic architecture and training procedure is similar to the usual FFBP-ANN as in Figure 1.

To train the network, an open-loop, or series-parallel architecture (Figure 2a), is used to help the network learn a specific pattern. In Figure 2, u is the external input and y is the target

response; TDL is the tap delay line for creating step delays; $\hat{y}$ is the prediction of the network; w and b are weight and bias, respectively, and their subscripts h and o denote for hidden layers and the output layer, respectively. In this study, during the training process, selected climate variables (e.g., SST and relative humidity) serve as the external inputs and the observed hurricane parameters serve as the target response. Current hurricane parameters (i.e., $y(t)$) are regressed on current and previous climate variables (i.e., $u(t), u(t-1), u(t-2), \cdots u(t-n_u)$) and previous hurricane parameters (i.e., $y(t-1), y(t-2), \cdots y(t-n_y)$) for dynamic modeling. The data feedforward and error backpropagation for weight and bias adjustment are identical to the learning process in FFBP-ANN, and the training, validation, and testing processes are done in an open-loop network. While the trained network is ready to use, the configuration of the network is changed to a closed-loop or parallel architecture (Figure 2b) for the multi-step-ahead prediction purpose. Because the observed response does not exist to be used as the input variable, instead of using the observed response, the predicted network output response is fed back to the network as the input. The external input, the projected climate variables, together with the predicted hurricane parameters connected back to the input layer, are used to predict future hurricane parameters by using this closed-loop network.

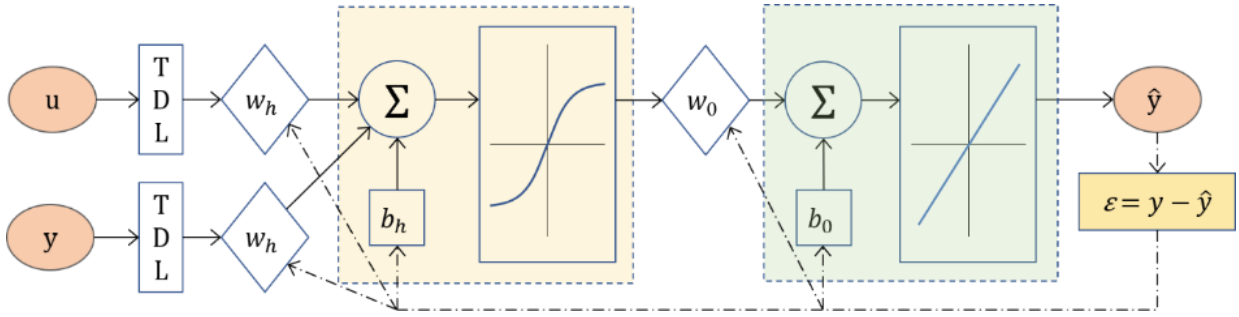

(a)

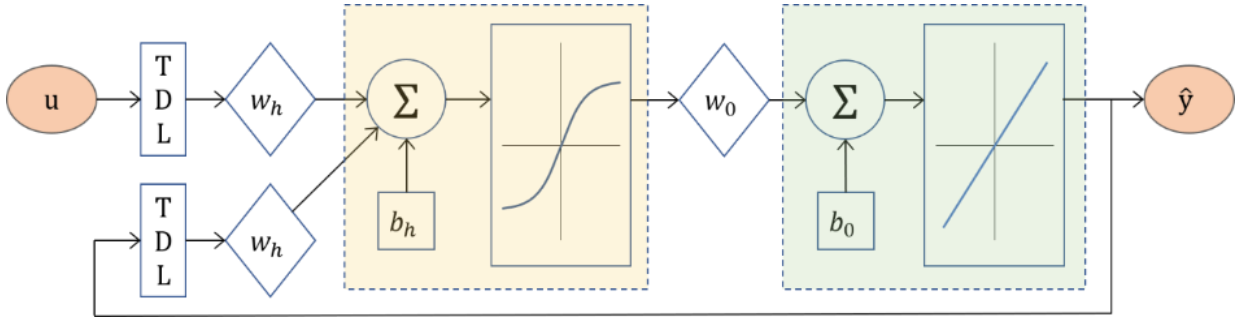

(b)

Figure 2. Configuration of the NARX network: (a) in open-loop form and (b) in close-loop form

CHAPTER 4: DEVELOPMENT OF CLIMATE-DEPENDENT HURRICANE SIMULATION FRAMEWORK

4.1 Stationary and Nonstationary Parameters in Hurricane Simulation

To simulate climate-dependent hurricane scenarios for future hurricane risk assessment, this study adopts and modifies the statistical hurricane simulation method described in Huang et al. (2001) by incorporating NARX ANNs-based nonstationary hurricane parameter prediction model. In the hurricane simulation model of this study, hurricanes are simulated from their landfall with parameters including annual occurrence rate, approach angle, translation wind speed, central pressure difference (CPD), the ratio of the high-intensity hurricane to all hurricanes (RHH), the radius of the maximum wind, and filling rate constant. Then, transition matrices are used to simulate subsequent hurricane tracks, with the filling rate constant determining the decay of hurricane intensity. The hurricane parameters are classified into stationary and nonstationary and modeled differently depending on the stationarity classification. The stationary hurricane parameters are assumed to follow the distribution under current climate conditions at any point in time and include RHH, annual occurrence rate, approach angle, translation wind speed, and filling rate constant. Transition matrices for both approach angle and translation wind speed are also assumed to be stationary. The nonstationary hurricane parameters are assumed to be affected by climate change. The CPD is independently modeled as nonstationary, and the radius of the maximum wind speed is modeled as a function of CPD (Vickery & Wadhera, 2008). Probabilistic models of stationary hurricane parameters and nonstationary hurricane parameters under current climate conditions are derived from historical hurricane data from 1944 to 2016, obtained from the International Best Track Archive for Climate Stewardship (IBTrACS v03r10) dataset published by Knapp et al. (2010). The IBTrACS dataset provides storm coordinates, central pressure, and

wind speed for every 6 hours as well as at landfall, and the storm track information is used to derive necessary hurricane parameters for hurricane simulation.

The CPD is assumed to be nonstationary in changing climate conditions since the hurricane intensity is expected to increase in changing climate conditions (Nakicenovic et al., 2000; Oouchi et al., 2006; Emanuel, 2008; Knutson et al., 2010). The site-specific annual mean CPD (MCPD) of hurricanes making landfall at the coastline of a study region is used for the nonstationary modeling. The increase in CPD projection will correspondingly lead to the increase in the frequency of high-intensity hurricanes, as suggested in several studies (Bengtsson et al., 2007; Emanuel, 2008; Knutson et al., 2008; Knutson et al., 2010).

The nonstationary hurricane parameter, MCPD, under climate change scenarios is predicted by using ANNs with selected climate variables. To distinguish different distribution attributes of high- and low-intensity hurricanes, the CPD distributions for high-intensity and low-intensity hurricanes are constructed separately. The high- and low-intensity hurricanes are fitted using category 1-2 and category 3-5 hurricanes in the Saffir-Simpson wind scale. The difference in the MCPD relative to the current climate condition is projected, which is used to shift CPD distributions of high- and low-intensity hurricanes. The RHH determines the probability of simulating high-intensity hurricanes. In a simulation, the number of simulated hurricanes is sampled from the Poisson distribution with a stationary annual occurrence rate in each study region, and RHH determines the number of hurricanes within the total number of hurricanes to be simulated using the probability distribution for the CPD of high-intensity hurricanes. In climate-dependent hurricane simulation, probabilistic models of site-specific stationary hurricane parameters are derived for each study region, and the nonstationary hurricane parameters are

predicted and applied to all study regions because of the constraint of data availability. Details about hurricane simulation will be provided in section 4.6.

4.2 Research Study Region

In this study, the southeastern U.S. coastal region is divided into 4 study regions for deriving the site-specific probabilistic models of stationary hurricane parameters and current conditions of nonstationary hurricane parameters to simulate hurricanes on specified coastlines. Hurricanes are simulated at the coastline of each region, as shown in Figure 3. Study regions are defined as follows:

Region 1: Texas (TX) state.

Region 2: Louisiana (LA), Mississippi (MS), and Alabama (AL) states.

Region 3a: Florida state by the coast of the Gulf of Mexico (FL_G).

Region 3b: Florida state by the coast of the Atlantic Ocean (FL_A).

Region 4: Georgia (GA), South Carolina (SC), and North Carolina (NC) states.

The division of the southeastern U.S. coastal states is based on a preliminary study on the validity of fitted distribution for hurricane parameters using historical data. The probability distribution fitting of hurricane parameters in each study region of the selected division has passed the goodness-of-fit test. Additional information for study regions is provided in Table 1. Note that the total exposure comprises the exposure of wooden and concrete masonry single-family residential buildings in study regions.

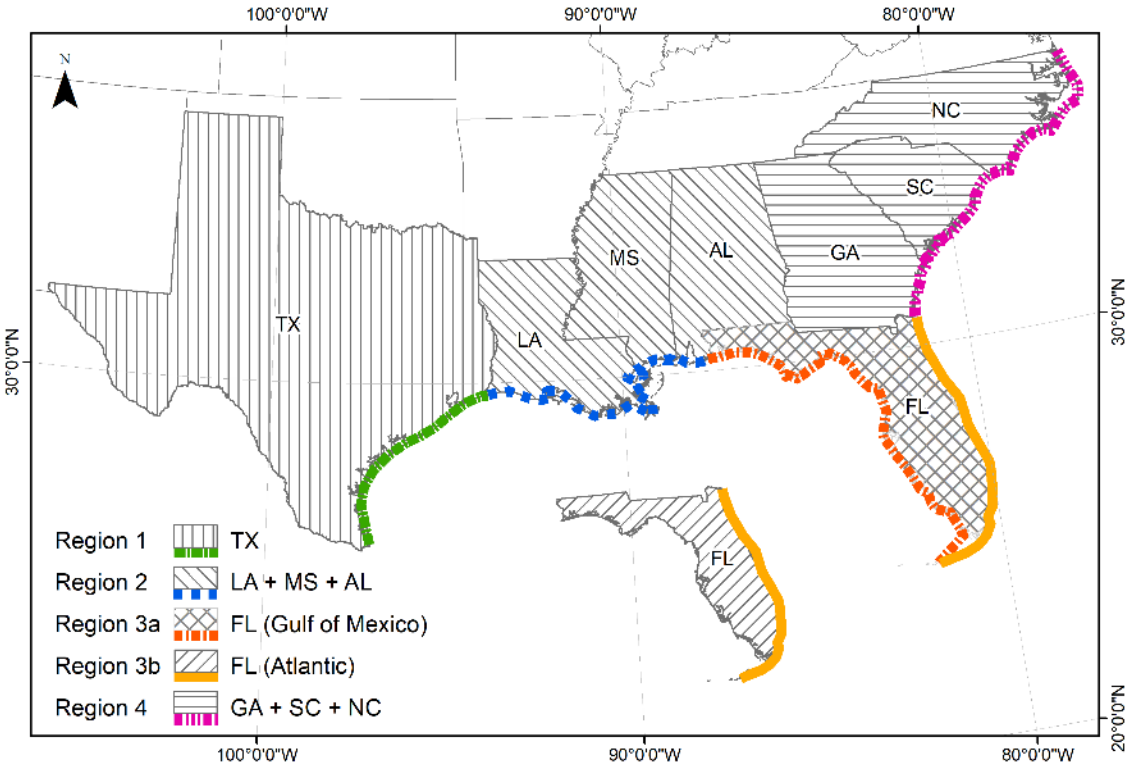

Figure 3. Study region for future hurricane wind and flood risk assessment

Table 1. Study region information

Regions	Coastlines of hurricane simulation	Length of coastlines (km)	Area of regions (km^2)	Total exposure (U.S. $1B)
Region 1	Texas (TX) state	595	685,841	2,367
Region 2	Louisiana (LA), Mississippi (MS), and Alabama (AL) states	993	378,770	1,089
Region 3a	Florida state by the coast of the Gulf of Mexico (FL_G)	1173	146,843	1,684
Region 3b	Florida state by the coast of the Atlantic Ocean (FL_A)	809		
Region 4	Georgia (GA), South Carolina (SC), and North Carolina (NC) states	974	360,137	2,560

4.3 Stationary Hurricane Parameters Modeling

The probabilistic models of hurricane parameters of each study region for the hurricane simulation are summarized in Table 2, including six site-specific hurricane parameters, which are hurricane annual occurrence rate (AOR), approach angle (AAG), translation wind speed (TWS), central pressure difference (CPD) for low- and high-intensity hurricanes, and the filling rate constant (FRC). The CPD of hurricanes is modeled for two intensity groups, low-intensity hurricanes (CPDLH) and high-intensity hurricanes (CPDHH). Distributions of CPDLH and CPDHH are fitted by using category 1-2 and category 3-5 historical hurricanes in the Saffir-Simpson wind scale, which corresponds to minor and major hurricanes, respectively. Note that category 3-5 hurricanes can still be simulated by using CPDLH distribution and vice versa. Furthermore, the mean values of CPD (MCPD) for hurricanes of all categories derived in this section represent baselines, and changes of MCPD from these baselines reflect the nonstationarity in MCPD.

Table 2. Probability distribution models of stationary hurricane parameters

Hurricane Parameter	Distribution	Distribution Parameter	Region 1: TX	Region 2: LA+MS+AL	Region 3a: FL_G	Region 3b: FL_A	Region 4: GA+SC+NC
AOR	Poisson	λ	0.236	0.403	0.333	0.264	0.375
AAG (degree)	Normal	μ	-30.134	-5.372	36.465	-57.512	-2.511
		σ	35.616	33.301	37.342	41.665	33.577
CPDLH (mb)	Weibull	u	41.251	44.069	38.491	39.598	45.555
		k	2.755	3.394	4.639	4.137	2.731
CPDHH (mb)	Weibull	u	66.536	82.528	70.060	70.916	72.354
		k	10.803	4.261	19.841	6.554	10.615
TWS (m/s)	Lognormal	λ	1.352	1.708	1.930	1.700	1.917
		ζ	0.391	0.547	0.466	0.333	0.501
FRC	Normal	μ	-2.868	-3.280	-3.340	-3.355	-3.120
		σ	0.490	0.508	0.649	0.393	0.732

For each hurricane parameter in each region, candidate distributions including normal, extreme value, exponential, Rayleigh, Weibull, lognormal, and Gamma distributions are tried to fit the data of the hurricane parameter. Bootstrap maximum likelihood estimation is used to determine probabilistic models of the hurricane parameters at landfall. The fitted candidate distribution is tested for the goodness of fit using the Kolmogorov–Smirnov test (K-S test) with a significance level of 0.05. The candidate distribution with the highest bootstrap likelihood and passing the K-S test for all study regions is chosen to model this parameter.

4.4 Adopted Climate Change Projection

In this research, climate-dependent hurricane simulation is based on climate change scenarios proposed by the IPCC (2013 and 2014). The IPCC projected climate scenarios are characterized by four representative concentration pathway (RCP) scenarios, the projection of greenhouse gas concentration. Four pathways are proposed for climate-related research: RCP2.6, RCP4.5, RCP6.0, and RCP8.5. The number associated with RCP represents the radiative forcing in a unit W/m^2, which quantifies the difference between sunlight absorbed by the earth and the energy radiated back to space (Shindell, 2013). Higher radiative forcing results in higher sea surface temperature and hence might induce hurricanes of higher intensity. The four projected pathways considered the possible change of future greenhouse gas emission, and within them, the RCP8.5 is the most extreme one, which represents the emissions increase throughout the 21st century. The worst situation, the RCP8.5 climate change scenario, is considered for climate-dependent hurricane parameters prediction in this study. The global SST increment projection based on concentration-driven Coupled Model Intercomparison Project Phase 5 (CMIP5) simulation is used. For RCP8.5 scenario, global mean SST is projected to increases 1.2°C for the

near-term projection (2015-2060) using 12 Atmosphere–Ocean General Circulation Models (AOGCMs) from the CMIP5. For the long-term projection (2081-2100), global mean SST is projected to increase 3.1℃ with the lower bound and upper bound being 2.1℃ and 4.0℃, respectively, using 39 AOGCMs from the CMIP5. For simplicity, the expected value, lower bound and upper bound of global SST are assumed to linearly increase to its long-term projection relative to the reference period, 1986 to 2005.

4.5 Nonstationary Hurricane Parameters Prediction

4.5.1 Climate variables for nonstationary hurricane parameters prediction

To depict the trend of future hurricane parameters, essential climate variables that predict the nonstationary hurricane parameters should be identified. The procedure of using the selected climate variables to predict nonstationary hurricane parameters is shown in Figure 4. Essential climate variables are identified from the climate variable candidates, and two time series regression models are used to predict nonstationary hurricane parameters from the IPCC projected global SST. For the climate variable candidates, two categories of climate variables are considered, which are SST variables and relative humidity variables. SST variables are derived from the Extended Reconstructed Sea Surface Temperature (ERSST) Version 5 dataset published by the National Centers for Environmental Information (Huang et al., 2017), and relative humidity variables are derived from International Comprehensive Ocean-Atmosphere Data Set (ICOADS) Release 3.0 provided by Freeman et al. (2017). Monthly values of both SST and relative humidity data are reported on a 2° × 2° grid, and the data for the period between 1944 and 2016 are extracted for the analysis.

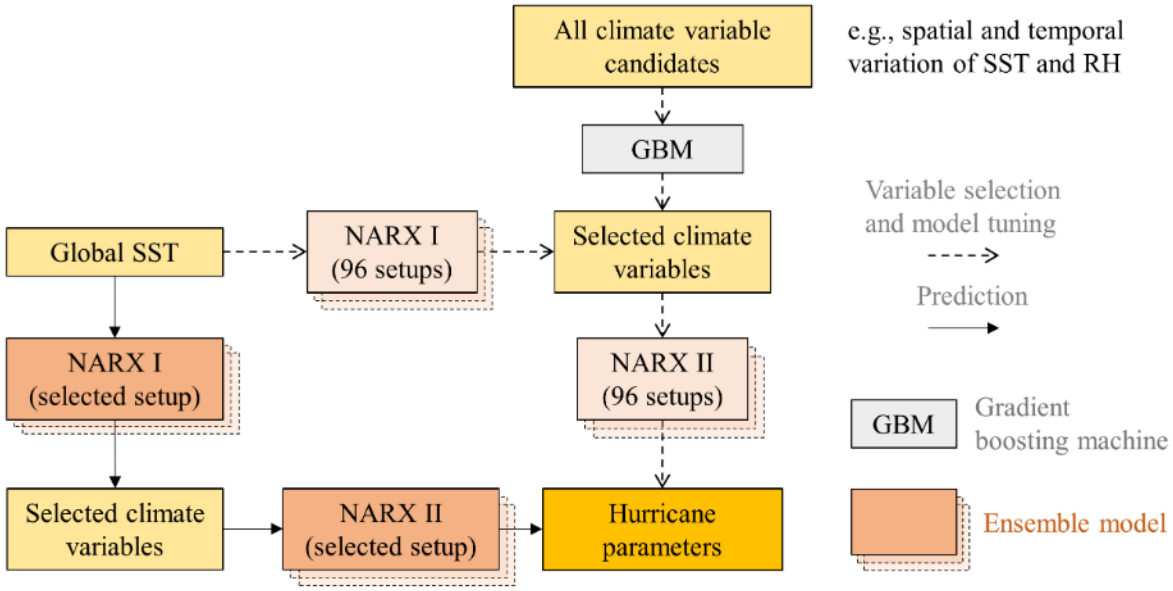

Figure 4. Flowchart of variable selection and nonstationary hurricane parameter prediction

Both SST and relative humidity are computed for six basins including the tropical Atlantic Ocean (equator to 32°N, from Americas to African coast; denoted as TA), non-tropical Atlantic Ocean (32°N to 66°30'N; denoted as NA), tropical Indian Ocean (15°S to 15°N, 40°E to 110°E; denoted as TI), non-tropical Indian Ocean (15°S to 60°S, 20°E to 147°E; denoted as NI), tropical Pacific Ocean (equator to 30°N, from 140°W to Americas; denoted as TP) and non-tropical Pacific Ocean (30°N to 60°N; denoted as NP). For each basin, the annual average, maximum, and minimum of the spatial mean, maximum, and minimum monthly values are determined for SST and relative humidity. Totally, 54 variables are obtained for each of SST and relative humidity, which are analyzed to identify the most influential climate variables to hurricane parameters by using variable selection. In addition to these 108 variables, two other variables, annual mean SST difference (SSTD) between the tropical Atlantic Ocean and the tropical Indian Ocean and between the tropical Atlantic Ocean and the tropical Pacific Ocean, are also considered as variable

candidates because of their potential influence on vertical wind shear which is directly related to the formation and intensity of the resulting hurricanes (Latif et al., 2007).

4.5.2 Climate variable selection

To develop an adequate model for the prediction of hurricane parameters, it is crucial to determine a set of input variables that collectively interpret the output variables. To enhance the capability of identifying the nonlinear relationship between climate variables and hurricane parameters, this study utilizes feature importance in gradient boosting as introduced in Hastie et al. (2009) to select climate variables for nonstationary hurricane parameters prediction. The details of the gradient boosting algorithm can be found in Friedman (2001 and 2002) and Mason et al. (2000). This study first establishes a gradient boosting model for the prediction of MCPD from all climate variables. Five-fold cross-validation mean square error (MSE) is used to determine the hyperparameters of these two models. In five-fold cross-validation, the training data is randomly separated into five portions, and in the K^{th} iteration, the K^{th} fold of data is held as the validation data, and the remaining data are used to train the model. The cross-validation error, the average test error of holdout test data, is then used to evaluate the model performance. The hyperparameters considered for tuning the ensemble model are the maximum number of splits, learning rate, and the number of trees. The maximum number of trees decides the number of individual models stacked up in the final model. The maximum number of splits decides the depth of each tree, which specifies the level of variable interaction in a tree. The learning rate or called shrinkage reduces the contribution of individual tree and hence slow down the learning process. Based on the minimum cross-validation error, the selected maximum number of splits, learning rate, and the number of trees are 5, 0.0005, and 1,500, respectively, for MCPD prediction. After fitting the model, the variables are sorted in descending order based on the relative importance, and the

number of selected climate variables is determined by using the elbow point on the relative importance plot, as shown in Figure 5. Figure 5 plots the relative importance of all 110 climate variables in descending order, and the green point represents the elbow point which determines the number of variables selected for each nonstationary hurricane parameter. Based on the rank-ordered relative importance, 12 climate variables is selected for MCPD prediction, and the selected climate variables are shown in Table 3.

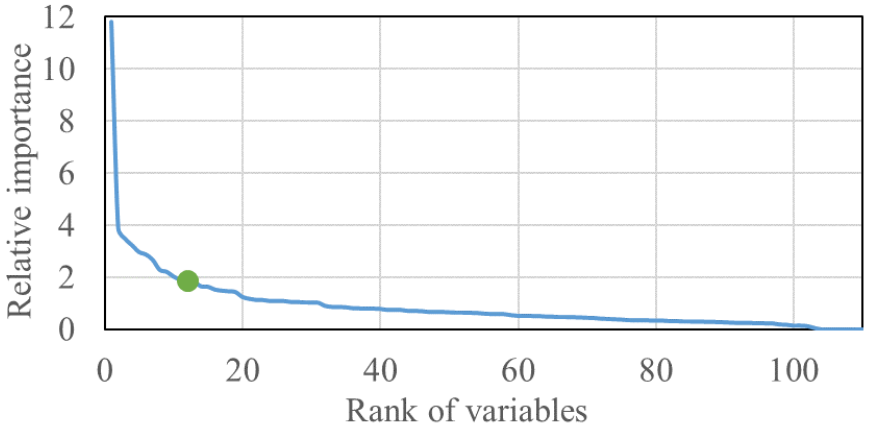

Figure 5. Rank-ordered relative importance of climate variable candidates for MCPD

Table 3. Selected climate variables for nonstationary hurricane parameter prediction

Hurricane parameters	Selected climate variables
MCPD	Annual mean of SSTD between TA and TI
	Annual mean of NA regional mean SST
	Annual minimum of TI regional minimum SST
	Annual minimum of NI regional minimum relative humidity
	Annual maximum of TP regional minimum SST
	Annual minimum of NA regional maximum SST
	Annual minimum of TA regional minimum relative humidity
	Annual mean of NP regional maximum relative humidity
	Annual maximum of NP regional minimum SST
	Annual maximum of NA regional mean relative humidity
	Annual minimum of NP regional mean SST
	Annual mean of SSTD between TA TP

4.5.3 NARX network setup and ensemble modeling of hurricane parameter prediction

The nonstationary hurricane parameter, MCPD, under climate change scenarios is modeled as time series models by using the NARX ANNs with selected climate variables. The basic concept of NARX ANNs is introduced in section 3.3. For enhancing the accuracy of hurricane parameter prediction, different network setups are investigated. In this study, five NARX network attributes are investigated (Table 4): 1) training algorithm, 2) transfer function (i.e., the activation function) in the hidden layer, 3) the number of hidden layers, 4) the number of hidden nodes in each hidden layer, and 5) the number of steps of feedback delay. A total of 96 combinations of network setups are considered. Network ensemble is adopted to improve the model performance, and the nested cross-validation is adopted to find the most suitable network configuration for the ensemble model for the time series prediction. As discussed in Varma and Simon (2006), the nested cross-validation can provide a closely unbiased estimate of the true error. To implement this procedure, the observation time series of dependent variables are divided into six folds to form five pairs of training and test sets. In the first pair, the first fold (chronologically) is used to train the network, and the second fold is used to test the model. In the second pair, the first two folds are used to train, and the third fold is used to train, and so on. This procedure is an expanding window approach, and discussion of this approach can be found in Hyndman (2016) and Bergmeir et al. (2018). In the expanding window approach, the potential issue is the later cross-validation models contain more information than the previous cross-validation model and could have a bias evaluation of the model configuration by simply averaging the performance of all cross-validation models. An alternative approach is a sliding window approach. The training data of the later cross-validation model does not include the data to train the previous model. This approach ensures fairness across all cross-validation models. However, since the time span of the training data is

fixed and shorter than the one in the expanding window approach, it cannot capture the variability longer than the time span well. The performance of the ensemble model with a certain network configuration is determined based on the average MSE of the five test sets. This procedure is conducted to construct both NARX I and NARX II models, and the selected network attributes for each model are shown Table 5.

Table 4. NARX network setup for investigation for nonstationary hurricane parameter prediction

Network Attributes	Tested Setups
Training algorithm	Levenberg-Marquardt algorithm Resilient backpropagation algorithm
Transfer function	Hyperbolic tangent sigmoid function Log-sigmoid transfer function Symmetric saturating linear transfer function
Number of hidden layers	1 or 2 hidden layers
Number of hidden nodes	10 or 15 hidden nodes in a hidden layer
Number of feedback delay	2 to 5 steps of tapped delay applied to variables

Table 5. Selected NARX network setup for nonstationary hurricane parameter prediction

Network attributes	NARX I (MCPD)	NARX II (MCPD)
Training algorithm	Resilient backpropagation	Resilient backpropagation
Transfer function	hyperbolic tangent sigmoid function	hyperbolic tangent sigmoid function
Number of hidden layers	2	1
Number of hidden nodes	15	15
Feedback delay (steps)	5	2

Using the projected global SST (section 4.4), corresponding climate variables and hurricane parameters are predicted by following the procedure shown in Figure 4. The selected climate variables are first predicted by using the ensemble NARX I model with selected setups and the projected global SST. With the projected climate variables, the MCPD is then projected by ensemble NARX II models with selected setups. The predictions of the selected model for MCPD compared to the observed values are shown in Figure 6, respectively. Grey dotted lines are the predictions from 400 individual networks of the selected ensemble model, and the blue solid line is the ensemble result of all networks. The red dashed line is the historical record. It is found that the ensemble model for MCPD prediction captures the general trend of the observed values well. Using the IPCC projected global SST, corresponding climate variables and hurricane parameters are predicted, as shown in Figure 7. The five-year moving average of prediction of MCPD for mean RCP8.5 scenario (solid line) as well as the upper bound (dashed line) and the lower bound (dash-dotted line) are shown in Figure 7. The shaded area in the figure shows the prediction interval representing the parameter uncertainty estimated by using neural network dropout as described in Zhu and Laptev (2017), Pearce et al. (2018), and Gal and Ghahramani (2016). Under the mean RCP8.5 scenario, compared to the current climate conditions (mean value between the year 1986 to 2005), MCPD increases 36% and 81%, respectively, for the near-term projection (2020-2030) and the long-term projection (2090-2100). Pant and Cha (2018) conducted a simple linear regression and found a 1-degree increase in SST results in a 1.92 mb increase in the CPD. Based on this relationship, compared to current climate conditions, the mean CPD would increase over 6.5 mb (25%) in the year 2100 under the RCP8.5 climate change scenario. Furthermore, Knutson et al. (2015) suggested a 4.5% increase in hurricane maximum wind speed under RCP4.5 in the late 21st century in the Atlantic ocean based on dynamic downscaling of the

CMIP5 model, and Knutson et al. (2020) suggested a globally 5% increase in maximum wind speed under RCP8.5 in the year 2055. Given that the CPD is approximately proportional to the square of wind speed, the CPD prediction in this study is reasonable compared to these previous findings.

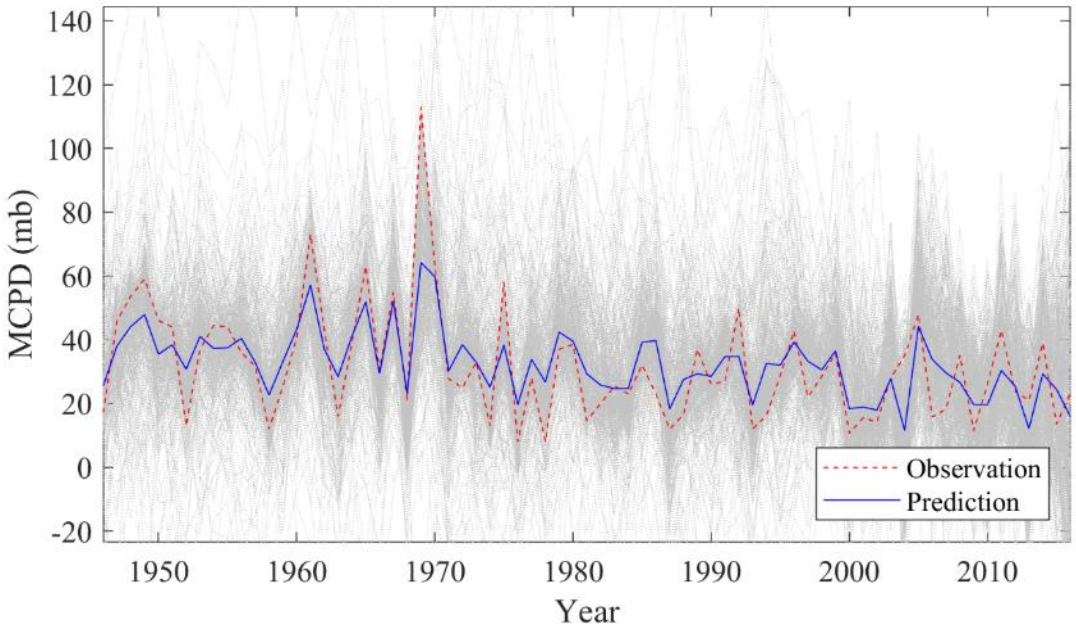

Figure 6. Comparison of hurricane MCPD prediction and observed data

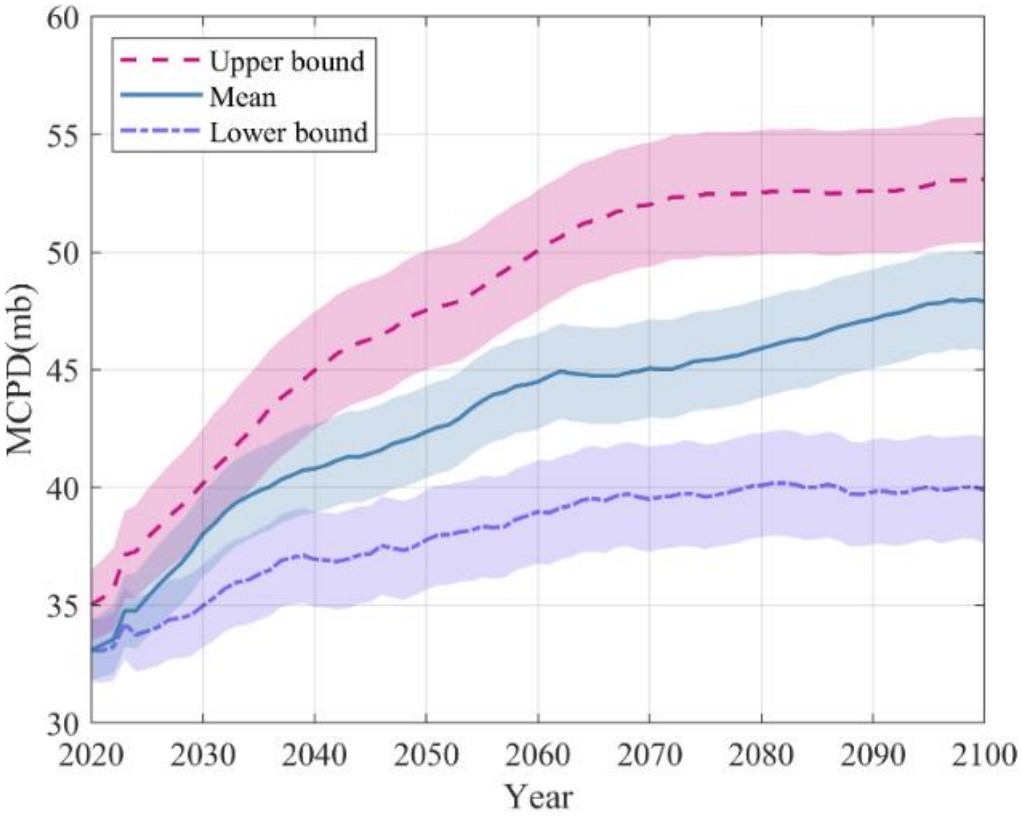

Figure 7. Prediction of nonstationary hurricane parameters MCPD under the mean, upper bound, and lower bound climate change scenario (RCP 8.5) projections

4.6 Hurricane Simulation

4.6.1 Landfalling hurricanes and initial conditions

Hurricane parameters are simulated by using Latin hypercube sampling for generating hurricanes at landfall with the region-specific annual occurrence rate following the Poisson distribution as in Table 2. Latin hypercube sampling (LHS) is adopted in this study for simulating hurricanes to reduce the number of simulations and retain the accuracy (Loh, 1995; Aistleitner et al., 2012). For each study region of each scenario in each simulation, the total number of hurricanes is determined by the annual occurrence rate, and then the numbers of high- and low-intensity hurricanes are determined by the RHH_{ldf}. The RHH for all hurricanes formed on the Atlantic Ocean (denoted as RHH_{all}) is converted to landfall RHH (denoted as RHH_{ldf}) by using a relationship established through a simple linear regression of historical data. The relationship between RHH_{ldf} and RHH_{all} used in this study is shown in Eq. (4).

$$RHH_{ldf} = 0.846RHH_{all} + 0.130\,. \tag{4}$$

Note that because of limited data, RHH_{ldf} derived here is applied for all study regions instead of a specific region. Since high-intensity hurricanes can be considered rare events, a 10-year time interval is used to avoid the non-occurrence as a limited number of simulations. During the 10-year period, landfall hurricane genesis is assumed to follow the Poisson distribution, and the genesis location is assumed to be uniformly distributed along the coastline of a study region (see Figure 3). The RHH determines the number of hurricanes simulated using region-specific CPDHH distribution to simulate CPD values.; on the other hand, the one minus RHH determines the number of hurricanes simulated using region-specific CPDLH distribution to simulate CPD values. Generated hurricanes associated with initial conditions simulated include location and site-

specific parameters, including translation wind speed, approach angle, filling rate constant, the radius of maximum wind speed (RMW), central pressure difference (CPDHH or CPDLH). Hurricane parameters are simulated using statistical models specified in Table 2. The RMW is calculated as a function of CPD by a formula adopted from Vickery and Wadhera (2008). The projected MCPD is used to calculate the MCPD change relative to current climate conditions (i.e., delta MCPD) and to update mean values of the CPDHH and CPDLH distributions under the changing climate conditions as shown in Eq. (5). Note that the projected MCPD is applied to all study regions to update region-specific CPDHH and CPDLH distributions due to the data availability.

$$\begin{aligned} Projected\ mean\ value\ of\ CPDHH &= Current\ mean\ value\ of\ CPDHH + \Delta MCPD \\ Projected\ mean\ value\ of\ CPDLH &= Current\ mean\ value\ of\ CPDLH + \Delta MCPD \end{aligned} . \quad (5)$$

4.6.2 Storm track and wind speed modeling

To simulate a complete storm track before and after landfall for the subsequent loss estimation, the translation wind speed and the approach angle of the storm are modeled with the discrete Markov chain. The transition probabilities are calculated based on past hurricane records. To predict the accumulated rainfall, hurricanes are simulated starting from 24 hours before their landfall. The before-landfall transition matrices are developed based on historical records, and hurricane intensity is assumed as constant before making landfall. Table 6 and Table 7 show transition matrices of the translation wind speed (V_T), and the approach angle (θ), for study region 1, respectively for demonstration purposes. The approach angle is taken clockwise positive from North. Both V_T and θ are functions of time starting from the landfall. To develop the one-step transition probability matrix, the changes in translation wind speed and approach angle are

discretized to seven states and the associated values have to be defined. For the translation wind speed, the state condition is defined as the ratio of the current translation speed to the translation speed of the previous step. For the approach angle, the state condition is defined as the difference between the current approach angle (in degree) and the approach angle of the previous step and normalized by dividing it by 90 degrees. As the current state being calculated, the continuous states are converted to discrete states by checking the closest state value (by row), and then the next state (by column) is decided by the conditional probabilities. The derivation of state values ensuring the validity of the transition matrices across all study regions.

From the simulated hurricanes, the maximum gradient wind speed is determined by using the physical model in Vickery et al. (2000):

$$\mathrm{V}_g = \frac{1}{2}(c \cdot \sin(\alpha) - fr) + \sqrt{\frac{1}{4}(c \cdot \sin(\alpha) - fr)^2 + \frac{B\Delta p}{\rho}\left(\frac{R_{max}}{r}\right)^B exp\left[-\left(\frac{R_{max}}{r}\right)^B\right]}, \quad (6)$$

where α is the heading angle, f is the Coriolis parameter, r is the distance from the storm center to the location of interest, ρ is the air density, Δp is the central pressure difference, B is the pressure profile parameter, R_{max} is the radius of the maximum wind speed. The gradient wind speed is converted to a maximum 1-minute sustained wind speed at the surface for wind damage and rainfall intensity estimation. A reduction factor of 0.6 is applied to convert the wind speed from the flight level to the surface level (Knaff et al., 2011), and 1.21 is applied to convert the 10-minute to the 1-minute wind speed assuming an open terrain condition (Harper et al., 2010). Consequently, 0.72 is used to obtain the maximum sustained wind speed.

Table 6. Translation wind speed transition matrix of study region 1

	$V_T(t)/V_T(t-1)$							
$V_T(t-1)/V_T(t-2)$	State value	0.351	0.566	0.781	0.996	1.211	1.426	1.641
	0.351	0.725	0.200	0.050	0.025	0.000	0.000	0.000
	0.566	0.423	0.308	0.154	0.038	0.077	0.000	0.000
	0.781	0.061	0.242	0.424	0.182	0.091	0.000	0.000
	0.996	0.015	0.059	0.147	0.324	0.221	0.118	0.118
	1.211	0.000	0.033	0.100	0.133	0.467	0.133	0.133
	1.426	0.000	0.000	0.111	0.111	0.167	0.389	0.222
	1.641	0.033	0.000	0.000	0.100	0.033	0.067	0.767

Table 7. Approach angle transition matrix of study region 1

	$[\theta(t)-\theta(t-1)]/90$							
$[\theta(t-1)-\theta(t-2)]/90$	State value	-0.114	-0.051	0.011	0.074	0.137	0.199	0.262
	-0.114	0.451	0.098	0.157	0.078	0.020	0.039	0.157
	-0.051	0.130	0.130	0.304	0.174	0.087	0.087	0.087
	0.011	0.136	0.136	0.227	0.136	0.091	0.136	0.136
	0.074	0.143	0.107	0.321	0.143	0.107	0.071	0.107
	0.137	0.050	0.000	0.200	0.150	0.250	0.300	0.050
	0.199	0.231	0.000	0.154	0.154	0.154	0.154	0.154
	0.262	0.206	0.088	0.118	0.118	0.059	0.118	0.294

CHAPTER 5: DEVELOPMENT OF HURRICANE WIND LOSS MODEL

5.1 Loss Estimation using ANN-based Surrogate Model

To evaluate the hurricane wind damage of simulated climate-dependent hurricane scenarios, a surrogate hurricane wind loss estimation model is developed. In the preliminary study, hurricane wind damage and economic loss were estimated by using HAZUS-MH. Wind loss estimation using HAZUS-MH is limited due to computational complexity and inefficiency. The computational complexity is caused by manual study region selection and input of storm track information, which makes the automatic loss estimation of simulated hurricane scenarios unachievable. Moreover, wind loss estimation using HAZUS-MH is also highly time-consuming due to the high-resolution loss estimation, which makes the number of hurricane simulations to be limited, resulting in a higher variation in risk assessment. Therefore, a computationally efficient surrogate model for hurricane wind loss estimation is developed to conduct hurricane wind risk assessment.

This study adopts ANNs for developing the surrogate model of hurricane wind loss estimation. The feasibility of using a statistical model as a surrogate model for disaster loss estimation has been proven in other studies. Kim et al. (2016) proposed a log-scale regression model to predict the ratio of claim payout to building appraised value based on claim payout data of Hurricane Ike in Texas. The study used wind speed, building age, building floor area, and the appraised value of building as explanatory variables, and the model was able to explain 32% of the variance in the observed data. Gudipati and Cha (2019) utilized ANNs for estimating seismic structural response and damage stage. The study constructed the model by using data of numerical analysis results with structural design parameters and seismic intensity parameters as explanatory variables. The developed neural network model significantly reduces the required computation

time and is able to explain over 95% of the variance in data generated by the numerical model. Specifically, ANNs are widely utilized in the prediction of hurricane characteristics such as hurricane trajectories (Alemany et al., 2019; Kordmahalleh et al., 2016), storm surge height (Chen et al., 2012; Rao & Mandal, 2005; Bajo & Umgiesser, 2010), and precipitation (Orlandini & Morlini, 2000; Hong et al., 2004). Furthermore, ANNs have been used in hurricane loss assessment for decades. Sandri (1996) investigated the application of a feedforward multilayer neural network with a modified backpropagation learning algorithm to model hurricane wind-induced damage potential of non-engineered buildings. The study showed that the ANN model is capable of recognizing the relationship between observed windstorm damage information and building grades. Zhao et al. (2013) classified historical storm surge economic losses into four levels and built ANN models to forecast damage extent, and the prediction accuracy reached 80%. Pilkington and Mahmoud (2016) developed classification ANNs to predict the hurricane impact based on a proposed hurricane impact level ranking system by using predictors including affected population and location, central pressure, wind speed, storm surge and precipitation at each landfall.

The loss assessment process using the proposed ANN-based surrogate model is shown in Figure 8. The surrogate model takes the hurricane hazard and the vulnerability as inputs and regional aggregated loss as output. The hurricane loss is evaluated at the census tract level. The hurricane hazard includes the maximum surface wind speed (3-sec wind gust), and maximum rainfall intensity predicted at the centroid of the census tract, and the vulnerability includes building type composition, dollar exposure of each building type, and topographic information of the census tract. For the loss assessment, building and content losses are considered, where the building loss includes structure and interior losses.

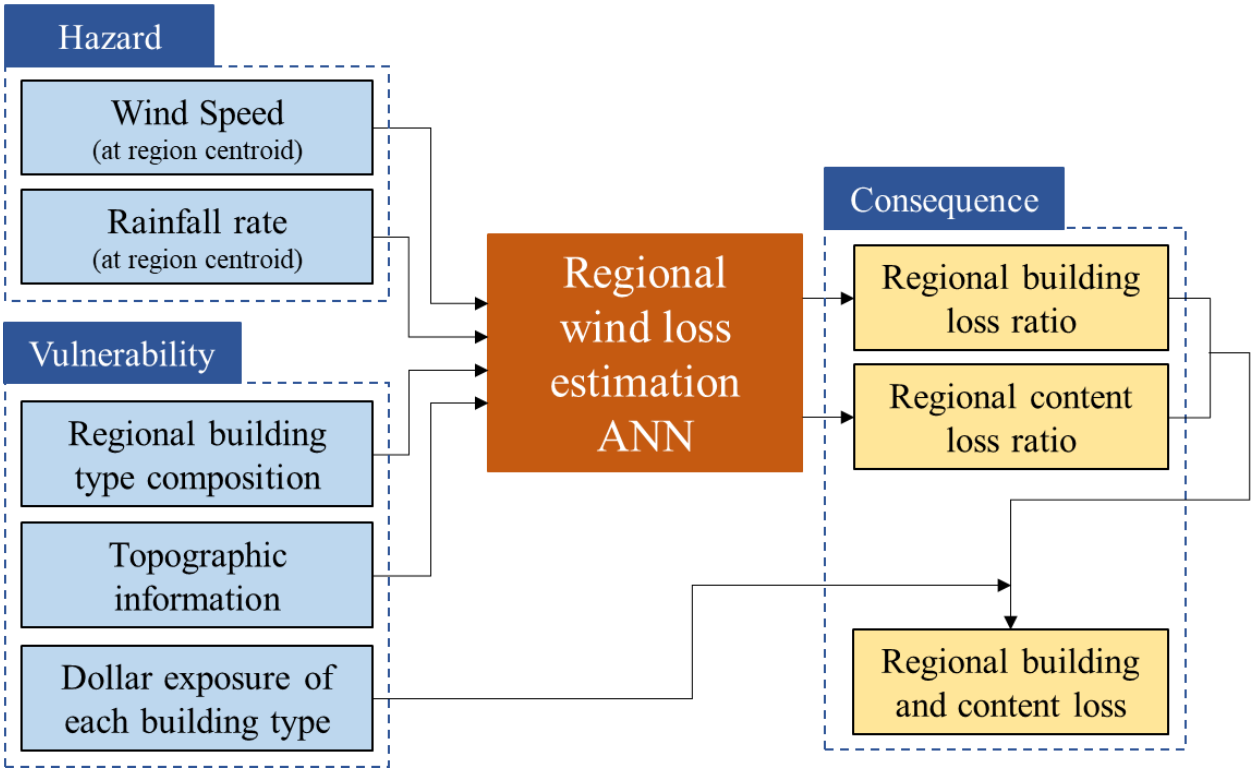

Figure 8. Hurricane wind loss assessment using the ANN-based surrogate model

5.2 Synthetic Data Generation and Model Development

The ANN-based surrogate model for hurricane wind loss assessment is developed using the loss data generated by the hurricane wind and rain ingress loss assessment model proposed by Pant and Cha (2018 and 2019). This model adopted existing methods (FEMA, 2013; Vickery et al., 2006; Gurley et al., 2005; Cope, 2004) to estimate hurricane losses of 32 prototypes of residential buildings, and it evaluates hurricane wind damage, wind-borne debris damage, and subsequent rain ingress damage, by considering the dependence between the component failure mechanisms. The mean loss of simulated hurricane events is evaluated using this model for hurricane-affected census tracts. The wind and rainfall intensities are recorded at the centroid of affected census tracts, and the computed aggregated losses are used to calculate the regional

building and content loss ratios. The synthetic data set has 35 independent variables, including recorded 3-second wind gust, maximum rain rate, surface roughness length, and 32 building type ratios, and has two dependent variables, including building and content loss ratios.

The model development process is shown in Figure 9. To generate the dataset for training the model, one thousand synthetic landfalling hurricanes are generated, and correspondingly, 57,460 rows of data are generated for constructing the surrogate wind loss model. To train the surrogate model, the generated synthetic data are split into the train, and test datasets and cross-validation is conducted on the training data to find the most suitable network configuration. The split ratio of 70% to 30% is used for training to test datasets. Five-fold cross-validation is conducted within the training data to evaluate the various network configurations, and network attributes are selected based on the cross-validation performance. The tested network configurations are shown in Table 8. Based on the cross-validation performance, the Levenberg-Marquardt back-propagation is adopted as a network training algorithm, and the hyperbolic tangent sigmoid function is adopted as an activation function in hidden neurons. Besides network input and output layers, the network structure of the candidate model is selected to have three hidden layers and five hidden neurons per layer. The square roots of the regional building and content loss ratio are chosen as the dependent variables for training the model. The candidate model with the selected configuration is then used for prediction to check if the performance on test data is acceptable, and the result of prediction versus target values on the original scale is shown in Figure 10. The test R-squared value is 0.96, and the test root mean square error (RMSE) is 0.04.

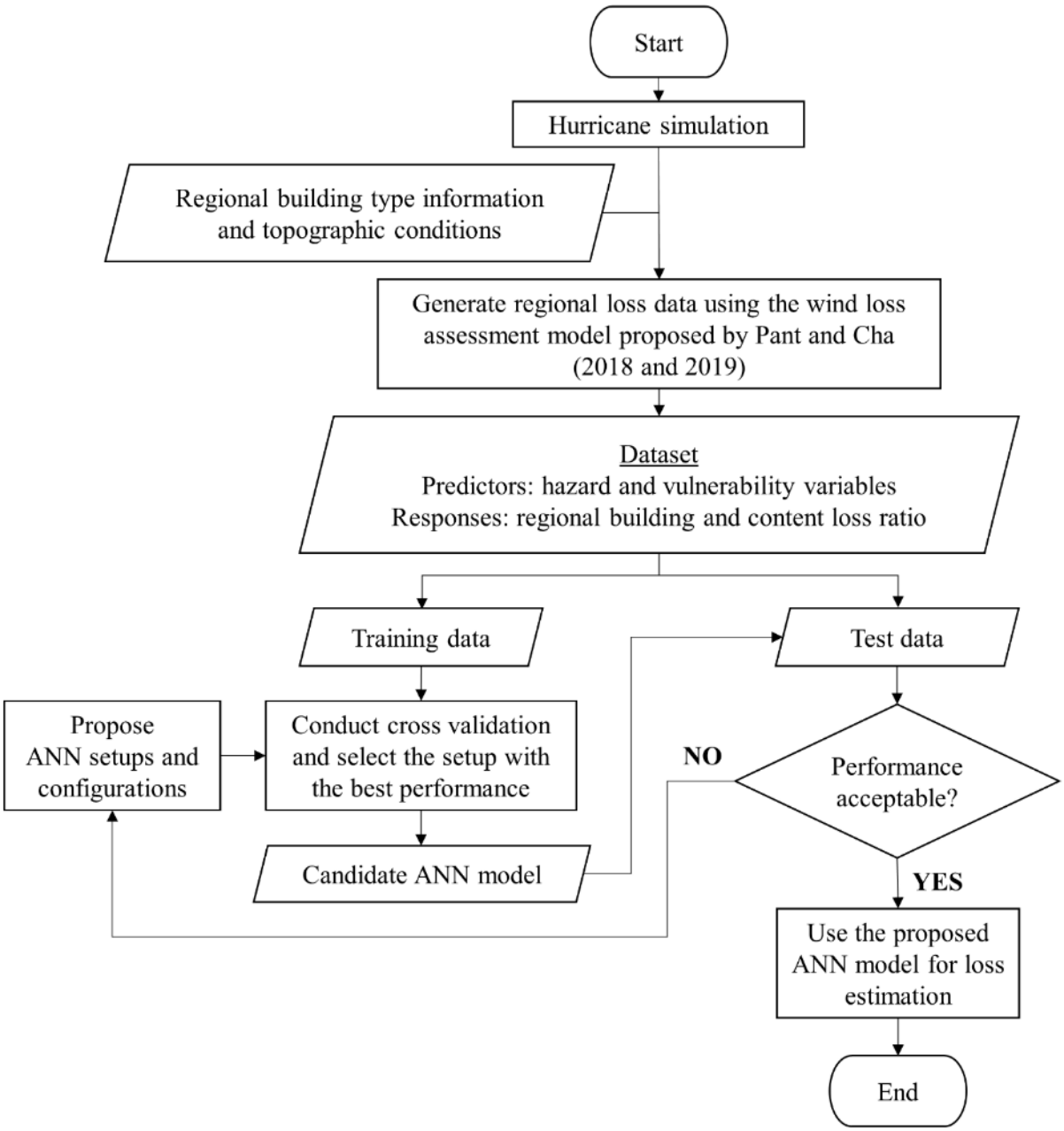

Figure 9. Flowchart of wind loss estimation surrogate model development

Table 8. Investigated Network setups for the wind loss prediction ANN

Network Attributes	Tested Setups
Training algorithm	1) Levenberg-Marquardt backpropagation 2) Resilient backpropagation 3) Gradient descent with momentum and adaptive learning rate backpropagation 4) Scaled conjugate gradient backpropagation
Transfer function in hidden layer	1) Hyperbolic tangent sigmoid function 2) Log-sigmoid transfer function 3) Normalized radial basis transfer function 4) Positive linear transfer function (ReLU) 5) Elliot symmetric sigmoid transfer function
Number of hidden layers	1 or 3 hidden layers
Number of hidden nodes	5, 10 or 15 hidden nodes
Output transformation	1) Response = loss ratio 2) Response = (loss ratio)$^{0.5}$ 3) Response = (loss ratio)$^{0.25}$

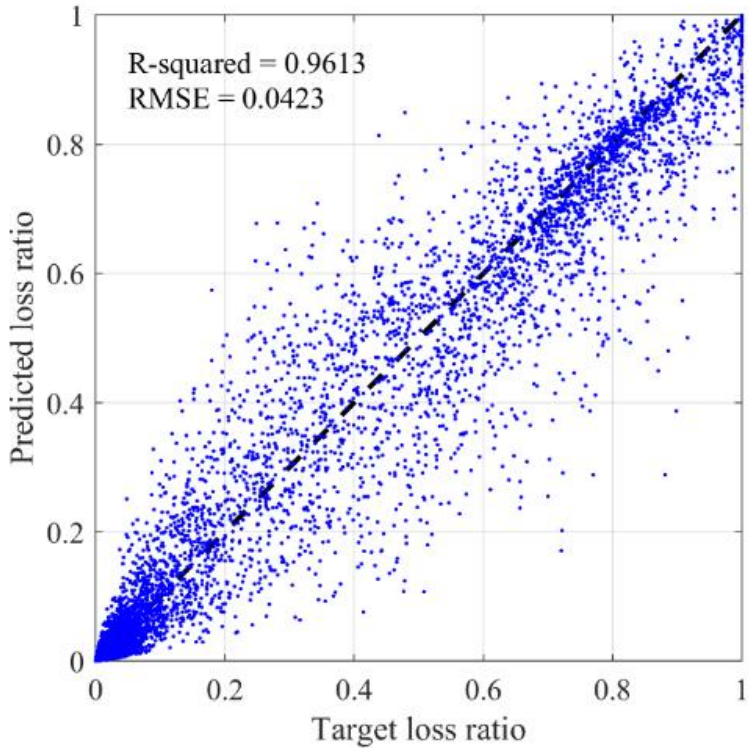

Figure 10. Test prediction of the ANN-based surrogate wind loss model

5.3 Model validation with HAZUS prediction

The proposed ANN-based surrogate wind loss model is further validated by using the loss data estimated by HAZUS-MH. The proposed wind loss model is used to estimate the losses from 328 synthetic hurricane scenarios that were generated in the preliminary study. In the preliminary study, the synthetic hurricanes were simulated at landfall, and the associated losses were estimated using HAZUS-MH. The recorded estimated property losses, including building and content losses, serve as the target values for the validation. The comparison of the wind loss estimations by the proposed model and HAZUS-MH is shown in Figure 11. A significant correlation between HAZUS estimation and surrogate model prediction is observed in the comparison result, while the surrogate model has a tendency of overestimating the loss for low-wind-loss cases. Therefore, it is concluded that the proposed surrogate model is sufficient to predict the change in the wind risk under climate change.

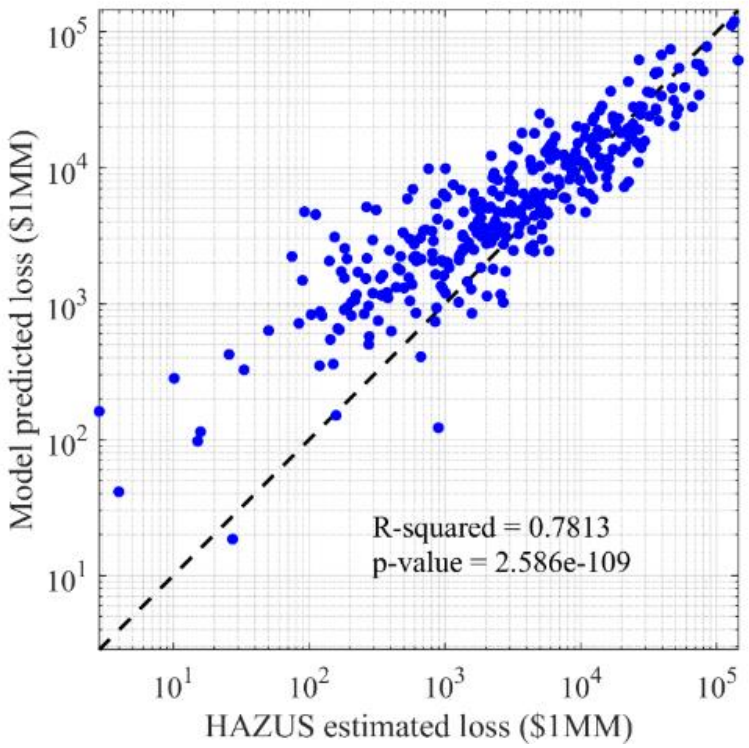

Figure 11. Comparison of the wind loss estimations by the proposed ANN-based surrogate model and HAZUS-MH

CHAPTER 6: DEVELOPMENT OF HURRICANE FLOOD LOSS MODEL

To efficiently assess the hurricane freshwater flood risk under climate change, the framework for a four-step statistical model that can be used as a surrogate loss assessment model is established, as shown in Figure 12. To assess the climate-dependent hurricane freshwater flood risk, hurricane storm tracks are simulated first with considering nonstationary hurricane parameters predicted by global sea surface temperatures (SST) as introduced in section 0. Then, the freshwater flood loss is estimated by the four-step loss assessment model. In the mode, first, an operational rainfall prediction model with calibrated accumulated total rainfall is used to simulate the rainfall intensity of simulated hurricanes. Secondly, the maximum stream stage increment is predicted at United States Geological Survey (USGS) stream gauge sites by using the rainfall intensity and topographic conditions. Thirdly, maximum flood depths during a hurricane event at centroids of census tracts affected by simulated hurricanes are predicted by using stream stage increment and site information of their surrounding stream gauge sites. Finally, the flood loss is determined using operational stage-damage curves at each census tract and aggregated throughout the hurricane-affected region to obtain the estimated hurricane flood loss. Details of the model development are introduced in this section.

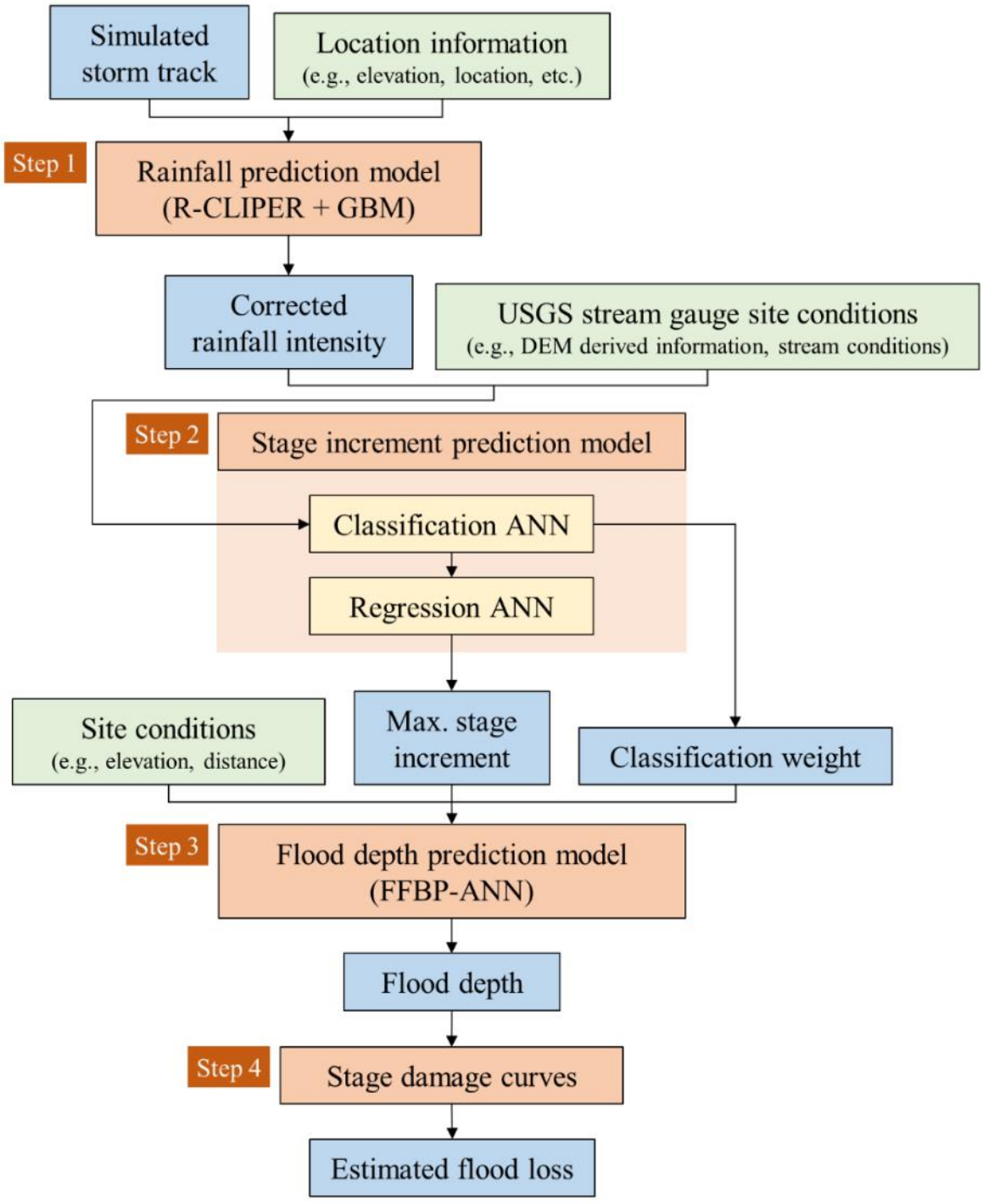

Figure 12. Schematic view of the four-step hurricane freshwater flood loss assessment model

6.1 Hurricane Rainfall Prediction

6.1.1 Operational rainfall evaluation model

This study develops a rainfall prediction model based upon the operational satellite-based Tropical Cyclone (TC) Rainfall Climatology and Persistence (R-CLIPER) Model developed by Marks Jr & DeMaria (2003) to simulate hurricane rainfall rate and accumulated rainfall. The R-CLIPER model was developed by using global satellite-based TC rainfall observation from the NASA Tropical Rain Measurement Mission (TRMM) satellite, and the detailed description and model development are provided in Lonfat et al. (2004) and Tuleya et al. (2007). Tuleya et al. (2007) assumed the rainfall is symmetrical about the storm center, which neglects the potential effect from vertical wind shear, local topography, interaction of the boundary layer with the surface while storm moving, interaction with baroclinic features (Lonfat et al., 2007). Lonfat et al. (2007) then developed a parametric model that generates a rainfall field composed of a rainfall field generated by the R-CLIPER model and the rainfall field associated with topography and vertical shear-generated asymmetry. For simplicity, this study adopts the symmetric assumption, and the operational R-CLIPER model is used for rainfall rate simulation. In Tuleya et al. (2007), the rainfall rate is calculated as:

$$RR(r, V_{max}) = \begin{cases} T_0 + (T_m - T_0) \cdot \left(\frac{r}{r_m}\right) & r < r_m \\ T_m \cdot exp\left(-\frac{r - r_m}{r_e}\right) & r > r_m \end{cases}, \quad (7)$$

where r = radius to the location of interest; V_{max} = the maximum surface wind speed; T_0 is the rain rate at r = 0; T_m is the maximum rain rate at $r = r_m$; r_m = radius of maximum rain rate; and r_e = radial extent of the storm rainfall. Moreover, the four parameters (T_0, T_m, r_m, r_e) in Eq. (7) were

derived from the least-squares fit of TRMM radial profile as a linear function of maximum wind speed V_{max}:

$$\begin{aligned} T_0 &= a_1 + b_1 U \\ T_m &= a_2 + b_2 U \\ r_m &= a_3 + b_3 U' \\ r_e &= a_4 + b_4 U \end{aligned} \tag{8}$$

where U is the normalized wind speed calculated as

$$U = 1 + \frac{V_{max} - 35}{35}, \tag{9}$$

and the maximum surface wind speed V_{max} here is given in knots. From Tuleya et al. (2007), the regression coefficients $a_1 \sim a_4$ are –1.10 in./day, –1.60 in./day, 64.5 km and 150 km, respectively, and $b_1 \sim b_4$ are 3.96 in./day, 4.80 in./day, –13.0 km and –16.0 km, respectively. The rainfall rate is determined for simulated six-hour-interval storm tracks. The accumulated rainfall amount and maximum rain rate are recorded at locations of interest (i.e., USGS stream gauge).

6.1.2 Rainfall intensity calibration using ensemble regression

A correction model is established to calibrate the R-CLIPER predicted accumulated rainfall. As pointed out in (Mudd et al., 2017), although the R-CLIPER model can predict the mean rainfall rate quite well, it is not able to capture extreme rainfall intensities. Tuleya et al. (2007) also stated that the prediction of the R-CLIPER model could be enhanced if the rainfall asymmetry is considered by incorporating environmental flow in the rainfall model. However, the main purpose of this study is not to predict hurricane rainfall intensity. The rainfall intensity is an intermediate variable in predicting the hurricane flood depth. Therefore, the following prediction will not be affected as long as the R-CLIPER predicted rainfall captures the rainfall tendency in

spatial distribution, and the simulated rainfall is used for the model development rather than using actual rainfall observation.

To make sure the prediction follows the same spatial tendency as actual rainfall, the relationship between the R-CLIPER predicted rainfall and actual rainfall observation is investigated. Historical hurricane rainfall observations of Hurricane Hermine, Hurricane Matthew, and Hurricane Harvey are collected from the National Weather Service (NWS) Advanced Hydrologic Prediction Service (AHPS). The actual accumulated rainfall is calculated by summing daily precipitation during the hurricane-affected period at locations of USGS stream gauges that are within 500 km radial distance from the storm center along the storm track. On the other hand, using the historical hurricane storm track information along with the R-CLIPER model, the synthetic accumulated rainfall is predicted at those USGS gauge locations for comparison. For these three hurricanes, there are 4087 synthetic accumulated rainfall samples, and corresponding actual accumulated rainfall observations at affected USGS stream gauge sites are calculated using the average of the three closest NWS observations. To predict actual accumulated rainfall amount, besides the R-CLIPER synthetic rainfall, the location (i.e., latitude and longitude), elevation, and distance to the coast of affected USGS stream gauge sites, are also used as predictors in this regression task. The actual accumulated rainfall is predicted by the five predictors by applying the least-squares-based gradient boosting. By virtue of the flexibility of gradient boosting, it is commonly utilized in hydrology-related modeling (Maloney et al., 2012; Erdal & Karakurt, 2013; Tisseuil et al., 2010; Kusiak et al., 2013). Boosting in statistical modeling is to combine a series of weak learners to be strong learners. A weak learner is a decision tree that uses binary split to predict within the feature space, and the tree is constructed by choosing the split to minimize the loss function. The gradient boosting adds new tree models upon the original sequence of trees one

by one and using gradient descent to minimize the loss while adding a new tree. For the regression problem in this study, the squared-error loss function is used.

To ensure the prediction power and avoid overfitting, model tuning is conducted to determine the hyperparameters, i.e., the parameters of the algorithm, of the gradient boosting. With the flexibility of the additive model, the GBM will overfit the training dataset unless some constraints are added. The hyperparameters considered for tuning the ensemble model are the maximum number of splits, learning rate, and the number of trees. A search grid is built with maximum number of splits = {1, 2, 4, 8, 16, 32, 64, 128, 256, 512}, learning rate = {0.025, 0.05, 0.1, 0.25, 0.5, 1}, and number of trees from 1 to 150. Five-fold cross-validation mean square error (MSE) is used to examine the model performance and for selecting the hyperparameters. In 5-folds cross-validation, the observed data is divided into 5 folds. In the K^{th} iteration, the K^{th} fold of data is held as the test data, and the remaining K-1 folds of data are used to train the model. The average of the test error of each holdout test data, i.e., the cross-validation error, is used to unbiasedly evaluate the model performance and for the further model selection. Based on the minimum cross-validation error, the selected maximum number of splits is 128, the learning rate is 0.01, and the number of trees is 200. The cross-validation holdout prediction is shown in Figure 13. The cross-validation root mean square error (RMSE) is 1.28 (in), and R-squared is 0.955. With the corrected rainfall prediction model, the predicted maximum rainfall rate and corrected accumulated rainfall are then used as the input variables for the stage increment model.

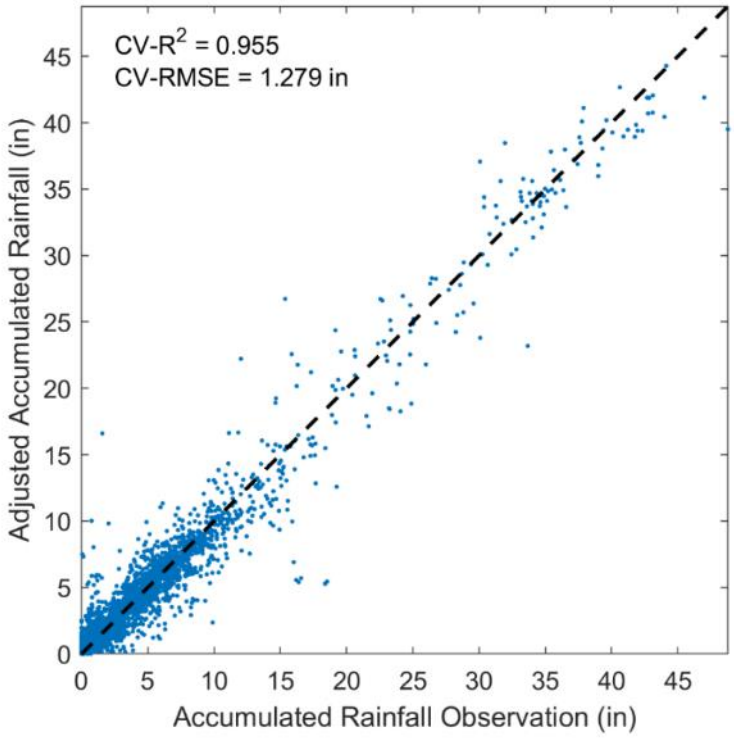

Figure 13. Actual accumulated rainfall vs. out-of-fold prediction of the correction model

6.2 Hurricane Rainfall-Induced River Stage Increment Prediction

6.2.1 Construction of dataset for development of stage increment prediction model

The stream condition is a key parameter to investigate riverine flooding. Thus, this study proposes a model for predicting the maximum stage increment of USGS stream gauges by using the associated site conditions and predicted rainfall intensity. To train the stage increment prediction model, a dataset is constructed using the observations from 42 U.S. landfalling hurricanes. The data collected at 2423 USGS stream gauge sites distributed across the study region, i.e., eight southeastern U.S. coastal states from Texas to North Carolina, are used in this study. Since the model is for stage increment attributed to rainfall, the data of the stage increment caused by storm surges are excluded. The National Storm Surge Hazard Maps developed by Zachry et al.

(2015) is used to identify the USGS stream gauges that are potentially affected by the storm surge. To encompass all potentially affected sites, the category 5 hurricane is used to delineate the storm surge hazard map. The data samples located within the storm surge affected area or have zero stage increment during the event are removed from the dataset. Accordingly, there are 1584 samples for training the stage increment prediction model. In the dataset, each observation represents an affected USGS stream gauge site that includes 13 site conditions as predictors and a logarithmic ratio of maximum stream stage increment to stream depth as the response. The affected USGS stream gauge sites are identified by a 500 km radial distance from the storm center along the historical hurricane storm track (IBTrACS v04r00) developed by Knapp et al. (2010).

The affected USGS stream gauge site condition variables include the rainfall intensity at the site location and the site topographic and geographic information. For the rainfall intensity, accumulated rainfall and maximum hourly rainfall rate predicted by the rainfall prediction model developed in the previous section are used. Other stream gauge site conditions including drainage area, elevation, curvature, slope, topography wetness index (TWI), surface roughness, stream discharge, and stream width under peak flow condition, longitude, latitude, and distance to the coast are also considered. Topographic variables (drainage area, elevation, curvature, and slope) are calculated based on geographic location and digital elevation model (DEM). The DEM adopted in this study is Shuttle Radar Topography Mission (SRTM) 90m Digital Elevation Database v4.1 developed by Jarvis et al. (2008), which is a 90-m spatial resolution DEM processed based on data from the NASA Shuttle Radar Topography Mission. The TWI is one of the popular factors used in flood risk assessment (Tehrany et al., 2013; Wang et al., 2015; Pourali et al., 2016). The TWI of a stream gauge site is generally defined as

$$\text{TWI} = \ln\left(\frac{a}{\tan(\beta)}\right), \tag{10}$$

where a = the upstream contributing area of the stream gauge site, and β = local slope given in radius. A high TWI value implies a large upstream contributing area and gentle local slope and hence has a higher potential for runoff (Wolock and McCabe Jr, 1995). The floodplain surface roughness is obtained from HAZUS-MH, which was originally derived from the national land-use database. It depends on the height and density of vegetation and building and obstructions upstream to the location of interest (FEMA, 2018). The stream information, including stream discharge and stream width under bankfull condition (mean annual peak flow), is obtained from Andreadis et al. (2013), and these variables provide a basic flow condition. The distance to the coast is calculated as the minimum distance from a stream gauge site to the coastline.

For the calculation of the response variable, instead of directly predicting the stage increment, a transformation of the response variable, a normalized stream stage increment, is used, which is expressed as

$$y = \ln\left(\frac{SI}{SD}\right), \tag{11}$$

where y is the model response variable, SI is the maximum stage increment in an event, and SD is the stream depth under mean peak flow condition. The maximum stream stage increment SI is taken as the difference between daily maximum stage at the beginning of the event and the daily maximum stage during the event. The SD is obtained from Andreadis et al. (2013). To derive the maximum stream stage increment, the stream gauge height variation during the hurricane-affected period is extracted from the USGS Water Data for the Nation (USGS, 2019b), and the hurricane-

affected period is obtained from the Tropical Cyclone Rainfall Data of National Oceanic and Atmospheric Administration (NOAA, 2019).

6.2.2 Classification and regression ANN models

To predict the maximum stage increment, a two-step ANN model is developed: the first is a classification ANN to label the stage increment samples to higher and lower levels, and the second is regression ANNs to establish a relationship between predictor and response variables at each level. The developed classification and regression models are combined to predict stage increment. The stage increment data are heterogeneous since observations are collected from different hurricanes, watersheds and have quite distinctive local topography and flow conditions, and hence the prediction performance is restricted by using a single regression model. It is found from a preliminary study that the prediction accuracy is improved if a sample can be categorized to a certain range, and the regression model is built corresponding to the range. In this study, a two-step ANN model comprising a classification model and regression models associated with the number of designations is developed to improve the prediction performance of the stage increment prediction model. A similar approach is found in (Contento et al., 2019) for modeling storm surge. Three classification options are considered in this study: classifications with 2, 3, and 4 classes. Data quantiles are used as class boundaries to divide the response variable into different classes. For instance, for four-class classification, 0.25, 0.5, and 0.75 quantiles are used to distinguish the four classes of response and create a balanced dataset. The different scales of stage increment ratio are separated and labeled, and a regression ANN is trained for each class.

For determining the most suitable classification and regression models for this problem, combinations of hyperparameters and ANN setups are investigated, including training algorithm, transfer function, number of hidden layers, and number of hidden nodes. The investigated network

setups are listed in Table 9. The choice of training algorithm decides how the network optimizes its prediction performance, and the transfer function affects the behavior between the input and output of each hidden node. A hidden node is a computational unit that combines input and generates responses, and a hidden layer contains one or more several hidden nodes. The network architecture includes the number of hidden layers and the number of hidden nodes in each hidden layer. To evaluate the model performance under these ANN setups, 5-fold cross-validation is conducted. The cross-validation test error rate, sensitivity, and specificity are used to find the best setting for the classification ANN, and the cross-validation MSE and R-squared are used to find the best setting for the regression ANN. The classification ANN predicts posterior probabilities that a sample is part of a class. The final classification is determined by the highest posterior probability. During this process, a variable, classification weight, indicting the certainty of classification is generated. For each sample, if the highest posterior probability of a class is much higher than the second-highest one, then the sample is regarded as possessing higher classification certainty. Comparing to other samples, it is assigned a higher classification weight. The weight is calculated as

$$w_{i,c} = \frac{FPP_i - SPP_i}{\sum_{\forall i \in c} w_i}, \tag{12}$$

where w_i is the classification weight for the ith sample in class c, the FPP_i and the SPP_i are the highest and the second-highest posterior probability predicted by the classification ANN for the ith sample in class c. The classification weights are used for actual regression model training after the determination of the network setup, and it is also used in the flood depth prediction model. The selected classification and regression ANN setups are shown in Table 10 and Table 11, respectively. It is obvious that the regression performance is better when there are more separations

in the dataset, but consequently, the classification performance is worse. While the data are separated into more classes, it is harder for the classifier to distinguish samples based on the predictors used in this problem. The final selection of the number of classes is based on the combined model prediction performance.

Table 9. Investigated network setups for the stage increment prediction ANN

Network Attributes	Tested Setups for Classification ANN	Tested Setups for Regression ANN
Training algorithm	1) Levenberg-Marquardt backpropagation 2) Resilient backpropagation 3) Bayesian regularization backpropagation	1) Levenberg-Marquardt backpropagation 2) Resilient backpropagation
Transfer function in hidden layer	1) Hyperbolic tangent sigmoid function 2) Log-sigmoid transfer function 3) Symmetric saturating linear function 4) Positive linear transfer function (ReLU)	1) Hyperbolic tangent sigmoid function 2) Symmetric saturating linear function 3) Positive linear transfer function (ReLU)
Transfer function in output layer	Log-sigmoid transfer function	Linear transfer function
Number of hidden layers	1 or 2 hidden layers	2, 3, 5 hidden layers
Number of hidden nodes	10, 20, 30 hidden nodes	5, 10, 20 hidden nodes

Table 10. Selected setups and test performance of the classification ANN

Number of Response classes	Network setup	Selected setup	CV-error rate	Sensitivity for the last class	Specificity for the last class
Two	Training algorithm	Levenberg-Marquardt	0.2820	0.6763	0.7634
	Transfer function	hyperbolic tangent sigmoid function			
	Number of hidden layers	1			
	Number of hidden nodes	10			
Three	Training algorithm	Levenberg-Marquardt	0.4662	0.6511	0.7831
	Transfer function	hyperbolic tangent sigmoid function			
	Number of hidden layers	2			
	Number of hidden nodes	10			
Four	Training algorithm	Levenberg-Marquardt	0.5750	0.6491	0.7641
	Transfer function	Positive linear transfer function			
	Number of hidden layers	1			
	Number of hidden nodes	30			

Table 11. Selected setups and performance of the regression ANN

Number of response classes	Network setup	Selected setup	Cross-Validation test MSE (ft^2)	Cross-Validation R^2
Two	Training algorithm	Levenberg-Marquardt	3.835	0.529
	Transfer function	Symmetric saturating linear function		
	Number of hidden layers	2		
	Number of hidden nodes	10		
Three	Training algorithm	Levenberg-Marquardt	3.615	0.701
	Transfer function	Positive linear transfer function		
	Number of hidden layers	1		
	Number of hidden nodes	10		
Four	Training algorithm	Levenberg-Marquardt	3.094	0.779
	Transfer function	Symmetric saturating linear function		
	Number of hidden layers	2		
	Number of hidden nodes	10		

The number of class division is determined based on the accuracy of the model prediction result. The 5-fold cross-validation MSE of the combined models with selected ANN model setups is used for this purpose. The ensemble technique is applied in the development of the stage increment model to reduce the variability in the model prediction attributed to different model initialization. The advantage of the ANN ensemble can be found in Dietterich (2000) and Zhou et al. (2002). The number of ANN model ensembles is set as 100 for both classification and regression ANNs. For regression ANN, the prediction is stabilized with the use of the average of predicted values. For classification ANN, the predicted posterior probabilities for classification are averaged and hence lead to lower classification weight for ambiguous samples in the boundary. The combined model prediction performances are shown in Table 12. The model performance is significantly improved by considering the classification weight. It is observed that the correctness of classification dominates the combined model prediction performance, so the performance of the combined model is better when the smaller number of classes is chosen.

Table 12. Stage increment prediction model performance

Number of classes	Non-weighted Prediction		Weighted Prediction	
	CV-RMSE (ft)	CV-R-squared	CV-RMSE (ft)	CV-R-squared
Two	2.956	0.162	0.247	0.235
Three	3.082	0.121	0.273	0.228
Four	3.416	0.146	0.390	0.228

6.3 Flood Depth Prediction

A model is developed to predict the flood depth at the location of interest by using the maximum stage increment of the surrounding USGS stream gauge sites. Historical high-water mark (HWM) data of Hurricane Matthew and Hurricane Harvey assessed from USGS (2019a) are used as the flood depth observations to develop the model. Variables used to predict the HWM, besides the maximum stage increment, include the USGS stream gauge site elevation, distance from the USGS stream gauge site to the HWM, and the classification weight generated by the stage increment prediction model. For each HWM, the surrounding 3 USGS stream gauge sites are identified, and the corresponding constructed datasets have 12 predictors (4 per site). For each valid sample, the HWM observation needs to have 3 USGS sites within 50 km radial distance enclosing the HWM. Under this constraint, there are 218 valid samples for training the model. Similar to the stage increment prediction modeling, to exclude the influence of storm surge during hurricane events, the HWM observations in the coastal region affected by storm surges are removed. Note that the HWM of the final data might result from fluvial or pluvial flooding or the combined effect. Furthermore, ground saturation and water table are not explicitly considered in this model since the temporal resolution of the model was not sufficient to capture their impact.

The most suitable network model for flood depth prediction is selected by evaluating the network performance of different network configurations as well as variables used. The FFBP-ANN with Bayesian regularization backpropagation training algorithm is selected in this study. Based on the preliminary study, the Bayesian regularization backpropagation algorithm outperforms other training algorithms tested in Table 9 in this regression modeling. Unlike the usual training algorithm, which tries to minimize the sum of squared error as the loss function, the Bayesian regularization applies Bayesian inference for minimizing the cost function and hence

introducing a sum of squared network weights in the minimizer. This sum of squared network weights term regularizes network development and avoids overfitting. Accordingly, in the model training process, the training data does not need to be further divided into training and validation sets to avoid overfitting. The detail of this algorithm is provided in MacKay (1992) and Foresee & Hagan (1997). In this study, 65% of observed data are used for training, and the remaining 35% of data are used for testing. Since the training algorithm is determined, the network architecture and variable used are the remaining model setups for selecting the most suitable ANN model. The final model selection is based on the best model performance on test data. For the network architecture, 10 and 20 hidden nodes in either 1 or 2 hidden layers are tested. The transfer function adopted in the hidden layer is the hyperbolic tangent sigmoid function.

The ensemble prediction technique is also utilized for flood depth prediction to enhance the model performance, and bootstrap sampling is adopted to generate a dataset for each individual model. To train an individual model, data are sampled with replacement from the 218 observations with the probability based on the certainty of HWM observation. One-and-a-half times the original sample size (i.e., 327 samples) are bootstrap sampled to develop each individual model. In the USGS HWM observation dataset, each observation was associated with a quality evaluation which is assigned with an observation weight (as shown in Table 13). Then in bootstrap sampling, the probability of each observation being sampled is calculated as its observation weight divided by the sum of observation weights of all samples. The process is repeated to develop one hundred individual models, and the model prediction is the ensemble average of all models. The test prediction is shown in Figure 14. It can be found that the model captures the trend in flood depth prediction but have a tendency of overestimating the flood depth for low flood depth cases. To reduce the effect of overestimation, instead of an ensemble average of all models, the predictions

from individual models are sorted, and the lowest ten percent of predicted values are used to compute the ensemble prediction.

Table 13. USGS HWM observation quality and assigned observation weight

Quality appraisal	Uncertainty	Observation weight
Excellent	± 0.05 ft	5
Good	± 0.10 ft	4
Fair	± 0.20 ft	3
Poor	± 0.40 ft	2
Very Poor	> 0.40 ft	1
Unknown	-	1

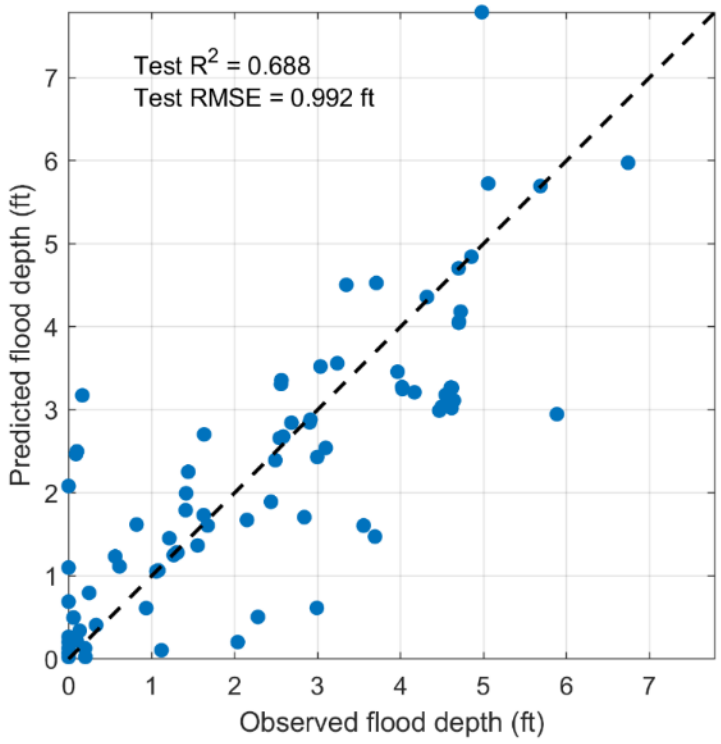

Figure 14. Test prediction of flood depth prediction model

6.4 Flood Loss Estimation

6.4.1 Stage damage curves and loss aggregation

The aggregated flood loss is estimated by using predicted flood depth at the census tract level. In a simulated hurricane event, census tracts are identified as affected by the hurricanes when their centroid fell into the affected region, which is determined by delineating the boundary of all affected USGS gauge sites. Using the flood depth prediction model, hurricane rainfall-induced flood depths are predicted at the centroids of the census tracts affected by the simulated hurricane event. Then, the predicted flood depth is used to estimate the total loss for the event with the stage damage curves. The aggregated loss of an event is calculated as

$$aggregated\ loss = \sum_{j=1}^{Nt} \sum_{i=1}^{Nc} f_{SD,i}\left(d_{f,j}\right) \cdot D_{ij}, \quad (13)$$

where $f_{SD,i}$ is the stage damage function for ith residential subcategory, Nc is the total number of residential subcategories which is 64 in this study, $d_{f,j}$ is the predicted flood depth at the centroid of jth census tract, D_{ij} is the total dollar exposure, including the structure and content exposure of ith residential subcategory in jth census tract, and Nt is the total number of census tracts affected by the hurricane event. The stage damage curves and the exposure information are obtained from Hazus-MH (FEMA, 2009). A total of 64 stage damage curves developed by the Federal Insurance Administration (FIA) and the U.S. Army Corps of Engineers (USACE) for both structure and content damage is used (Scawthorn et al., 2006). The categorization of stage damage curves adopted from HAZUS is listed in Table 14. The percentage of each residential subcategory is calculated at the census tract level by using a weighted average of the dollar exposure of census blocks.

Table 14. Categorization of stage damage curves in HAZUS-MH

Occupancy type	Variations
Single-family house	• Split level • With or without a basement • One story • Two floors • Three or more floors
Mobile house	• With or without a basement
Apartment unit	• With or without a basement • 1 to 2 stories • 3 to 4 stories • 5 or more stories
Average hotel/motel Average institutional dormitory Nursing Home	• With or without a basement • Low rise • Mid rise • High rise

6.4.2 Validation of loss estimation model using NFIP significant loss events

The four-step flood loss estimation model is validated with flood insurance payout data of historical hurricanes provided by FEMA (2019) as the actual loss data. FEMA lists significant flood events that have 1,500 paid losses paid by the National Flood Insurance Program (NFIP). Thirty-three hurricane events from the list are used for model validation (from 1979 Hurricane Frederic to 2017 Hurricane Harvey). For the historical hurricane events, storm track data are retrieved from IBTrACS v04r00, and corresponding aggregated losses of each event are predicted using the models developed in this study. The result is shown in Figure 15.

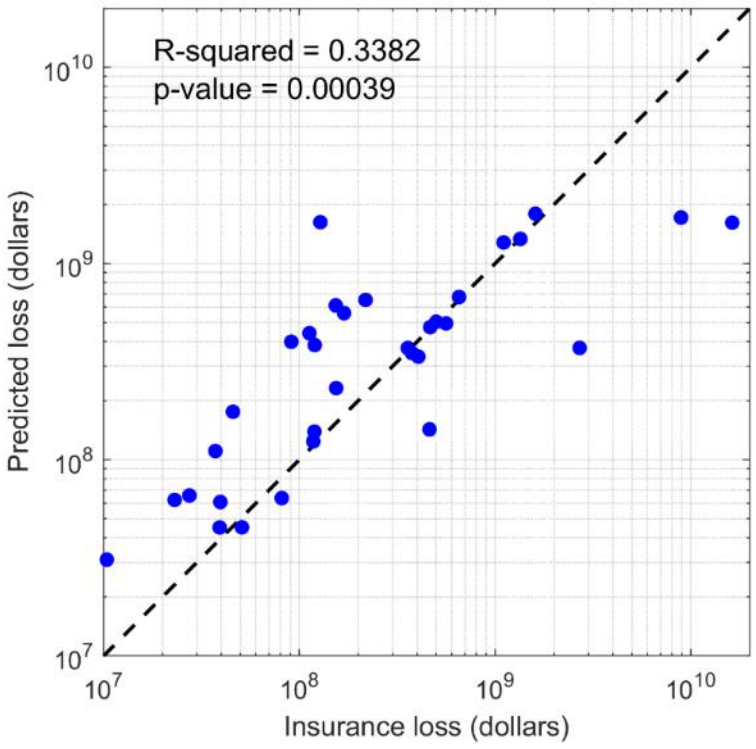

Figure 15. Predicted historical hurricane flood loss vs. NFIP claim payout

It is observed that the model prediction is proportional to the actual loss. The prediction is correlated with actual loss at a significance level of 0.01 (p-value = 0.00039). The prediction error results from several known reasons. Firstly, underestimation of losses may be observed for the events which have a significant portion of loss due to storm surge since the NFIP paid loss included the loss caused by both storm surge and freshwater flooding. On the other hand, losses can be overestimated as well. One main reason for overestimation is the overestimation in low flood depth, which can be seen in Figure 14. Based on the adopted stage-damage curves, a large portion of the loss is attributed to the first few feet of flood depth. Therefore, as the flood depth is overestimated, so is the estimated loss. Another possible reason for the overestimation is the discrepancy between actual flood loss and flood loss assessed by NFIP (Botts et al., 2014). Losses

are possible in some communities located outside of the NFIP 100-year floodplain, which would not have been included in the NFIP claim payout since they are not required to carry flood insurance. Furthermore, the assumption of constant dollar exposure causes prediction errors as well. For simplicity, this study adopted the default building inventory used in Hazus-MH to calculate the base exposure amount for all historical events, which might overestimate the actual exposure for earlier events and underestimate the exposure for later events. Since the model prediction captures the overall loss trend but not the actual loss, the percentage increase in loss is used to investigate the future change in flood loss under climate change scenarios.

CHAPTER 7: HURRICANE RISK ASSESSMENT RESULTS

7.1 Hurricane simulation

Given the efficiency of the developed surrogate model for hurricane wind and freshwater loss assessment, the number of hurricane scenarios in wind and freshwater flood risk assessment is not critically restricted by the computation power. Comparing to the detailed loss estimation by HAZUS-MH, the saved time can be used to generate more samples. Synthetic hurricanes are simulated for climate scenarios listed in Table 15 to investigate the climate change impact on hurricane wind and freshwater flood risks. Under a stratified sampling framework, hurricanes are simulated at each of five sections of coastline, as shown in Figure 3. The loss of each region under each scenario is estimated by aggregating losses resulted from hurricanes simulated across all regions. For synthetic hurricane events simulated on each region, Latin hypercube sampling is adopted to sample hurricane parameters to reduce the required number of simulations, and hurricanes are simulated for a 10-year span to reduce the chance of non-occurrence under a limited number of simulations. As the baseline for comparison, a total of 20,000 years of hurricane events is simulated for scenario 1, the current climate conditions, which characterizing the average of hurricane conditions between 1986 to 2005. For other climate change scenarios in Table 15, a total of 10,000 years of events are simulated, and the required number of simulations is verified in the convergence analysis in a preliminary study. As a result, the numbers of landfalling hurricanes simulated for scenario 1 and the rest are about 32,000 and 16,000, respectively.

Table 15. Climate scenarios for hurricane wind and freshwater flood risk investigation

Scenario	Description
1	Current climate condition (1986-2005)
2	2020-2030 under RCP8.5 lower-bound
3	2090-2100 under RCP8.5 lower-bound
4	2020-2030 under RCP8.5 mean
5	2090-2100 under RCP8.5 mean
6	2020-2030 under RCP8.5 upper-bound
7	2090-2100 under RCP8.5 upper-bound

Simulated hurricane attributes are summarized in Table 16 to Table 18. The total number of hurricanes simulated for each study region is shown in Table 16, where NH denotes non-major hurricanes and MH denotes major hurricanes. Table 17 shows the ratio of the number of major (category 3 and above) hurricanes to the number of all simulated hurricanes for each scenario. The change in ratios of high-intensity hurricanes is different in regions. Under current climate conditions, region 2 (LA+MS+AL) has the highest ratio of high-intensity hurricanes, while under changing climate conditions, the ratio is surpassed by region 4 (GA+SC+NC). In the most extreme case (scenario 7), upper bound projection of RCP8.5 scenario in the year 2090 to 2100, it is predicted that almost 60% of the landfalling hurricane along the coastline of region 4 will be high-intensity hurricanes. Table 18 shows the mean values of the changes in central pressure difference, maximum sustained wind speed, maximum accumulated rainfall, and maximum rain rate under climate scenario 4 and scenario 5 relative to current climate conditions. The histograms of simulated hurricane CPD and maximum sustained wind speed at landfall for current climate conditions, climate change scenario 4 and scenario 5 are shown in Figure 16. Since the predicted change in nonstationary hurricane parameters, MCPD, is applied to all study regions, the change in hurricane attributes related to the hurricane intensity is relatively uniform across study regions. The maximum accumulated rainfall not only depends on hurricane intensity but also depends on

local topography, watershed, hurricane tracks, etc. Therefore, the change in simulated accumulated rainfall exhibits different trends across study regions.

Table 16. Total number of major and non-major hurricanes simulated for hurricane wind and freshwater flood loss estimation using ANN-based surrogate models

Region	Scenario 1		Scenario 2		Scenario 3		Scenario 4	
	NH	MH	NH	MH	NH	MH	NH	MH
Region1: TX	4691	30	2212	147	1931	428	2149	210
Region2: A+MS+AL	6612	1443	3051	975	2775	1251	2990	1036
Region3a: FL_G	6265	401	2633	701	2285	1047	2479	854
Region3b: FL_A	4821	458	2158	478	1962	677	2097	541
Region4: GA+SC+NC	6480	1019	2661	1087	2283	1468	2524	1226
Overall	28869	3351	12715	3388	11236	4871	12239	3867
	Scenario 5		Scenario 6		Scenario 7			
	NH	MH	NH	MH	NH	MH		
Region1: TX	1552	810	2011	352	1339	1021		
Region2: A+MS+AL	2457	1572	2893	1136	2175	1853		
Region3a: FL_G	1965	1371	2312	1022	1878	1456		
Region3b: FL_A	1660	980	2004	634	1480	1160		
Region4: GA+SC+NC	1837	1915	2336	1418	1531	2220		
Overall	9471	6648	11556	4562	8403	7710		

Table 17. Simulated ratio of the number of high-intensity hurricanes to the number of all hurricanes for each study region under climate scenarios

	Scenario						
Region	1	2	3	4	5	6	7
Region1: TX	0.6%	6.2%	18.1%	8.9%	34.3%	14.9%	43.3%
Region2: LA+MS+AL	17.9%	24.2%	31.1%	25.7%	39.0%	28.2%	46.0%
Region3a: FL_G	6.0%	21.0%	31.4%	25.6%	41.1%	30.7%	43.7%
Region3b: FL_A	8.7%	18.1%	25.7%	20.5%	37.1%	24.0%	43.9%
Region4: GA+SC+NC	13.6%	29.0%	39.1%	32.7%	51.0%	37.8%	59.2%
Overall	10.4%	21.0%	30.2%	24.0%	41.2%	28.3%	47.8%

Table 18. Percentage increase in mean values of maximum CPD, maximum sustained wind speed, maximum accumulated rainfall, and maximum rainfall rate distributions of simulated hurricanes (in %)

	Maximum CPD		Maximum sustained wind speed		Maximum accumulated rainfall		Maximum rain rate	
Region	Sce. 4	Sce. 5	Sce. 4	Sce. 5	Sce. 4	Sce. 5	Sce. 4	Sce. 5
Region1: TX	19.3	44.0	9.9	21.3	3.5	7.0	9.9	20.6
Region2: LA+MS+AL	17.8	38.0	9.3	19.0	5.1	10.6	9.5	18.7
Region3a: FL_G	18.9	42.2	9.6	20.4	1.5	3.9	9.8	19.1
Region3b: FL_A	18.3	43.3	9.4	20.9	1.8	3.0	10.1	22.3
Region4: GA+SC+NC	17.2	39.8	8.9	19.5	1.1	1.7	9.6	21.6
Overall	18.2	40.9	9.4	20.0	2.9	6.0	9.7	20.3

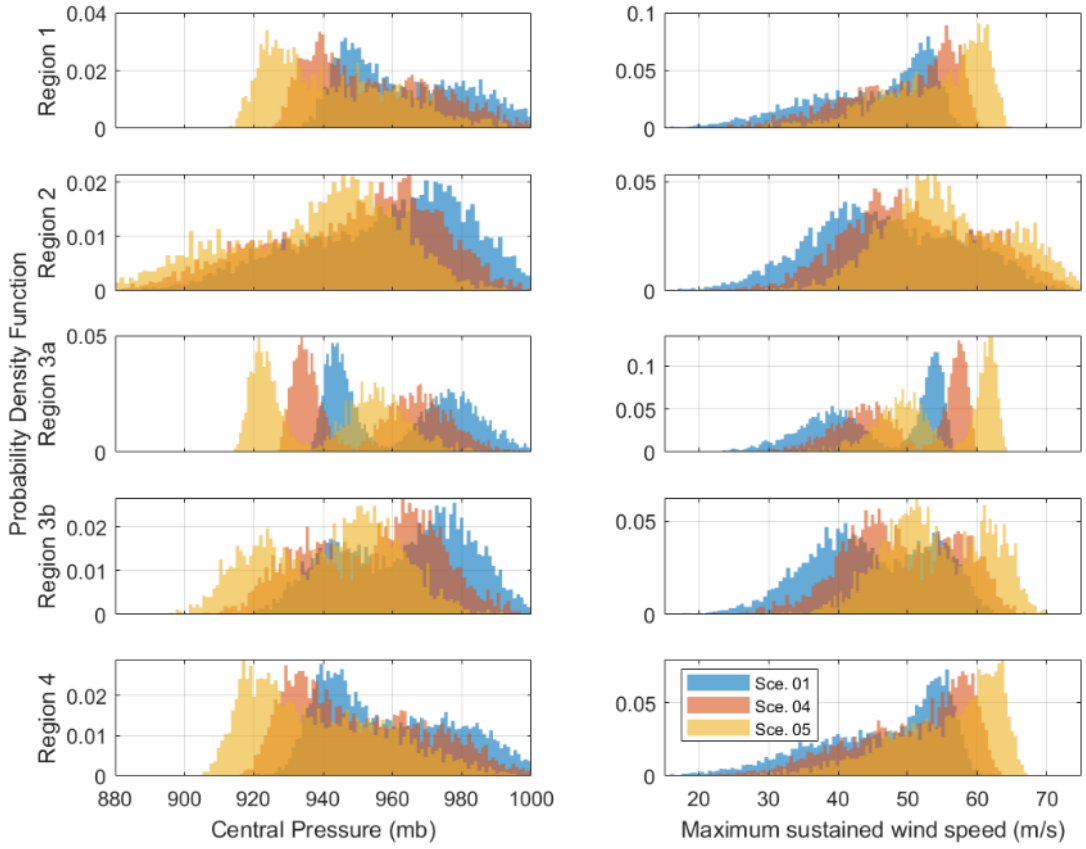

Figure 16. Simulated hurricane CPD and maximum sustained wind speed histograms for hurricane loss estimation

7.2 Wind and flood loss estimation

The hurricane wind and rain-ingress loss and hurricane rainfall-induced freshwater flood loss of simulated hurricane events under climate change scenarios are estimated by the surrogate hurricane wind and flood loss models. The hurricane loss is predicted at the census tract level and aggregated as the county and region-level estimated loss. The changes in hurricane hazards and aggregated loss at county level under climate scenario 5, the long-term projection of IPCC RCP8.5 scenario, are demonstrated in Figure 17 and Figure 18. During hurricane simulation, the decadal maximum values of a 3-sec wind gust, wind loss, rainfall, rain rate, flood depth, and flood loss are recorded at the county level. The maximum values are then fitted with extreme values distribution, and the corresponding annual maximum values are derived. Figure 17 shows the number of valid samples for fitting the extreme value distributions for each county, and Figure 18 shows the changes in hurricane hazard and losses. In Figure 17, there are more wind damage samples closer to the coastline as expected. In contrast, the flood damage prediction depends on the location of USGS stream gauges, i.e., the stream distribution, and thus, it shows a more irregular distribution of valid samples. The number of valid samples can be used as the indicator of confidence in prediction when comparing the change in hurricane hazard at the county level. Wind gust and rain rate show similar change patterns as shown in Figure 18 (a) and (c), respectively, which is due to the direct relationship between the two (Eqs. (7) to (9)). The accumulated rainfall depends on topography and storm movement, thus the changing pattern in accumulated rainfall (Figure 18(b)) is observed to be different from those in wind gust and rain rate. According to the plots, climate change has a higher impact on the inland area than on the coastal area for the flood risk and has an opposite trend for the wind risk. Hurricane wind loss increases significantly along the coastal region under climate change scenario 5. For the freshwater flood risk, it was observed that climate

change might have a higher impact on the inland area than the coastal area. This is suspected because of the increased average duration of hurricanes. The average duration of hurricanes will be increased due to the increased hurricane intensity, and hence the probability of hurricanes affecting an inland area with rainfall will be increased. The difference in the individual locations might be the result of differences in vulnerability of residential buildings, terrain conditions, and increment of rainfall amount.

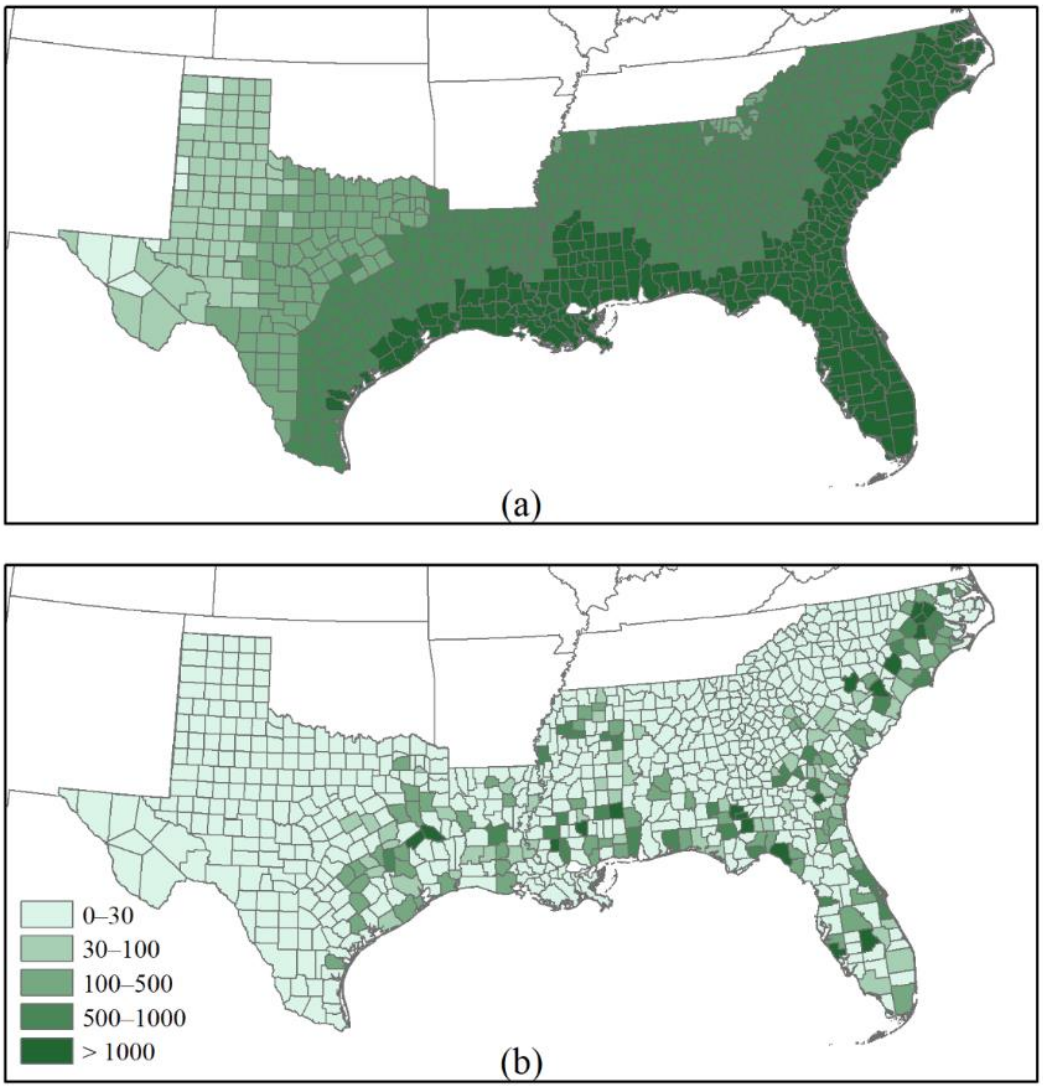

Figure 17. Spatial distribution of hurricane loss samples for (a) wind and (b) flood

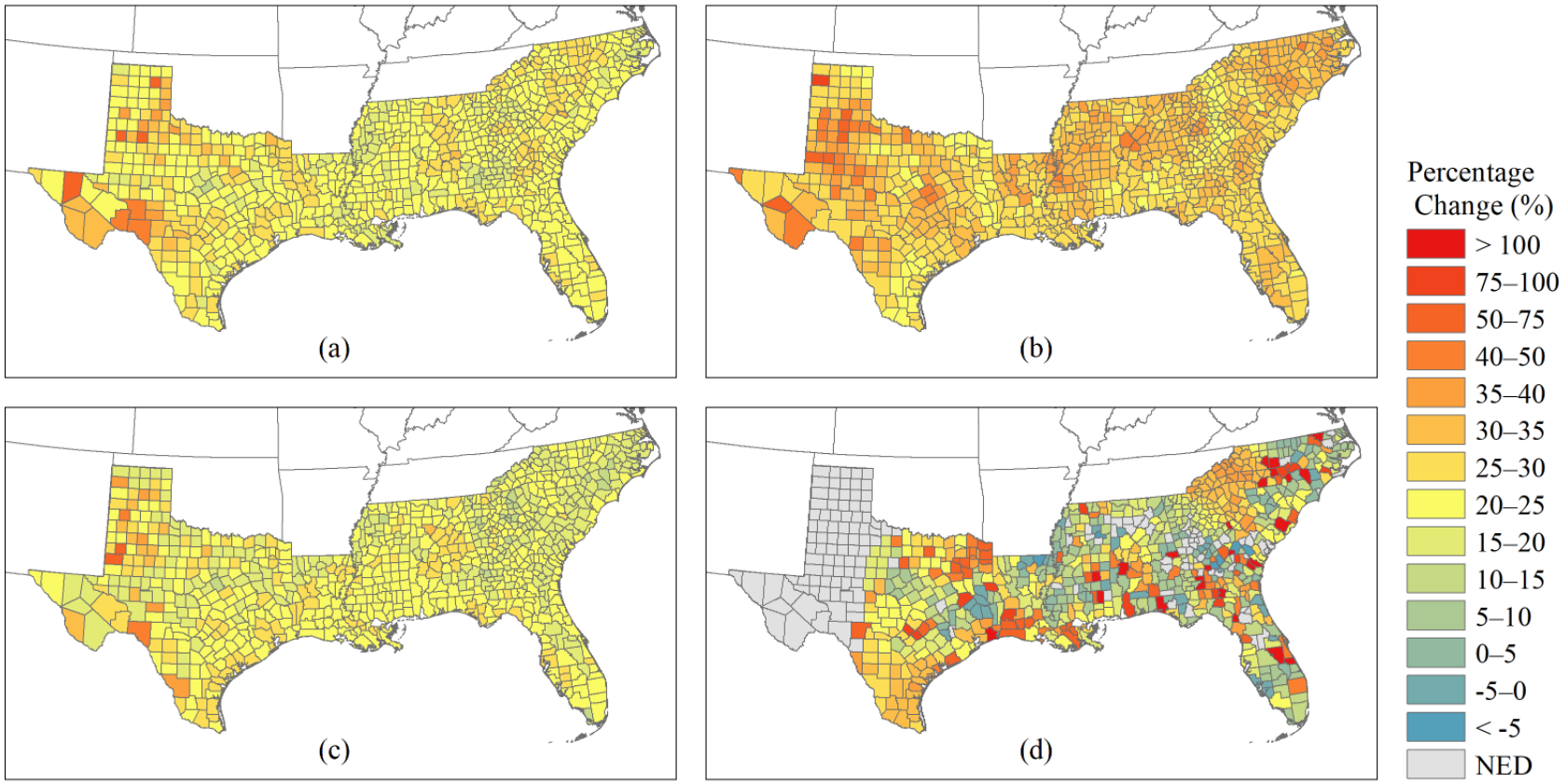

Figure 18. Percentage change in (a) annual maximum rain rate (AEP = 0.01), (b) annual maximum accumulated rainfall (AEP = 0.01), (c) annual maximum 3-sec wind gust (AEP = 0.00143), (d) annual maximum flood depth (AEP = 0.01), (e) accumulated wind loss, (f) accumulated flood loss (g) maximum wind loss, and (h) maximum flood loss at county-level under IPCC RCP8.5 long-term projection

Figure 18 (continued)

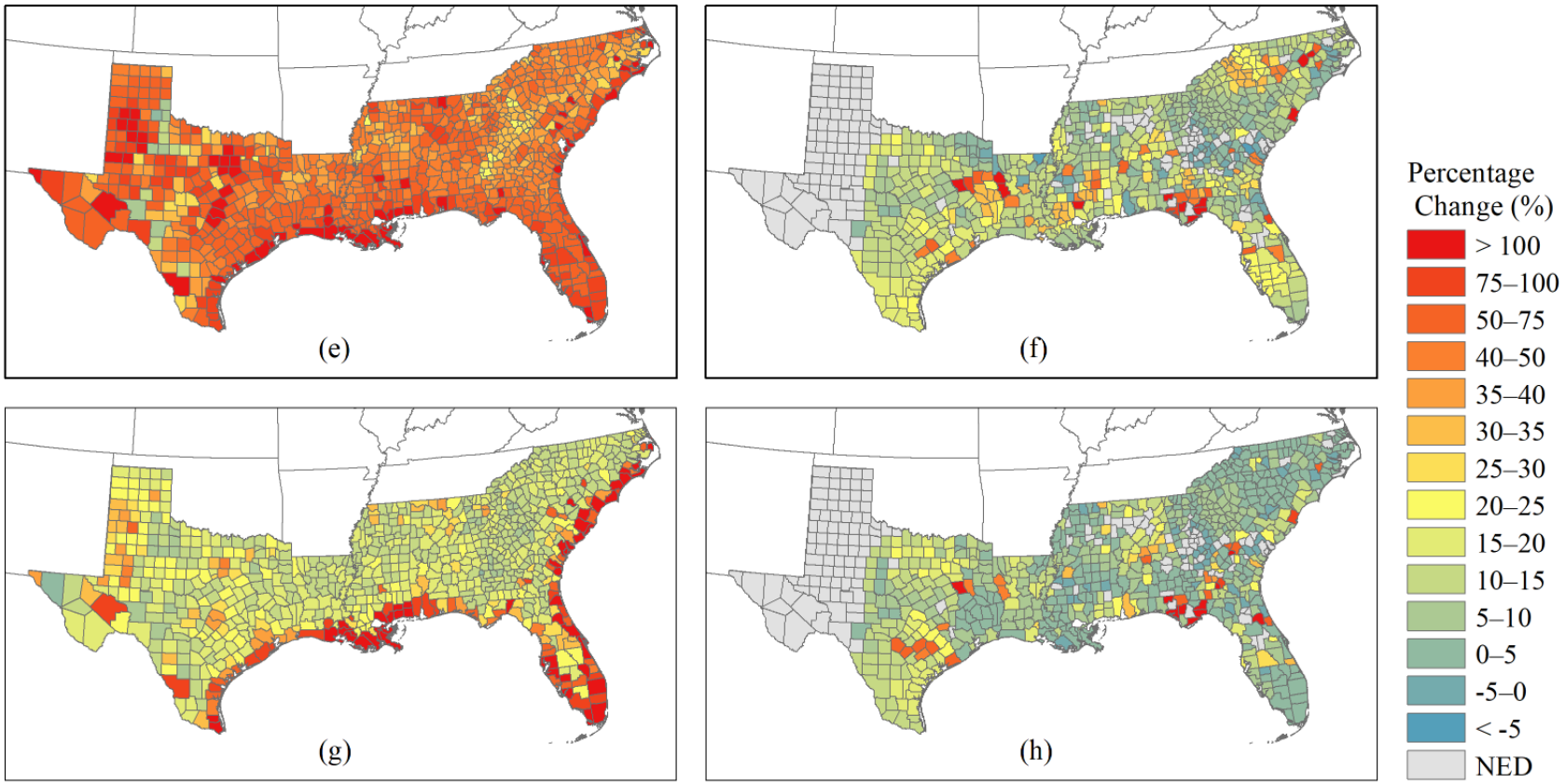

Table 19 shows the expected 10-year accumulated hurricane wind and freshwater flood losses and corresponding standard error (SE) for four study regions, and Table 20 shows the percentage change relative to current climate conditions. Note that since the development of the hurricane freshwater flood loss model is based on historical insurance loss data, the loss predicted in this study accounts for actual loss only partially. In contrast, the wind loss model predicts the loss ratio of total exposure. Therefore, there is a discrepancy between the predicted wind and freshwater flood losses.

Table 19. Expected 10-year accumulated losses and SEs for hurricane wind and freshwater flood (U.S. $1M)

Scenario	Region 1: TX		Region 2: LA+MS+AL		Region 3: FL		Region 4: GA+SC+NC	
	Wind and rain-ingress total loss							
	Mean	SE	Mean	SE	Mean	SE	Mean	SE
1	7174	193	12444	296	29561	418	15573	273
2	10328	375	16533	522	38759	761	20128	453
3	13852	531	21557	668	47093	970	24389	547
4	11746	446	17799	564	41964	846	21670	495
5	20358	799	27974	830	59544	1192	31347	728
6	12590	477	18897	572	44304	882	24103	570
7	23095	856	31891	924	68154	1351	35249	769
Scenario	Freshwater flood insurance loss							
	Mean	SE	Mean	SE	Mean	SE	Mean	SE
1	561	9	1077	13	1478	18	4182	52
2	627	14	1185	20	1568	26	4454	78
3	686	15	1259	21	1598	26	4516	78
4	639	15	1225	21	1583	27	4341	77
5	696	15	1306	21	1623	27	4639	83
6	644	14	1232	20	1631	28	4562	80
7	727	15	1336	21	1676	28	4727	79

Table 20. Percentage increase in the expected 10-year accumulated wind and freshwater flood loss

	Region 1: TX		Region 2: LA+MS+AL		Region 3: FL		Region 4: GA+SC+NC	
Scenario	Wind	Flood	Wind	Flood	Wind	Flood	Wind	Flood
2	44.0%	11.7%	32.9%	10.0%	31.1%	6.1%	29.2%	6.5%
3	93.1%	22.2%	73.2%	16.9%	59.3%	8.1%	56.6%	8.0%
4	63.7%	13.9%	43.0%	13.7%	42.0%	7.1%	39.2%	3.8%
5	183.8%	24.1%	124.8%	21.2%	101.4%	9.8%	101.3%	10.9%
6	75.5%	14.8%	51.9%	14.3%	49.9%	10.3%	54.8%	9.1%
7	221.9%	29.6%	156.3%	24.0%	130.6%	13.3%	126.4%	13.0%

The estimated losses are found to increase in all climate change scenarios, even under the lower bound projection of IPCC8.5 scenario, and wind loss has a more significant increase than the freshwater flood loss. Compared to current climate conditions, the expected wind loss and flood loss increase by 29.2 – 221.9% and 3.8 – 29.6%, respectively, across the study region in six climate change scenarios. The amount of the change in risk varies by region: region 1, Texas, has the highest percentage increase in both expected wind loss and flood loss for all climate change scenarios. Compared with other regions, region 4 has the least percentage increase in wind loss except for the change in wind loss under scenarios 6, where region 3 has the lowest percentage change in wind loss. Compared to region 1 and region 2, region 3 and region 4 have a lower percentage increase in flood losses. In most cases, the percentage increase in wind and flood loss followed the same trend across study regions for near-term and long-term projections, with the order of severity being Region 1 > Region 2 > Region 3 > Region 4 for most of the climate change scenarios.

In general, the expected wind loss shows a more dramatic increase compared with the expected flood loss. The different extents of increment in hurricane wind and flood losses are suspected due to their different sensitivities to wind speed. Figure 19 plots the estimated mean

value and ±1 standard deviation bounds of wind and flood structure and content loss ratios against the wind gust. The nonstationary hurricane parameter adopted and predicted in this study is MCPD, which is directly related to hurricane wind intensity. However, the flood loss ratio is the function of flood depth, which is related to rainfall intensity, topography conditions, watershed, stream conditions, hurricane translation speed, etc., and is found insensitive to wind speed, unlike the loss ratio of wind and rain-ingress damage.

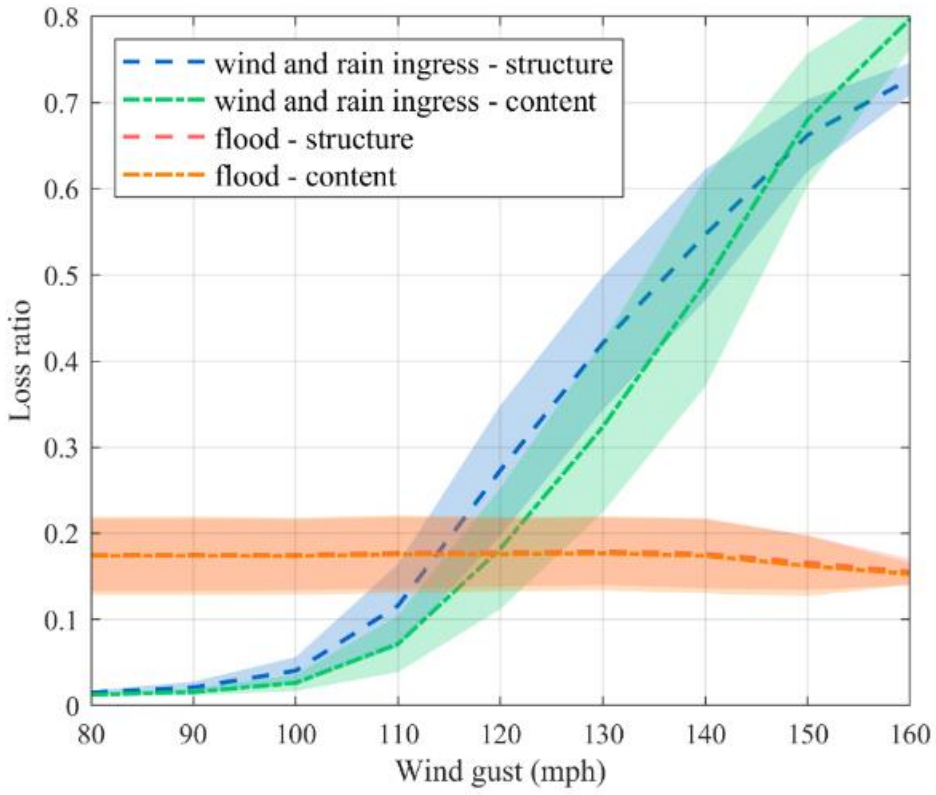

Figure 19. Wind and flood loss ratio versus wind gust

CHAPTER 8: CONCLUSIONS

Hurricane causes tremendous losses every year, and the climate change might worsen the hurricane risk due to the increasing hurricane intensity and the increasing number of high-intensity hurricanes as a result of the rising global temperature. Future hurricane risk assessment is essential for the development and evaluation of climate change impact mitigation strategies. Hence, by conducting climate-dependent hurricane simulation and estimating the consequent change in expected losses, hurricane wind and freshwater flood risks to residential buildings under the IPCC projected RCP8.5-related scenarios are investigated. This study investigates the climate change impact on hurricane wind and flood risks by using machine learning techniques, especially artificial neural networks. To simulate hurricanes considering climate change, the nonstationary hurricane characteristics under changing climate conditions are predicted by utilizing NARX-ANN with the IPCC projected global SST. To efficiently evaluate the hurricane wind loss in a vast region, the southeastern U.S. coastal states from Texas to North Carolina, an ANN-based surrogate model is developed. An existing model proposed by Pant and Cha (2018 and 2019) is adopted to generate hurricane loss data for training the ANN-based surrogate wind loss model. The ANN model takes regional hurricane wind and rainfall intensity and composition of building types as input to predict the regional building and content loss ratios. The developed model is further validated with the synthetic hurricane loss data evaluated by using HAZUS-MH. On the other hand, to assess hurricane rainfall-induced freshwater flood loss, a four-step hurricane freshwater flood loss estimation model is developed. With simulated storm tracks, the rainfall rate and accumulated rainfall are predicted by using the operational R-CLIPER model. Furthermore, by using the ensemble regression technique, the R-CLIPER simulated accumulated rainfall is adjusted based on location and elevation. Then, a combined model consisting of classification and

regression ANNs is constructed to predict the maximum stream gauge height increment ratio at USGS stream gauge sites by rainfall intensity and topographic and geographic conditions. Followed by the predicted stage increment, ANN is further used to predict the flood depth at the location of interest during a hurricane event based on the stream stage increment of surrounding stream gauges. With simulated hurricane storm tracks, associated rainfall, stream stage increment, and flood depth are predicted, and the aggregated flood loss is estimated by using the operational stage-damage curves. For simplification and to focus on the climate change impact on hurricane risks, current inventory and exposure are used in loss estimation, and changes in building stocks, population, and inflation are not considered in this study.

The climate change impact on the hurricane risk varies temporally and spatially and is also different for hurricane wind and freshwater flooding. For regional risk assessment, under IPCC RCP8.5 mean projection, the near-term (2020-2030) and long-term (2090-2100) expected hurricane wind loss relative to current climate conditions increase by 39% to 64% and 101% to 184%, respectively. The highest increase in hurricane wind risk occurs in region 1, and the least occurs in region 4. Under the same scenario, the near-term (2020-2030) and long-term (2090-2100) expected hurricane freshwater flood loss relative to current climate conditions increase by 4% to 14% and 10% to 24%, respectively. Considering millions-to-billions dollar loss caused in a hurricane event, these increased amounts of risk are not negligible. The regions that have the highest and the least increase in hurricane flood risk are the same as the hurricane wind risk. Compared to flood risk, it is predicted to have a higher change in hurricane wind risk because the change in nonstationary hurricane parameter, MCPD, induces more high-wind speed hurricanes in the changing climate conditions, and flood loss is less sensitive to the wind speed. Based on the analysis in this study, the flood loss is directly related to the flood depth, which is less related to

wind speed. Thus, the predicted change in hurricane wind risk is more dramatic than in flood risk. However, both changes in risk are not negligible. The results of this study indicate different regional prioritizations for climate change impact mitigation toward hurricane wind and flood hazards. For county-level risk assessment, the climate change impact appears highly nonuniform within study regions. Within a state, climate change impact varies from coastal to inland counties. Generally speaking, climate change has a higher impact on hurricane wind risk to the coastal counties and a higher impact on hurricane flood risk to the inland counties.

It should be noted that simplification and assumptions in model development and loss estimation are made in this study to investigate the climate change impact on the hurricane risk in extensive regions, which are summarized below.

(1) In climate-dependent hurricane simulation, projected SST and relative humidity are used as external variables for nonstationary hurricane parameters prediction. Instead of sea surface relative humidity used in this study, relative humidity above the surface (e.g., 600-hPa RH) or the column relative humidity would be the better variables to predict hurricane activities. Environment wind shear, an important factor affecting hurricane formation and intensity, is not modeled in hurricane simulation. Lin et al. (2013) showed that ocean heat content might be a better predictor for hurricane activity prediction comparing to SST. Moreover, the use of climate variables might also affect the prediction result. Lee et al. (2020) examined the projection of future tropical cyclone frequency and found an opposite trend projected by using different moisture variables, namely, column relative humidity and saturation deficit. Thus, the choice of climate variable for nonstationary hurricane parameter prediction should be further investigated to improve the power and authenticity of the model prediction.

(2) Region-specific stationary hurricane characteristics are used in climate-dependent hurricane simulations, but nonstationary hurricane characteristics in this study are predicted for the whole study region due to data availability. Similarly, the maximum stage increment prediction model is developed for the whole study regions by selecting USGS stream gauge sites across study regions that are highly heterogeneous. The data heterogeneity and insufficient predictors are the main reasons limiting the model performance. Moreover, for the flood depth prediction model, although the HWM observations were distributed across North and South Carolinas and Texas, they might not well represent other study regions. The model performance can be improved by separating the current model to local models that use data collected from smaller regions to reduce the heterogeneity or investigating other informative predictors that can be more efficiently explain the variation in response variables. Besides data heterogeneity, the other issue that resulted from limited data is data dependency. Data collected from a specific event might possess certain attributes different from data from other events due to spatial or temporal dependency. If predictors cannot distinguish data from each event, i.e., the spatial or temporal dependency cannot be recognized by the model, the induced data dependency could diminish the model prediction capability or even lead to a biased model prediction. The solution to address this issue is to incorporate more predictors to capture the variability in data from different sources or supplementing more samples from different events.

(3) The model is developed by excluding the potential effect from storm surges, i.e., without considering observations along coastlines, but it is also applied to estimate the loss in those regions, which might cause the loss of accuracy in loss estimation. The coastal flooding can be freshwater flooding, storm surge flooding, or compound flooding, including both

components. The developed freshwater flood assessment model predicts the freshwater flood components and might underestimate the actual flood loss in coastal regions subjected to storm surges. Approximately 25% of total loss exposure in the study region is estimated to be associated with the storm surge-affected regions, based on the National Storm Surge Hazard Maps (Zachry et al., 2015) and HAZUS-MH database. To accurately estimate coastal flood loss for coastal regions, storm surge needs to be taken into account along with freshwater flooding.

(4) For the flood loss estimation model, the local flood control measures are not considered in the flood depth prediction. Although the effectiveness of local water management and community resilience in flood control has been reflected on the collected flood depth data, the flood depth prediction can be enhanced by explicitly incorporating the local flood controls such as canals, levees, pumping stations, detention basins, drainage systems, etc. as predictors into the model. Likewise, the inclusion of community characteristics and environmental conditions such as soil type, ground surface permeability, saturation, water table, vegetation water absorption, etc., can further improve the performance of the flood depth prediction model.

(5) The main purpose of this study is to raise awareness by providing an initial risk assessment rather than to predict the varying future risk with different climate adaptation strategies. Therefore, the climate change scenario adopted in this study is the worst case, and the current inventory and exposure are used in loss estimation. According to Crompton and McAneney (2008), losses can be overestimated if the improvement of quality of replaced buildings is not considered. For a more accurate future risk assessment, the varying conditions, such as the potential changes in vulnerabilities due to building code change, exposures due to

urbanization, building stock, population growth and distribution, economic inflation, etc., need to be considered. However, these changes are complex to model, and the uncertainties in the changes are high for long-term prediction. Thus, their impacts on future risk require a separate in-depth investigation and have not been considered in this study. Loss normalization should be conducted by considering these factors to compare the current and future losses or compare losses of different regions.

REFERENCES

Aistleitner, C., Hofer, M., & Tichy, R. (2012). A central limit theorem for Latin hypercube sampling with dependence and application to exotic basket option pricing. *International Journal of Theoretical and Applied Finance*, *15*(7), 1250046. https://doi.org/10.1142/S021902491250046X

Akbari Asanjan, A., Yang, T., Hsu, K., Sorooshian, S., Lin, J., & Peng, Q. (2018). Short-Term Precipitation Forecast Based on the PERSIANN System and LSTM Recurrent Neural Networks. *Journal of Geophysical Research: Atmospheres*, *123*(22), 12,543-12,563. https://doi.org/10.1029/2018JD028375

Alemany, S., Beltran, J., Perez, A., & Ganzfried, S. (2019). Predicting Hurricane Trajectories Using a Recurrent Neural Network. *AAAI Conference on Artificial Intelligence*, *33*, 468–475. https://doi.org/10.1609/aaai.v33i01.3301468

Alexander, L. V., Zhang, X., Peterson, T. C., Caesar, J., Gleason, B., Klein Tank, A. M. G., Haylock, M., Collins, D., Trewin, B., Rahimzadeh, F., & Tagipour, A. (2006). Global observed changes in daily climate extremes of temperature and precipitation. *Journal of Geophysical Research Atmospheres*, *111*(D5), 1–22. https://doi.org/10.1029/2005JD006290

Andreadis, K. M., Schumann, G. J., & Pavelsky, T. (2013). A simple global river bankfull width and depth database. *Water Resources Research*, *49*(10), 7164–7168. https://doi.org/10.1002/wrcr.20440

Anthes, R. A., Corell, R. W., Holland, G., Hurrell, J. W., MacCracken, M. C., & Trenberth, K. E. (2006). Hurricanes and global warming - Potential linkages and consequences. *Bulletin of the American Meteorological Society*, *87*(5), 623–628. https://doi.org/10.1175/BAMS-87-5-617

Atallah, E., Bosart, L. F., & AIYYER, A. R. (2007). Precipitation distribution associated with landfalling tropical cyclones over the eastern United States. *Monthly Weather Review*, *135*(6), 2185–2206. https://doi.org/10.1175/MWR3382.1

Bajo, M., & Umgiesser, G. (2010). Storm surge forecast through a combination of dynamic and neural network models. *Ocean Modelling*, *33*(1–2), 1–9. https://doi.org/10.1016/j.ocemod.2009.12.007

Baños, R., Manzano-Agugliaro, F., Montoya, F. G., Gil, C., Alcayde, A., & Gómez, J. (2011). Optimization methods applied to renewable and sustainable energy: A review. *Renewable and Sustainable Energy Reviews*, *15*(4), 1753–1766. https://doi.org/10.1016/j.rser.2010.12.008

Bender, M. A., Knutson, T. R., Tuleya, R. E., Sirutis, J. J., Vecchi, G. A., Garner, S. T., & Held, I. M. (2010). Modeled impact of anthropogenic warming on the frequency of intense Atlantic hurricanes. *Science*, *327*(5964), 454–458. https://doi.org/10.1126/science.1180568

Bengtsson, L., Hodges, K. I., Esch, M., Keenlyside, N., Kornblueh, L., Luo, J. J., & Yamagata, T. (2007). How may tropical cyclones change in a warmer climate? *Tellus, Series A: Dynamic Meteorology and Oceanography*, *59 A*(4), 539–561.

https://doi.org/10.1111/j.1600-0870.2007.00251.x

Bergmeir, C., Hyndman, R. J., & Koo, B. (2018). A note on the validity of cross-validation for evaluating autoregressive time series prediction. *Computational Statistics & Data Analysis*, *120*, 70–83. https://doi.org/10.1016/j.csda.2017.11.003

Bhatia, K., Vecchi, G., Murakami, H., Underwood, S., & Kossin, J. (2018). Projected response of tropical cyclone intensity and intensification in a global climate model. *Journal of Climate*, *31*(20), 8281–8303. https://doi.org/10.1175/JCLI-D-17-0898.1

Biswas, M. K., Carson, L., Newman, K., Bernardet, L., Kalina, E., Grell, E., & Frimel, J. (2017). *COMMUNITY HWRF USERS GUIDE v3.9a*. https://doi.org/10.7289/V5/TM-OAR-GSD-51

Bjarnadottir, S., Li, Y., & Stewart, M. G. (2011). A probabilistic-based framework for impact and adaptation assessment of climate change on hurricane damage risks and costs. *Structural Safety*, *33*(3), 173–185. https://doi.org/10.1016/j.strusafe.2011.02.003

Bjarnadottir, S., Li, Y., & Stewart, M. G. (2014). Regional loss estimation due to hurricane wind and hurricane-induced surge considering climate variability. *Structure and Infrastructure Engineering*, *10*(11), 1369–1384. https://doi.org/10.1080/15732479.2013.816973

Botts, H., Jeffery, T., Kolk, S., & Suhr, L. (2014). *2014 CoreLogic Storm Surge Report*. https://www.pia.org/IRC/storm/hurricane/2014stormsurgereport.pdf

Brodley, C. E., & Smyth, P. (1995). The process of applying machine learning algorithms. *Applying Machine Learning in Practice IMLC-95*.

Cangialosi, J. (2018). *The State of Hurricane Forecasting: A Look at Model and NHC Accuracy*. WeatherNation. https://www.weathernationtv.com/news/state-hurricane-forecasting-look-model-nhc-accuracy/

Carswell, Jr, W. J., & Lukas, V. (2018). *The 3D elevation program—Flood risk management*. https://pubs.usgs.gov/fs/2017/3081/fs20173081.pdf

CBO. (2019). *Expected Costs of Damage From Hurricane Winds and Storm-Related Flooding* (Issue April). www.cbo.gov/publication/55019

Chan, K. T. F. (2019). Are global tropical cyclones moving slower in a warming climate? *Environmental Research Letters*, *14*(10). https://doi.org/10.1088/1748-9326/ab4031

Chen, W. B., Liu, W. C., & Hsu, M. H. (2012). Predicting typhoon-induced storm surge tide with a two-dimensional hydrodynamic model and artificial neural network model. *Natural Hazards and Earth System Science*, *12*(12), 3799–3809. https://doi.org/10.5194/nhess-12-3799-2012

Cheng, C. T., Ou, C. P., & Chau, K. W. (2002). Combining a fuzzy optimal model with a genetic algorithm to solve multi-objective rainfall-runoff model calibration. *Journal of Hydrology*, *268*(1–4), 72–86. https://doi.org/10.1016/S0022-1694(02)00122-1

Chu, P.-S., & Wang, J. (1998). Modeling Return Periods of Tropical Cyclone Intensities in the Vicinity of Hawaii*. *Journal of Applied Meteorology*, *37*(9), 951–960. https://doi.org/10.1175/1520-0450(1998)037<0951:MRPOTC>2.0.CO;2

Clark, K. M. (1986). A Formal Approach to Catastrophe Risk Assessment and Management. *Proceedings of the Casualty Actuarial Society*.

Contento, A., Xu, H., & Gardoni, P. (2019). Risk Analysis for Hurricanes Accounting for the Effects of Climate Change. In *Climate Adaptation Engineering*. Elsevier Inc. https://doi.org/10.1016/b978-0-12-816782-3.00002-4

Cope, A. D. (2004). *Predicting the vulnerability of typical residential buildings to hurricane damage*. University of Florida.

Coppola, D. P. (2015). Introduction to International Disaster Management: Third Edition. In *Introduction to International Disaster Management: Third Edition*. Elsevier Inc. https://doi.org/10.1016/C2014-0-00128-1

Coumou, D., & Rahmstorf, S. (2012). A decade of weather extremes. *Nature Climate Change*, *2*(7), 491–496. https://doi.org/10.1038/nclimate1452

Crompton, R. P., & McAneney, K. J. (2008). Normalised Australian insured losses from meteorological hazards: 1967-2006. *Environmental Science and Policy*, *11*(5), 371–378. https://doi.org/10.1016/j.envsci.2008.01.005

Cui, W., & Caracoglia, L. (2016). Exploring hurricane wind speed along US Atlantic coast in warming climate and effects on predictions of structural damage and intervention costs. *Engineering Structures*, *122*, 209–225. https://doi.org/10.1016/j.engstruct.2016.05.003

Czajkowski, J., Villarini, G., Montgomery, M., Michel-Kerjan, E., & Goska, R. (2017). Assessing Current and Future Freshwater Flood Risk from North Atlantic Tropical Cyclones via Insurance Claims. *Scientific Reports*, *7:41609*, 1–10. https://doi.org/10.1038/srep41609

Demaria, M., & Kaplan, J. (1994). Sea Surface Temperature and the Maximum Intensity of Atlantic Tropical Cyclones. *Journal of Climate*, *7*(9), 1324–1334. https://doi.org/10.1175/1520-0442(1994)007<1324:sstatm>2.0.co;2

DHS. (2017). *FEMA Needs to Improve Management of its Flood Mapping Programs*. https://www.documentcloud.org/documents/4066233-OIG-17-110-Sep17.html

Dietterich, T. G. (2000). Ensemble Methods in Machine Learning. *Proceedings of the First International Workshop on Multiple Classifier Systems*, 1–15. https://link.springer.com/chapter/10.1007/3-540-45014-9_1

Elsner, J. B., Kossin, J. P., & Jagger, T. H. (2008). The increasing intensity of the strongest tropical cyclones. *Nature*, *455*(7209), 92–95. https://doi.org/10.1038/nature07234

Emanuel, K. A. (1987). The dependence of hurricane intensity on climate. *Nature*, *326*(6112), 483–485. https://doi.org/10.1038/326483a0

Emanuel, K. A. (1991). The Theory of Hurricanes. *Annual Review of Fluid Mechanics*, *23*(1), 179–196. https://doi.org/10.1146/annurev.fl.23.010191.001143

Emanuel, K. A. (2008). The hurricane-climate connection. *Bulletin of the American Meteorological Society*, *89*(5), ES10–ES20. https://doi.org/10.1175/BAMS-89-5-Emanuel

Emanuel, K. A. (2013). Downscaling CMIP5 climate models shows increased tropical cyclone activity over the 21st century. *Proceedings of the National Academy of Sciences of the United States of America*, *110*(30), 12219–12224. https://doi.org/10.1073/pnas.1301293110

Emanuel, K. A. (2017). Assessing the present and future probability of Hurricane Harvey's rainfall. *National Academy of Sciences of the United States of America*, *114*(48), 12681–12684. https://doi.org/10.1073/pnas.1716222114

Emanuel, K. A., Ravela, S., Vivant, E., & Risi, C. (2006). A statistical deterministic approach to hurricane risk assessment. *Bulletin of the American Meteorological Society*, *87*(3), 299–314. https://doi.org/10.1175/BAMS-87-3-299

Erdal, H. I., & Karakurt, O. (2013). Advancing monthly streamflow prediction accuracy of CART models using ensemble learning paradigms. *Journal of Hydrology*, *477*, 119–128. https://doi.org/10.1016/j.jhydrol.2012.11.015

FEMA. (2009). *HAZUS-MH MR4 Flood Model Technical Manual*. https://www.fema.gov/media-library/assets/documents/24609?id=5120

FEMA. (2013). *Hazus—MH 2.1 Technical manual: Hurricane Model*. https://www.fema.gov/sites/default/files/2020-09/fema_hazus_hurricane-model_technical-manual_2.1.pdf

FEMA. (2018). *Hazus Flood Model User Guidance*. https://www.fema.gov/media-library/assets/documents/24609

FEMA. (2019). *Significant Flood Events*. https://www.fema.gov/significant-flood-events

Foresee, F. D., & Hagan, M. T. (1997). Gauss-Newton approximation to bayesian learning. *IEEE International Conference on Neural Networks - Conference Proceedings*, *3*, 1930–1935. https://doi.org/10.1109/ICNN.1997.614194

Freeman, E., Woodruff, S. D., Worley, S. J., Lubker, S. J., Kent, E. C., Angel, W. E., Berry, D. I., Brohan, P., Eastman, R., Gates, L., Ji, Z., Lawrimore, J., Rayner, N. A., & Smith, S. R. (2017). ICOADS Release 3.0: a major update to the historical marine climate record. *International Journal of Climatology*, *37*(5), 2211–2232. https://doi.org/10.1002/joc.4775

Friedman, J. H. (2001). Greedy Function Approximation: A Gradient Boosting Machine. *Annals of Statistics*, 1189–1232.

Friedman, J. H. (2002). Stochastic gradient boosting. *Computational Statistics and Data Analysis*, *38*(4), 367–378. https://doi.org/10.1016/S0167-9473(01)00065-2

Gal, Y., & Ghahramani, Z. (2016). Dropout as a Bayesian approximation: Representing model uncertainty in deep learning. *33rd International Conference on Machine Learning, ICML 2016*, *3*, 1651–1660.

Garfin, G., Franco, G., Blanco, H., Comrie, A., Gonzalez, P., Piechota, T., Smyth, R., & Waskom, R. (2014). Southwest: the third national climate assessment. In J. M. Melillo, T. C. Richmond, & G. W. Yohe (Eds.), *Climate change impacts in the United States: the third National Climate Assessment* (pp. 462–486). US Global Change Research Program. https://doi.org/10.7930/J08G8HMN

Geeraerts, J., Troch, P., De Rouck, J., Verhaeghe, H., & Bouma, J. J. (2007). Wave overtopping at coastal structures: prediction tools and related hazard analysis. *Journal of Cleaner Production*, *15*(16), 1514–1521. https://doi.org/10.1016/j.jclepro.2006.07.050

Geman, S., Bienenstock, E., & Doursat, R. (1992). Neural Networks and the Bias/Variance Dilemma. *Neural Computation*, *4*(1), 1–58. https://doi.org/10.1162/neco.1992.4.1.1

Gudipati, V. K., & Cha, E. J. (2019). A framework for optimization of target reliability index for a building class based on aggregated cost. *Structural Safety*, *81*(November 2018), 101873. https://doi.org/10.1016/j.strusafe.2019.101873

Gurley, K., Pinelli, J. P., Subramanian, C., Cope, A., Zhang, L., Murphree, J., & Artiles, A. (2005). Development Calibration and Validation of Vulnerability Matrices of the Florida Public Hurricane Loss Projection Model. In *Florida Public Hurricane Loss Projection Model (FPHLPM) engineering team final report: Vol. III*.

Hall, T. M., & Jewson, S. (2007). Statistical modelling of North Atlantic tropical cyclone tracks. *Tellus, Series A: Dynamic Meteorology and Oceanography*, *59 A*(4), 486–498. https://doi.org/10.1111/j.1600-0870.2007.00240.x

Hallegatte, S. (2007). The use of synthetic hurricane tracks in risk analysis and climate change damage assessment. *Journal of Applied Meteorology and Climatology*, *46*(11), 1956–1966. https://doi.org/10.1175/2007JAMC1532.1

Harper, B. A., Kepert, J. D., & Ginger, J. D. (2010). *Guidelines For Converting Between Various Wind Averaging Periods In Tropical Cyclone Conditions*. World Meteorological Organization. https://www.wmo.int/pages/prog/www/tcp/documents/WMO_TD_1555_en.pdf

Hastie, T., Tibshirani, R., & Friedman, J. (2009). *The Elements of Statistical Learning* (2nd ed.). Springer New York. https://doi.org/10.1007/978-0-387-84858-7

Hein, J. E., & Jenkins, J. C. (2017). Why does the United States lack a global warming policy? The corporate inner circle versus public interest sector elites. *Environmental Politics*, *26*(1), 97–117. https://doi.org/10.1080/09644016.2016.1244966

Holland, G., & Bruyère, C. L. (2014). Recent intense hurricane response to global climate change. *Climate Dynamics*, *42*(3–4), 617–627. https://doi.org/10.1007/s00382-013-1713-0

Hong, Y., Hsu, K. L., Sorooshian, S., & Gao, X. (2004). Precipitation estimation from remotely sensed imagery using an artificial neural network cloud classification system. *Journal of Applied Meteorology*, *43*(12), 1834–1852. https://doi.org/10.1175/jam2173.1

Hsu, K. L., Gao, X., Sorooshian, S., & Gupta, H. V. (1997). Precipitation estimation from remotely sensed information using artificial neural networks. *Journal of Applied Meteorology*, *36*(9), 1176–1190. https://doi.org/10.1175/1520-0450(1997)036<1176:PEFRSI>2.0.CO;2

Huang, B., Thorne, P. W., Banzon, V. F., Boyer, T., Chepurin, G., Lawrimore, J. H., Menne, M. J., Smith, T. M., Vose, R. S., & Zhang, H.-M. (2017). Extended Reconstructed Sea Surface Temperature, Version 5 (ERSSTv5): Upgrades, Validations, and Intercomparisons. *Journal of Climate*, *30*(20), 8179–8205. https://doi.org/10.1175/JCLI-D-16-0836.1

Hyndman, R. J. (2016). *Cross-validation for time series*. https://robjhyndman.com/hyndsight/tscv/

Iliadis, L. S., & Maris, F. (2007). An Artificial Neural Network model for mountainous water-resources management: The case of Cyprus mountainous watersheds. *Environmental Modelling and Software*, *22*(7), 1066–1072. https://doi.org/10.1016/j.envsoft.2006.05.026

Ilonen, J., Kamarainen, J. K., & Lampinen, J. (2003). Differential evolution training algorithm for feed-forward neural networks. *Neural Processing Letters*, *17*(1), 93–105. https://doi.org/10.1023/A:1022995128597

IPCC. (2013). *Climate change 2013 the physical science basis: Working Group I contribution to the fifth assessment report of the intergovernmental panel on climate change* (T. F. Stocker, D. Qin, G.-K. Plattner, M. Tignor, S. K. Allen, J. Boschung, A. Nauels, Y. Xia, V. Bex, & P. M. Midgley (eds.)). Cambridge University Press. https://doi.org/10.1017/CBO9781107415324

IPCC. (2014). *Climate Change 2014: Synthesis Report. Contribution of Working Groups I, II and III to the Fifth Assessment Report of the Intergovernmental Panel on Climate Change* (R. K. Pachauri & L. A. Meyer (eds.)). IPCC. https://www.ipcc.ch/report/ar5/syr/

IPCC. (2018). *Global Warming of 1.5°C*. https://www.ipcc.ch/sr15/

Jain, A. K., Murty, M. N., & Flynn, P. J. (1999). Data clustering: A review. *ACM Computing Surveys*, *31*(3), 264–323. https://doi.org/10.1145/331499.331504

Jang, J. R. (1993). ANFIS : Adap tive-Ne twork-Based Fuzzy Inference System. *IEEE Transactions on Systems, Man, and Cybernetics*, *23*(3), 665–685.

Jarvis, A., Reuter, H. I., Nelson, A., & Guevara, E. (2008). *Hole-filled SRTM for the globe Version 4*. CGIAR-CSI SRTM 90m Database. https://cgiarcsi.community/data/srtm-90m-digital-elevation-database-v4-1/

Kia, M. B., Pirasteh, S., Pradhan, B., Mahmud, A. R., Sulaiman, W. N. A., & Moradi, A. (2012). An artificial neural network model for flood simulation using GIS: Johor River Basin, Malaysia. *Environmental Earth Sciences*, *67*(1), 251–264. https://doi.org/10.1007/s12665-011-1504-z

Kim, J. M., Woods, P. K., Park, Y. J., Kim, T., & Son, K. (2016). Predicting hurricane wind damage by claim payout based on Hurricane Ike in Texas. *Geomatics, Natural Hazards and Risk*, *7*(5), 1513–1525. https://doi.org/10.1080/19475705.2015.1084540

Kim, S., Moon, I., & Chu, P. (2020). An increase in global trends of tropical cyclone translation speed since 1982 and its physical causes. *Environmental Research Letters*, *15*(9). https://doi.org/https://doi.org/10.1088/1748-9326/ab9e1f

Knaff, J. A., Demaria, M., Molenar, D. A., Sampson, C. R., & Seybold, M. G. (2011). An automated, objective, multiple-satellite-platform tropical cyclone surface wind analysis. *Journal of Applied Meteorology and Climatology*, *50*(10), 2149–2166. https://doi.org/10.1175/2011JAMC2673.1

Knapp, K. R., Kruk, M. C., Levinson, D. H., Diamond, H. J., & Neumann, C. J. (2010). The

international best track archive for climate stewardship (IBTrACS) unifying tropical cyclone data. *Bulletin of the American Meteorological Society*, *91*(3), 363–376. https://doi.org/10.1175/2009BAMS2755.1

Knutson, T. R., Camargo, S. J., Chan, J. C. L., Emanuel, K., Ho, C.-H., Kossin, J., Mohapatra, M., Satoh, M., Sugi, M., Walsh, K., & Wu, L. (2019). Tropical Cyclones and Climate Change Assessment: Part II. Projected Response to Anthropogenic Warming. *Bulletin of the American Meteorological Society*, 1–62. https://doi.org/10.1175/bams-d-18-0194.1

Knutson, T. R., Camargo, S. J., Chan, J. C. L., Emanuel, K., Ho, C.-H., Kossin, J., Mohapatra, M., Satoh, M., Sugi, M., Walsh, K., & Wu, L. (2020). Tropical Cyclones and Climate Change Assessment: Part II: Projected Response to Anthropogenic Warming. *Bulletin of the American Meteorological Society*, *101*(3), E303–E322. https://doi.org/10.1175/BAMS-D-18-0194.1

Knutson, T. R., McBride, J. L., Chan, J., Emanuel, K., Holland, G., Landsea, C., Held, I., Kossin, J. P., Srivastava, A. K., & Sugi, M. (2010). Tropical cyclones and climate change. *Nature Geoscience*, *3*(3), 157–163. https://doi.org/10.1038/ngeo779

Knutson, T. R., Sirutis, J. J., Garner, S. T., Vecchi, G. A., & Held, I. M. (2008). Simulated reduction in Atlantic hurricane frequency under twenty-first-century warming conditions. *Nature Geoscience*, *1*(6), 359–364. https://doi.org/10.1038/ngeo202

Knutson, T. R., Sirutis, J. J., Zhao, M., Tuleya, R. E., Bender, M., Vecchi, G. A., Villarini, G., & Chavas, D. (2015). Global projections of intense tropical cyclone activity for the late twenty-first century from dynamical downscaling of CMIP5/RCP4.5 scenarios. *Journal of Climate*, *28*(18), 7203–7224. https://doi.org/10.1175/JCLI-D-15-0129.1

Kordmahalleh, M. M., Sefidmazgi, M. G., & Homaifar, A. (2016). A sparse recurrent neural network for trajectory prediction of atlantic hurricanes. *GECCO 2016 - Proceedings of the 2016 Genetic and Evolutionary Computation Conference*, 957–964. https://doi.org/10.1145/2908812.2908834

Kossin, J. P. (2018). A global slowdown of tropical-cyclone translation speed. *Nature*, *558*(7708), 104–107. https://doi.org/10.1038/s41586-018-0158-3

Kossin, J. P., Knapp, K. R., Olander, T. L., & Velden, C. S. (2020). Global increase in major tropical cyclone exceedance probability over the past four decades. *Proceedings of the National Academy of Sciences*, *117*(22), 201920849. https://doi.org/10.1073/pnas.1920849117

Kusiak, A., Wei, X., Verma, A. P., & Roz, E. (2013). Modeling and prediction of rainfall using radar reflectivity data: A data-mining approach. *IEEE Transactions on Geoscience and Remote Sensing*, *51*(4), 2337–2342. https://doi.org/10.1109/TGRS.2012.2210429

Landsea, C. W., Vecchi, G. A., Bengtsson, L., & Knutson, T. R. (2010). Impact of duration thresholds on Atlantic tropical cyclone counts. *Journal of Climate*, *23*(10), 2508–2519. https://doi.org/10.1175/2009JCLI3034.1

Lanzante, J. R. (2019). Uncertainties in tropical-cyclone translation speed. *Nature*, *570*(7759), E6–E15. https://doi.org/10.1038/s41586-019-1223-2

Latif, M., Keenlyside, N., & Bader, J. (2007). Tropical sea surface temperature, vertical wind shear, and hurricane development. *Geophysical Research Letters*, *34*(1), 12–15. https://doi.org/10.1029/2006GL027969

Lee, C.-Y., Camargo, S. J., Sobel, A. H., & Tippett, M. K. (2020). Statistical–Dynamical Downscaling Projections of Tropical Cyclone Activity in a Warming Climate: Two Diverging Genesis Scenarios. *Journal of Climate*, *33*(11), 4815–4834. https://doi.org/10.1175/jcli-d-19-0452.1

Lee, C. Y., Tippett, M. K., Camargo, S. J., & Sobel, A. H. (2015). Probabilistic multiple linear regression modeling for tropical cyclone intensity. *Monthly Weather Review*, *143*(3), 933–954. https://doi.org/10.1175/MWR-D-14-00171.1

Lee, C. Y., Tippett, M. K., Sobel, A. H., & Camargo, S. J. (2018). An environmentally forced tropical cyclone hazard model. *Journal of Advances in Modeling Earth Systems*, *10*(1), 223–241. https://doi.org/10.1002/2017MS001186

Lehmann, R. J. (2020). *Do no harm: Managing retreat by ending new subsidies*. https://www.rstreet.org/wp-content%0A/uploads/2020/02/195.pdf

Li, Q., Wang, C., & Zhang, H. (2016). A probabilistic framework for hurricane damage assessment considering non-stationarity and correlation in hurricane actions. *Structural Safety*, *59*, 108–117. https://doi.org/10.1016/j.strusafe.2016.01.001

Li, Y., Van De Lindt, J. W., Dao, T., Bjarnadottir, S., & Ahuja, A. (2012). Loss analysis for combined wind and surge in hurricanes. *Natural Hazards Review*, *13*(1), 1–10. https://doi.org/10.1061/(ASCE)NH.1527-6996.0000058

Lin, I. I., Goni, G. J., Knaff, J. A., Forbes, C., & Ali, M. M. (2013). Ocean heat content for tropical cyclone intensity forecasting and its impact on storm surge. *Natural Hazards*, *66*(3), 1481–1500. https://doi.org/10.1007/s11069-012-0214-5

Liong, S.-Y., Lim, W.-H., & Paudyal, G. N. (2000). RIVER STAGE FORECASTING IN BANGLADESH: NEURAL NETWORK APPROACH. *JOURNAL OF COMPUTING IN CIVIL ENGINEERING*, *14*(January), 1–8.

Liu, F. (2014). *Projections of Future US Design Wind Speeds Due to Climate Change for Estimating Hurricane Losses*. Clemson University, Clemson, SC.

Loh, W.-L. (1995). On the convergence rate to normality of Latin Hypercube Sampling U-statistics. *Purdue University Tech Report*, *95*(2).

Lohninger, H. (1999). *Teach/Me - Data Analysis* (1st ed.). Springer US.

Lonfat, M., Marks Jr, F. D., & Chen, S. S. (2004). Precipitation Distribution in Tropical Cyclones Using the Tropical Rainfall Measuring Mission (TRMM) Microwave Imager: A Global Perspective. *Monthly Weather Review*, *132*(7), 1645–1660.

Lonfat, M., Rogers, R., Marchok, T., & Marks, F. D. (2007). A parametric model for predicting hurricane rainfall. *Monthly Weather Review*, *135*(9), 3086–3097. https://doi.org/10.1175/MWR3433.1

MacKay, D. J. C. (1992). Bayesian Interpolation. *Neural Computation*, *4*(3), 415–447. https://doi.org/10.1162/neco.1992.4.3.415

Maloney, K. O., Schmid, M., & Weller, D. E. (2012). Applying additive modelling and gradient boosting to assess the effects of watershed and reach characteristics on riverine assemblages. *Methods in Ecology and Evolution*, *3*(1), 116–128. https://doi.org/10.1111/j.2041-210X.2011.00124.x

Mann, M. E., & Emanuel, K. A. (2006). Atlantic Hurricane Trends Linked to Climate Change. *Eos, Transactions American Geophysical Union*, *87*(24), 233–241.

Marks Jr, F. D., & DeMaria, M. (2003). *Development of a Tropical Cyclone Rainfall Climatology and Persistence (R-CLIPER) Model*.

Martinez, A. B. (2020). Improving normalized hurricane damages. *Nature Sustainability*, *3*, 517–518. https://doi.org/10.1038/s41893-020-0550-5

Mason, L., Baxter, J., Bartlett, P. L., & Frean, M. R. (2000). Boosting algorithms as gradient descent. *Advances in Neural Information Processing Systems*, 512–518.

Maune, D. F. (2016). *FEMA's Romance with LiDAR*. LiDAR Magazine. https://lidarmag.com/2016/05/28/femas-romance-with-lidar/

Mudd, L., Rosowsky, D., Letchford, C., & Lombardo, F. (2017). Joint probabilistic wind-rainfall model for tropical cyclone hazard characterization. *Journal of Structural Engineering (United States)*, *143*(3), 1–17. https://doi.org/10.1061/(ASCE)ST.1943-541X.0001685

Mudd, L., Wang, Y., Letchford, C., & Rosowsky, D. (2014a). Assessing Climate Change Impact on the U.S. East Coast Hurricane Hazard: Temperature, Frequency, and Track. *Natural Hazards Review*, *15*(3), 04014001. https://doi.org/10.1061/(ASCE)NH.1527-6996.0000128

Mudd, L., Wang, Y., Letchford, C., & Rosowsky, D. (2014b). Hurricane wind hazard assessment for a rapidly warming climate scenario. *Journal of Wind Engineering and Industrial Aerodynamics*, *133*, 242–249. https://doi.org/10.1016/j.jweia.2014.07.005

Mudd, L., Wang, Y., Rosowsky, D., & Letchford, C. (2013). Assessing climate change impact on the US east coast hurricane hazard , II : sea surface temperature and hurricane frequency. *Safety, Reliability, Risk and Life-Cycle Performance of Structures & Infrastructures*, 1471–1478. https://doi.org/10.13140/RG.2.1.2495.7280

Mustafa, M. R., Rezaur, R. B., Saiedi, S., & Isa, M. H. (2012). River suspended sediment prediction using various multilayer perceptron neural network training algorithms-A case study in Malaysia. *Water Resources Management*, *26*(7), 1879–1897. https://doi.org/10.1007/s11269-012-9992-5

Nakamura, J., Lall, U., Kushnir, Y., & Rajagopalan, B. (2015). HITS: Hurricane Intensity and Track Simulator with North Atlantic Ocean Applications for Risk Assessment. *Journal of Applied Meteorology and Climatology*, *54*(7), 1620–1636. https://doi.org/10.1175/JAMC-D-14-0141.1

Nakicenovic, N., & Swart, R. (2000). *Special report on emissions scenarios: a special report of Working Group III of the Intergovernmental Panel on Climate Change*.

https://www.ipcc.ch/site/assets/uploads/2018/03/sres-en.pdf

National Hurricane Center. (2009). *Technical Summary of the National Hurricane Center Track and Intensity Models*. https://www.nhc.noaa.gov/pdf/model_summary_20090724.pdf

Nayak, P. C., Sudheer, K. P., Rangan, D. M., & Ramasastri, K. S. (2004). A neuro-fuzzy computing technique for modeling hydrological time series. *Journal of Hydrology*, *291*(1–2), 52–66. https://doi.org/10.1016/j.jhydrol.2003.12.010

Neelakantan, T. R., Lingireddy, S., & Brion, G. M. (2002). Effectiveness of different artificial neural network training algorithms in predicting protozoa risks in surface waters. *Journal of Environmental Engineering*, *128*(6), 533–542. https://doi.org/10.1061/(ASCE)0733-9372(2002)128:6(533)

NOAA. (2019). *Tropical Cyclone Rainfall Data*. https://www.wpc.ncep.noaa.gov/tropical/rain/tcrainfall.html

Olsen, R. (2015). *Adapting Infrastructure and Civil Engineering Practice to a Changing Climate*. American Society of Civil Engineers. https://doi.org/10.1061/9780784479193

Oouchi, K., Yoshimura, J., Yoshimura, H., Mizuta, R., Kusunoki, S., & Noda, A. (2006). Tropical Cyclone Climatology in a Global-Warming Climate as Simulated in a 20 km-Mesh Global Atmospheric Model: Frequency and Wind Intensity Analyses. *Journal of the Meteorological Society of Japan. Ser. II*, *84*(2), 259–276. https://doi.org/10.2151/jmsj.84.259

Orlandini, S., & Morlini, I. (2000). Artificial neural network estimation of rainfall intensity from radar observations. *Journal of Geophysical Research: Atmospheres*, *105*(D20), 24849–24861.

Pant, S., & Cha, E. J. (2018). Effect of Climate Change on Hurricane Damage and Loss for Residential Buildings in Miami-Dade County. *Journal of Structural Engineering (United States)*, *144*(6), 04018057. https://doi.org/10.1061/(ASCE)ST.1943-541X.0002038

Pant, S., & Cha, E. J. (2019). Wind and rainfall loss assessment for residential buildings under climate-dependent hurricane scenarios. *Structure and Infrastructure Engineering*, *15*(6), 771–782. https://doi.org/10.1080/15732479.2019.1572199

Patricola, C. M., & Wehner, M. F. (2018). Anthropogenic influences on major tropical cyclone events. *Nature*, *563*(7731), 339–346. https://doi.org/10.1038/s41586-018-0673-2

Pearce, T., Zaki, M., Brintrup, A., & Neely, A. (2018). High-quality prediction intervals for deep learning: A distribution-free, ensembled approach. *35th International Conference on Machine Learning, ICML 2018*, *9*, 6473–6482.

Pilkington, S. F., & Mahmoud, H. N. (2016). Using artificial neural networks to forecast economic impact of multi-hazard hurricane-based events. *Sustainable and Resilient Infrastructure*, *1*(1–2), 63–83. https://doi.org/10.1080/23789689.2016.1179529

Pinelli, J. P., Gurley, K. R., Subramanian, C. S., Hamid, S. S., & Pita, G. L. (2008). Validation of a probabilistic model for hurricane insurance loss projections in Florida. *Reliability Engineering and System Safety*, *93*(12), 1896–1905.

https://doi.org/10.1016/j.ress.2008.03.017

Poff, N. L. R., Tokar, S., & Johnson, P. (1996). Stream hydrological and ecological responses to climate change assessed with an artificial neural network. *Limnology and Oceanography*, *41*(5), 857–863. https://doi.org/10.4319/lo.1996.41.5.0857

Pourali, S. H., Arrowsmith, C., Chrisman, N., Matkan, A. A., & Mitchell, D. (2016). Topography Wetness Index Application in Flood-Risk-Based Land Use Planning. *Applied Spatial Analysis and Policy*, *9*(1), 39–54. https://doi.org/10.1007/s12061-014-9130-2

Rao, S., & Mandal, S. (2005). Hindcasting of storm waves using neural networks. *Ocean Engineering*, *32*(5–6), 667–684. https://doi.org/10.1016/j.oceaneng.2004.09.003

Risser, M. D., & Wehner, M. F. (2017). Attributable Human-Induced Changes in the Likelihood and Magnitude of the Observed Extreme Precipitation during Hurricane Harvey. *Geophysical Research Letters*, *44*(24), 12,457-12,464. https://doi.org/10.1002/2017GL075888

Rivas-Perea, P., Cota-Ruiz, J., Venzor, J. A. P., Chaparro, D. G., & Rosiles, J.-G. (2013). LP-SVR Model Selection Using an Inexact Globalized Quasi-Newton Strategy. *Journal of Intelligent Learning Systems and Applications*, *05*(01), 19–28. https://doi.org/10.4236/jilsa.2013.51003

Rogers, L. L., & Dowla, F. U. (1994). Optimization of groundwater remediation using artificial neural networks with parallel solute transport modeling. *Water Resources Research*, *30*(2), 457–481. https://doi.org/10.1029/93WR01494

Rosowsky, D. V., Mudd, L., & Letchford, C. (2016). Assessing climate change impact on the joint wind-rain hurricane hazard for the northeastern U.S. coastline. In P. Gardoni, C. Murphy, & A. Rowell (Eds.), *Risk Analysis of Natural Hazards: Interdisciplinary Challenges and Integrated Solutions* (pp. 113–134). Springer. https://doi.org/10.1007/978-3-319-22126-7_8

Rumpf, J., Weindl, H., Höppe, P., Rauch, E., & Schmidt, V. (2007). Stochastic modelling of tropical cyclone tracks. *Mathematical Methods of Operations Research*, *66*(3), 475–490. https://doi.org/10.1007/s00186-007-0168-7

Rumpf, J., Weindl, H., Höppe, P., Rauch, E., & Schmidt, V. (2009). Tropical cyclone hazard assessment using model-based track simulation. *Natural Hazards*, *48*(3), 383–398. https://doi.org/10.1007/s11069-008-9268-9

Sandri, P. (1996). *An artificial neural network for wind-induced damage potential to nonengineered buildings*. Texas Tech University.

Scawthorn, C., Flores, P., Blais, N., Seligson, H., Tate, E., Chang, S., Mifflin, E., Thomas, W., Murphy, J., Jones, C., & Lawrence, M. (2006). HAZUS-MH flood loss estimation methodology. II. Damage and loss assessment. *Natural Hazards Review*, *7*(2), 72–81. https://doi.org/10.1061/(ASCE)1527-6988(2006)7:2(72)

Schaal, S. (1999). Is imitation learning the route to humanoid robots? *Trends in Cognitive Sciences*, *3*(6), 233–242.

Seneviratne, S. I., Nicholls, N., Easterling, D., Goodess, C. M., Kanae, S., Kossin, J., Luo, Y., Marengo, J., McInnes, K., Rahimi, M., Reichstein, M., Sorteberg, A., Vera, C., & Zhang, X. (2012). Changes in climate extremes and their impacts on the natural physical environment. In C. B. Field, V. Barros, T. F. Stocker, D. Qin, D. J. Dokken, K. L. Ebi, M. D. Mastrandrea, K. J. Mach, G.-K. Plattner, S. K. Allen, M. Tignor, & P. M. Midgley (Eds.), *Managing the Risks of Extreme Events and Disasters to Advance Climate Change Adaptation* (pp. 109–230). A Special Report of Working Groups I and II of the Intergovernmental Panel on Climate Change (IPCC). Cambridge University Press. https://doi.org/10.1017/CBO9781139177245

Shen, W., Tuleya, R. E., & Ginis, I. (2000). A sensitivity study of the thermodynamic environment on GFDL model hurricane intensity: Implications for global warming. *Journal of Climate*, *13*(1), 109–121. https://doi.org/10.1175/1520-0442(2000)013<0109:ASSOTT>2.0.CO;2

Shindell, D. (2013). Radiative Forcing in the AR5. *Climate Change 2013: The Physical Science Basis*, 1–11. http://climate.envsci.rutgers.edu/climdyn2013/IPCC/IPCC_WGI12-RadiativeForcing.pdf

Solomon, A., Goddard, L., Kumar, A., Carton, J., Deser, C., Fukumori, I., Greene, A. M., Hegerl, G., Kirtman, B., Kushnir, Y., & Newman, M. (2011). Distinguishing the roles of natural and anthropogenically forced decadal climate variability: implications for prediction. *Bulletin of the American Meteorological Society*, *92*(2), 141–156. https://doi.org/10.1175/2010BAMS2962.1

Stewart, M. G., & Deng, X. (2015). Climate Impact Risks and Climate Adaptation Engineering for Built Infrastructure. *ASCE-ASME Journal of Risk and Uncertainty in Engineering Systems, Part A: Civil Engineering*, *1*(1), 1–12. https://doi.org/10.1061/AJRUA6.0000809

Tehrany, M. S., Pradhan, B., & Jebur, M. N. (2013). Spatial prediction of flood susceptible areas using rule based decision tree (DT) and a novel ensemble bivariate and multivariate statistical models in GIS. *Journal of Hydrology*, *504*, 69–79. https://doi.org/10.1016/j.jhydrol.2013.09.034

Tippett, M. K., Camargo, S. J., & Sobel, A. H. (2011). A poisson regression index for tropical cyclone genesis and the role of large-scale vorticity in genesis. *Journal of Climate*, *24*(9), 2335–2357. https://doi.org/10.1175/2010JCLI3811.1

Tisseuil, C., Vrac, M., Lek, S., & Wade, A. J. (2010). Statistical downscaling of river flows. *Journal of Hydrology*, *385*(1–4), 279–291. https://doi.org/10.1016/j.jhydrol.2010.02.030

Tokar, A. S., & Johnson, P. A. (1999). Rainfall-runoff modeling using Artificial Neural Networks. *Journal of Hydrologic Engineering*, *4*(3), 232–239. https://doi.org/10.1061/(ASCE)1084-0699(1999)4:3(232)

Tonn, G., & Czajkowski, J. (2018). *An Analysis of U . S . Tropical Cyclone Flood Insurance Claim Losses : Storm Surge vs . Freshwater*. https://pdfs.semanticscholar.org/2b75/7dad5905e55c8dba94cc58555757f77ebf6a.pdf

Trenberth, K. E., Cheng, L., Jacobs, P., Zhang, Y., & Fasullo, J. (2018). Hurricane Harvey Links to Ocean Heat Content and Climate Change Adaptation. *Earth's Future*, *6*(5), 730–744.

https://doi.org/10.1029/2018EF000825

Tuleya, R. E., DeMaria, M., & Kuligowski, R. J. (2007). Evaluation of GFDL and simple statistical model rainfall forecasts for U.S. landfalling tropical storms. *Weather and Forecasting*, *22*(1), 56–70. https://doi.org/10.1175/WAF972.1

USGS. (2019a). *USGS Flood Event Viewer*. https://stn.wim.usgs.gov/FEV

USGS. (2019b). *USGS Water Data for the Nation*. https://doi.org/10.5066/F7P55KJN

Van Aalst, M. K. (2006). The impacts of climate change on the risk of natural disasters. *Disasters*, *30*(1), 5–18. https://doi.org/10.1111/j.1467-9523.2006.00303.x

Van Oldenborgh, G. J., Van Der Wiel, K., Sebastian, A., Singh, R., Arrighi, J., Otto, F., Haustein, K., Li, S., Vecchi, G., & Cullen, H. (2017). Attribution of extreme rainfall from Hurricane Harvey, August 2017. *Environmental Research Letters*, *12*(12), 124009. https://doi.org/10.1088/1748-9326/aa9ef2

Varma, S., & Simon, R. (2006). Bias in error estimation when using cross-validation for model selection. *BMC Bioinformatics*. https://doi.org/10.1186/1471-2105-7-91

Vecchi, G. A., & Knutson, T. R. (2008). On estimates of historical North Atlantic tropical cyclone activity. *Journal of Climate*, *21*(14), 3580–3600. https://doi.org/10.1175/2008JCLI2178.1

Vecchi, G. A., Swanson, K. L., & Soden, B. J. (2008). Whither Hurricane Activity? *Science*, *322*(5902), 687–689. https://doi.org/10.1126/science.1164396

Vickery, P. J., Skerlj, P. F., Lin, J., Twisdale, L. A., Young, M. A., & Lavelle, F. M. (2006). HAZUS-MH hurricane model methodology. II: Damage and loss estimation. *Natural Hazards Review*, *7*(2), 94–103. https://doi.org/10.1061/(ASCE)1527-6988(2006)7:2(94)

Vickery, P. J., Skerlj, P. F., & Twisdale, L. A. (2000). Simulation of hurricane risk in the US using empirical track model. *Journal of Structural Engineering*, *126*(10), 1222–1237.

Vickery, P. J., & Wadhera, D. (2008). Statistical models of Holland pressure profile parameter and radius to maximum winds of hurricanes from flight-level pressure and H* wind data. *Journal of Applied Meteorology and Climatology*, *47*(10), 2497–2517. https://doi.org/10.1175/2008JAMC1837.1

Villarini, G., Smith, J. A., Baeck, M. L., Marchok, T., & Vecchi, G. A. (2011). Characterization of rainfall distribution and flooding associated with U.S. landfalling tropical cyclones: Analyses of Hurricanes Frances, Ivan, and Jeanne (2004). *Journal of Geophysical Research Atmospheres*, *116*(23). https://doi.org/10.1029/2011JD016175

Wang, Y., & Rosowsky, D. V. (2018). Hazard-based regional loss estimation considering hurricane intensity, size and sea surface temperature change. *Sustainable and Resilient Infrastructure*, *3*(4), 151–164. https://doi.org/10.1080/23789689.2017.1364564

Wang, Z., Lai, C., Chen, X., Yang, B., Zhao, S., & Bai, X. (2015). Flood hazard risk assessment model based on random forest. *Journal of Hydrology*, *527*, 1130–1141. https://doi.org/10.1016/j.jhydrol.2015.06.008

Wolock, D. M., & McCabe Jr, G. J. (1995). Comparison of Single and Multiple Flow Direction Algorithms for Computing Topographic Parameters in TOPMODEL. *Water Resources Research*, *31*(5), 1315–1324. https://doi.org/10.1029/95WR00471

Wuebbles, D. J., Kunkel, K., Wehner, M., & Zobel, Z. (2014). Severe Weather in United States Under a Changing Climate. *Eos, Transactions American Geophysical Union*, *95*(18), 149–156. https://doi.org/10.1002/2014EO180001

Zachry, B. C., Booth, W. J., Rhome, J. R., & Sharon, T. M. (2015). A national view of storm surge risk and inundation. *Weather, Climate, and Society*, *7*(2), 109–117. https://doi.org/10.1175/WCAS-D-14-00049.1

Zahmatkesh, Z., Karamouz, M., Goharian, E., & Burian, S. J. (2015). Analysis of the effects of climate change on urban storm water runoff using statistically downscaled precipitation data and a change factor approach. *Journal of Hydrologic Engineering*, *20*(7), 1–11. https://doi.org/10.1061/(ASCE)HE.1943-5584.0001064

Zhang, G., Murakami, H., Knutson, T. R., Mizuta, R., & Yoshida, K. (2020). Tropical cyclone motion in a changing climate. *Science Advances*, *6*(17), 1–8. https://doi.org/10.1126/sciadv.aaz7610

Zhao, L. Di, Yang, M. Y., Bian, C. P., & Hao, Q. (2013). Using neural networks forecast the economic losses caused by storm surge. *Advanced Materials Research*, *798*, 987–991. https://doi.org/10.4028/www.scientific.net/AMR.798-799.987

Zhou, Z. H., Wu, J., & Tang, W. (2002). Ensembling neural networks: Many could be better than all. *Artificial Intelligence*, *137*(1–2), 239–263. https://doi.org/10.1016/S0004-3702(02)00190-X

Zhu, L., & Laptev, N. (2017). Deep and Confident Prediction for Time Series at Uber. *IEEE International Conference on Data Mining Workshops, ICDMW*, *2017-Novem*, 103–110. https://doi.org/10.1109/ICDMW.2017.19